PELLET FEED GRINDING PROCESS OPTIMIZATION THROUGH SIMULATION TOOLS AND MATHEMATICAL MODELING

Patrícia Mundim Campos Faria

Dissertação de Mestrado apresentada ao Programa de Pós-graduação em Engenharia Metalúrgica e de Materiais, COPPE, da Universidade Federal do Rio de Janeiro, como parte dos requisitos necessários à obtenção do título de Mestre em Engenharia Metalúrgica e de Materiais.

Orientadores: Luís Marcelo Marques Tavares
Raj Rajamani

Rio de Janeiro
Junho de 2015

PELLET FEED GRINDING PROCESS OPTIMIZATION THROUGH SIMULATION TOOLS AND MATHEMATICAL MODELING

Patrícia Mundim Campos Faria

DISSERTAÇÃO SUBMETIDA AO CORPO DOCENTE DO INSTITUTO ALBERTO LUIZ COIMBRA DE PÓS-GRADUAÇÃO E PESQUISA DE ENGENHARIA (COPPE) DA UNIVERSIDADE FEDERAL DO RIO DE JANEIRO COMO PARTE DOS REQUISITOS NECESSÁRIOS PARA A OBTENÇÃO DO GRAU DE MESTRE EM CIÊNCIAS EM ENGENHARIA METALÚRGICA E DE MATERIAIS.

Examinada por:

Prof. Luís Marcelo Marques Tavares, Ph.D.

Prof. Rodrigo Magalhães de Carvalho, D.Sc.

Eng. Douglas Batista Mazzinghy, D.Sc.

Prof. Aubrey Njema Mainza, Ph.D.

RIO DE JANEIRO, RJ - BRASIL

JUNHO DE 2015

Faria, Patrícia Mundim Campos

Pellet Feed Grinding Process Optimization Through Simulation Tools And Mathematical Modeling/ Patrícia Mundim Campos Faria. - Rio de Janeiro: UFRJ/COPPE, 2015.

XXVII, 189 p.: il.; 29,7 cm.

Orientadores: Luís Marcelo Marques Tavares

Raj Rajamani

Dissertação (mestrado) - UFRJ/ COPPE/ Programa de Engenharia Metalúrgica e de Materiais, 2015.

Referências Bibliográficas: p. 152-161.

1. Comminution. 2. Ball mill optimization. 3. Simulation and modeling. I. Tavares, Luís Marcelo Marques *et al.* II. Universidade Federal do Rio de Janeiro, COPPE, Programa de Engenharia Metalúrgica e de Materiais. III. Título.

Para meu marido Rodolfo e meus filhos Théo e Luca.

AGRADECIMENTOS

Primeiramente agradeço a Deus.

E depois a todos que contribuíram com a execução deste trabalho, em especial:

Ao meu marido Rodolfo por estar sempre ao meu lado, me apoiando e me incentivando nas horas mais difíceis. Seu apoio foi fundamental para que este trabalho tivesse um princípio, um meio e um fim;

Ao meu filho Théo que entendeu que em vários momentos tive que me ausentar de suas brincadeiras para finalizar esta dissertação e ao meu filho Luca que espero que mesmo dentro da barriga tenha entendido a minha ausência em curtir mais a sua gestação;

A minha mãe Neide que sempre me incentivou a estudar e buscar novos desafios;

A minha irmã Andréa e a toda minha família pela paciência nos momentos de estresse e pela torcida pelo sucesso deste trabalho;

A Vale S/A pela oportunidade de desenvolver este trabalho, em especial ao Diretor Maurício Max, ao Gerente Executivo Rodrigo Araújo, a Supervisora Simonny Guachalla por terem acreditado no meu potencial para aprender e aplicar o aprendizado adquirido, as amigas e colegas de trabalho Tatiane Alvarenga e Cátia Casagrande e a todos que direta ou indiretamente contribuíram para realização deste estudo;

Ao meu orientador Prof. Luís Marcelo Marques Tavares por todo ensinamento passado ao longo destes quatro anos de orientação.

Ao meu co-orientador Prof. Raj Rajamani pela troca de experiências durante o intercambio realizado na Universidade de Utah.

Resumo da Dissertação apresentada à COPPE/UFRJ como parte dos requisitos necessários para a obtenção do grau de Mestre em Ciências (M.Sc.)

OTIMIZAÇÃO DO PROCESSO DE MOAGEM DE PELLET FEED ATRAVÉS DE FERRAMENTAS DE SIMULAÇÃO E MODELAGEM MATEMÁTICA

Patrícia Mundim Campos Faria

Junho/2015

Orientadores: Luís Marcelo Marques Tavares
Raj Rajamani

Programa: Engenharia Metalúrgica e de Materiais

O presente trabalho utilizou técnicas de modelagem e simulação tradicionais e mais avançadas a fim de obter o melhor desempenho operacional de um moinho de bolas em um circuito fechado que produz finos para o processo de pelotização.

No caso das técnicas tradicionais, a aplicação da abordagem do modelo do balanço populacional, que mostra como informações de testes de moagem em batelada e medições apropriadas da distribuição do tempo de residência em moinhos contínuos de escala piloto podem descrever o desempenho de um moinho industrial, é demonstrada. As variáveis: concentração de sólidos, tamanho superior de bola e enchimento de polpa, foram investigadas usando esta metodologia e, de acordo com os resultados simulados, uma condição operacional ótima foi proposta para o moinho industrial da Vale S/A, correspondendo ao tamanho máximo de bolas de 25 mm e percentagem de sólidos entre 76 e 80%.

Além disso, o revestimento do moinho foi periodicamente escaneado a laser e essas medições forneceram dados importantes para entender as mudanças que ocorrem na movimentação da carga à medida que o revestimento se desgasta e também forneceram dados para as simulações em DEM que integrou seus resultados ao modelo mecanicista de moinho de bolas desenvolvido na UFRJ.

Abstract of Dissertation presented to COPPE/UFRJ as a partial fulfillment of the requirements for the degree of Master of Science (M.Sc.)

PELLET FEED GRINDING PROCESS OPTIMIZATION THROUGH SIMULATION TOOLS AND MATHEMATICAL MODELING

Patrícia Mundim Campos Faria

June/2015

Advisors: Luís Marcelo Marques Tavares
Raj Rajamani

Department: Metallurgical and Materials Engineering

The present work made use of traditional and more advanced modeling and simulation techniques in order to reach the best operational performance of a selected closed-circuit ball mill producing fines for pelletizing process.

In the case of traditional tools, the application of the population balance model approach, showed how information from batch grinding tests and proper measurements of residence time distributions of a pilot-scale continuous mill can describe industrial mill performance is demonstrated. The variables: solids concentration, top ball size and slurry filling, were investigated using this methodology and according to simulated results an optimal operational condition was defined for Vale's industrial mill, corresponding to 25 mm of top ball size and solids concentration between 76 and 80%.

Further, the mill liner was periodically laser scanned and these measurements provided important data to understand how media motion changes as liners wore. In addition, this provided data for DEM – based simulation of mill and integrating its outcome with the UFRJ ball mill mechanistic model.

LIST OF FIGURES

LIST OF TABLES

LIST OF SYMBOLS

Latin

A	Model parameter in t_{10} equation
A_B	Constant in Bond's power equation
a_c, b_c, c	Constants that must be fitted to the data in BARRIOS *et al.*'s equation
$A_{i,b}$	Rate of appearance of material in class i due to body fracture
$A_{i,s}$	Rate of appearance of material in class i due to surface fracture
a_{ij}	Breakage function in density form, corresponding to the mechanism of surface breakage
B	Top ball size
b	Width of weir in overflow discharge mills
b'	Model parameter in t_{10} equation
B_{i1}	Feed size cumulative breakage distribution function
b_{i1}	Feed size individual breakage distribution function
b_{ij}	Breakage function in density form
B_{ij}	Cumulative breakage distribution function
d	Intermediate ball size
D	Mill diameter inside liners
d^*	Original size of the particle
d'	Fitting parameter
d_A	Model parameter
d_m	Distance between the center of the mill and the center of gravity of the charge
d_i	Representative size of particles contained in the ith class
$D_{i,b}$	Rate of disappearance of material in class i due to body fracture
$D_{i,s}$	Rate of disappearance of material in class i due to surface fracture
d_j	Mean size of the particles caught by the colliding steel ball
d_o	Model parameter
d^s	Scrap ball size
D_t	Trunnion diameter
E	Specific energy input to mill
$E(t)$	Residence time distribution in a mill
$E_{50,i}$	Median particle fracture energy of particles contained in size i
$E_{50b,j}$	Median mass-specific particle fracture energy of particles in size class i that are broken as a result of the impact of magnitude E

E_∞	Model parameter
eE	Fraction of the impact energy that is absorbed by each particle captured in an impact event
E_i^*	Maximum fracture energy of particles contained in class i
$E_{max,i}$	Upper truncation value of the distribution
$F_3(d)$	Ball size distribution
F_{80}	Size where 80% of feed particles are smaller
f_c	Fractional volume filling
F_i	Zero order production rate constants
$F_i(E, t)$	Distribution of fracture energies of the material contained in size class i that did not suffer any impact event during the time interval
$F_i(E,0)$	Fracture probability distribution of the original material
$F_i^*(E, t+\Delta t)$	Distribution of fracture energies of the particles in size class i that were captured in an impact event, but which did not fracture
g	Acceleration due to gravity
$G_i(t)$	Fraction of material in the class i that has been damaged but remained in the original size range
h	Initial bed height
H	Total mass of material to be ground, known as hold-up
h_b	Height in Morrell's equation
$H_i(t)$	Fraction of material that appeared due to body and surface breakage
$I_i(t)$	Fraction of material that was not captured in the time interval
J_b	Fraction of the mill volume that is occupied by balls
J_t	Fraction of the mill volume that is occupied by the total charge (media and material)
k	Calibration constant
K_D	Parameter determined from Donda's grindability test
K_e	Elastic constant of the contact
K_g	Geometric constant of the contact
K_i	Elastic stiffness of each of the bodies in contact
K_L	Loading factor in King's equation
kW_b	Kilowatts per ton of media in the mill pinion
L	Mill length inside liners
L_c	Centerline length of the mill
L_d	Mean length of the conical ends
L_e	Effective length of the mill including the conical ends
$m_1(0)$	Top size mass fraction at time 0

$m_1(t)$	Top size mass fraction at time t
m_b	Mass of grinding media
M_c	Total mass charge in the mill
$m_i(t)$	Mass fraction of the material in the ith size interval at any time t
$m_{i,batch}$	Batch response in mathematical description of material transport through the mill
$m_{i,MP}$	Continuous response in mathematical description of material transport through the mill
m_j	Mass of particles contained in size class j captured in each stressing event
M_{MF}	Mass flow rate of feed to the mill
M_{ore}	Ore mass
M_p	Mass flow rate of fresh feed to the mill
m_p	mass of particles that completely fill the interstices between the balls under static conditions
$\overline{m}_{p,i}$	Average weight of the particles contained in size class i
M_{slurry}	Slurry mass
M_{water}	Water mass
N	Mill rotation speed
n	Number of mixers in series
n_b	Total number of balls in balls charge
N_c	Mill critical speed
$N_{\text{cap},i}$	Number of particles caught between the media elements
n_e	Constant in energy equations
P	Mill power
$p(E)$	Distribution of stressing energies E in the mill
$p(e)$	Function that represents the energy split among particles
P_{80}	Size where 80% of product particles are smaller
P_{net}	Mill net power
P_{no_load}	No load power at Morrell's equation
Q	Volumetric discharge rate
Q^*	Dimensionless ball size and lifter geometry
Q_{max}	Maximum volumetric discharge rate
r	Radial position
r_c	Radius of the bed, also called radius of capture
r_{ci}	Radius of curvature of each of the bodies in contact
r_e	Radius of contact due to the elastic deformation in the vicinity of contact

R_f	Percentage retained on the desired mesh of the feed
r_g	Radius of contact due to geometry
r_i	Radial position of charge inner surface
r_m	Radius of mill inside liners
R_p	Percentage retained on the desired mesh of the product
r_t	Trunnion radius
S_1	Top feed size breakage rate function parameter
S_1^E	Top feed size specific selection function parameter
$S_i(t)$	Size discretized selection function for each ith size interval at any time t
S_i^E	Specific selection function for the ith size interval
S_s	Factor of ball size
t	Time
T	Torque required to turn the mill
t_{10}	Fraction of material passing 1/10th of the original particle size
T_f	Torque required to overcome friction
t_n	Percent passing in size d_j/n
U	Fraction of the voidage that is filled by slurry or solids
u	Velocity
V_B	Balls volume
V_{bulk}	Bulk volume of solids
V_m	Mill volume
V_{med}	Autogenous media volume
V_r	Tangential velocity of a particle at radial distance r
V_S	Slurry volume
V_{void}	Void volume
w_i	Mass of material captured between two grinding media elements
W_i	Work index in Bond's equation
x	Representative size
x_1	Initial or feed particle size
x_2	Final or product particle size

Greek

Δ	Maximum deformation of the bed during impact

λ	Model parameter
ϕ	Model parameter
ϕ_1	Function of dimensionless mill speed, ball load, particle load, ball size and lifter geometry in power equations
κ_i	First order surface breakage rate
α_n, β_n	Parameters that are fitted to the experimental data
ϕ_v	Volume fraction of solids in the slurry
α_1, α_2, α_3	Breakage function parameters
β	Volume shape factor
γ	Parameter in power equations
δ	Dirac delta function
ε	Bed porosity
ζ_j	Selection function adjustable parameters
θ	Factor that accounts for the rotation speed
θ'	Fitting parameter
θ_s	Angular displacement of shoulder position at the mill shell
θ_t	Angular displacement of toe position at the mill shell
θ_{tm}	Angular displacement of the grinding media toe position at the mill shell
θ_{tp}	Angular displacement of the pulp toe position at the mill shell
λ_b	Layer thickness
ξ	Factor that accounts for the mill filling
ρ_b	Ball density
ρ_{bulk}	Bulk density
ρ_c	Charge density
ρ_m	Media density
ρ_{ore}	Ore specific gravity
ρ_s	Slurry density
σ_∞	Model parameter
σ_i	Standard deviation of the lognormal distribution of particle fracture energies of particles contained in size class *i*
σ_i^2	Variance
τ	Mean residence time for material in the mill
τ'	Mean residence time of each mixer
φ_c	Fraction of mill critical speed
ω	Frequency of stressing events in the comminution machine

NOMENCLATURE

AG	Fully Autogenous Mill
DEM	Discrete Element Method
HPGR	High Pressure Grinding Rolls
JKMRC	Julius Kruttschnitt Mineral Research Centre
LTM	Laboratório de Tecnologia Mineral
MPL	Mineral Processing Laboratory
PBM	Population Balance Model
RMS	Root Mean Squares
RTD	Residence Time Distribution
SAG	Semi-autogenous Mill
UFRJ	Universidade Federal do Rio de Janeiro

1. INTRODUCTION

Grinding operations are of great importance to the mineral industries and in particular are one of the most important unit operations in the iron ore pelletizing process. Two groups of equipment can represent the traditional comminution process: crushers and mills. The first group generally represents the first stage of comminution and its objective is to reduce the particle size throughout the operational range utilized in mills. The second generally consist of tumbling mills with a grinding media charge made of steel balls or cylpebs, except for some cases in which grinding rods or ore fragments, called pebbles, are used. Ball mills often represent the last stage in the comminution process.

The major purpose of grinding circuits is to reduce the ore particle size, either in dry or wet circuits, through a combination of impact and abrasion, in order to liberate the ore mineral or to achieve the desired size for the subsequent process.

For many years in the past, iron ores that were charged to blast furnaces were only crushed and classified either at the mine site or at the iron and steel plant. In this case lump ores were preferred, although small portions of fine ores could be tolerated. As a result, a significant part of the fines that were not used formed continuously growing dumps with no economic use. Their limited use was because they reduced the blast furnace gas permeability and disturbed the furnace operation. Moreover, a large part of these fines was blown out of the blast furnace and had to be recovered as flue dust. Furthermore, these dusts represented a considerable iron value, which, much like the unused fine ore dumps, was lost. Many possibilities were examined, and tests to agglomerate the flue dust by sintering or briquetting and to recycle it to the blast furnace were started in various industrialized countries, although with differing intensities. In countries with comparatively small ore reserves, the sinter process development continued intensively and at about the same time, some researches were looking for an alternative process to sintering, especially in areas in which very fine ores or concentrates were available. This was the beginning of the pelletizing process (MEYER, 1980).

According to MEYER (1980), pellets are balls produced from concentrates and natural iron ores of different mineralogical and chemical composition with some remarkable properties such as:

- Uniform size distribution within a main range of 9-15 mm diameter;
- High and even porosity of 25-30%;
- High iron content: more than 63% iron;
- Practically no loss on ignition or volatiles;
- Uniform mineralogical composition in the form of an easily reducible hematite or hematite-bearing compounds;
- High and uniform mechanical strength;
- Limited amenability to abrade and good behavior during transportation and handling;
- Sufficient mechanical strength even at thermal stress under reducing atmosphere.

Because of these several properties, which are predetermined and definable, they differ from lump ore and, to a certain extent, also from sinter. To obtain the required properties and considering the great variety of raw materials that are taken into account, adequate production methods are to be adopted. The first stage is the green balls formation. Fine-grained iron ores having adequate size distribution are rolled with the addition of a wetting liquid, usually water, in suitable devices such as drums or discs. In this way, wet balls are formed, the so-called green pellets. During the ball formation, it is also possible to use other additives for improving the properties of green and fired pellets, e.g. bentonite used as a binder, and for changing the metallurgical properties of the indurated pellets, e.g. limestone or dolomite. In a second step the green pellets are dried and indurated to obtain the typical features of pellets. This is achieved, in most cases, by careful heating under oxidizing atmosphere to just below the softening point of the ores used. During this heating, not only the crystalline structure is changed but also others bonds appear, such as reactions between slag-forming constituents – both between each other and with iron oxides. The hot pellets are carefully cooled in order to maintain as far as possible the result crystalline structures and other bonds, as well as to avoid tension cracks.

Successful pellet production calls for an optimum efficiency and harmony between all three process steps (raw material preparation, formation and induration of green balls) with the preceding stage significantly influencing the subsequent one. An error made in the preceding stage can only be corrected to a limited extent in the subsequent process stages. Even during the induration process, no first-class pellet can be produced from a defective green ball. The purpose of the green ball formation is to generate pellets with

a substantially higher strength primarily with the aim of withstanding their transportation and the stresses occurring during metallurgical operations. The most important factors influencing green ball formation are the physical properties of fine-grained iron ores (grain size and size distribution, grain shape, surface condition – specific surface area, porosity, pore type). In other words, the adequate fineness and a suitable size distribution of the raw materials is an important prerequisite to pelletizing process and by controlling these factors the pellet quality can be improved.

With the exception of concentrates, which often are already obtained with sufficient fineness from the beneficiation plant, natural ores, coarser concentrates and additives have to be ground or reground. In the case of Vale's pelletizing plants located in Vitoria – Espírito Santo State (Brazil), the typical size specification required for a good green ball formation is around 80 to 87% passing 45 μm in the cyclone overflow, so that to achieve this target it is necessary to have about 40% of the mill discharge passing the 45 μm sieve. Currently, the pellet feed provided by Vale's beneficiation plants located in Minas Gerais State has around 10 % passing 45 μm. This amount of fines indicates that a regrinding process is essential to achieve the fineness suitable to the green ball formation. Figure 1.1 illustrates the flowsheet of one of the pelletizing plants at Vale. In this case the regrinding process with ball mills is the first stage of this process.

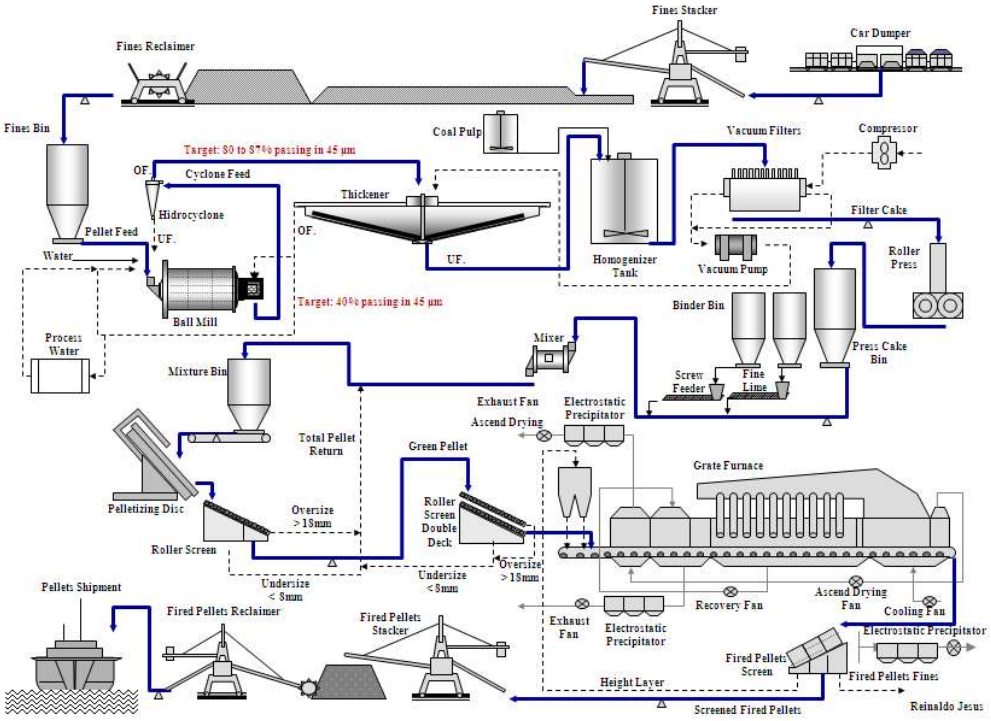

Figure 1.1: Pelletizing process flowchart

Grinding circuits involve high capital and operating costs and are notoriously inefficient (SIDDIQUE, 1977). Particle size reduction is directly proportional to energy consumption. In other words, for the same feed size distribution, the finer the mill product the greater is the energy required. Thus, the high energy consumption in the regrinding circuit is one of the major cost items of the pelletizing process. Therefore, there is considerable room to develop and apply simulation techniques and mathematical modeling to optimize this process, which could reduce the processing costs. This is a topic of special interest to Vale, which currently has eight pelletizing plants in operation in Brazil, with 21 conventional ball mills operating in wet grinding. In this context, this study is concerned with improving Vale's ball mill performance through simulation techniques and mathematical modeling.

As mentioned previously, the particle size reduction process is a highly energy intensive process and the understanding of how the energy is applied and utilized in these processes exist since the end of the 19th century. The first quantitative definitions, completely empirical, emerged during this period (Rittinger and Kick's law). Further, in the middle of the 1950s, Fred Bond, an engineer from Allis Chalmers, the leading mill

manufacturing company at the time, proposed an empirical methodology for mill scale up based on laboratory batch tests. The simple Bond equation has served the industry well as a basis for scale-up from laboratory-scale data.

From the 1970s on, significant advances were made in the development of detailed phenomenological grinding models derived from population balance considerations. In other words, the population balance applied to the comminution process becomes a mass balance for particle size classes and its use depends on the characterization of the functions which describe the motion of the mass through the size classes, for example, the breakage and selection functions. This approach became very popular as a modeling tool of comminution process. This type of model, in its complete form, is capable of describing the size distribution in a grinding mill as a function of time in batch grinding or steady state mill discharge in continuous mills, besides the dynamics of continuous mill operation. As such, according to this methodology the plant scale mill can be optimized via laboratory scale grinding mill tests. However, this approach has certainly important limitations: although it can describe effectively the process, the empirical modeling based on PBM has no intrinsic capabilities to allow simulating the process under conditions that are different from those that were used to fit its parameters (CARVALHO and TAVARES, 2013).

Owing to the limitations presented by the classical population balance model, some researchers already in the 1980s argued that major advances in modeling of comminution would have to occur through the development of more mechanistic models. Several studies were conducted with the aim of understanding the mechanisms involved in the particle size reduction and how these mechanisms are related to the implementation of efforts.

Considering the advance in understanding the particle breakage mechanisms, the proper description of the comminution environment in mills and crushers also became necessary. Responding to this need, MISHRA and RAJAMANI (1992) applied the Discrete Element Method (DEM) to simulate the grinding environment, considering a ball mill as a set of circular slices. Also in the beginning of the 1990s, several results involving the characterization of the individual particle breakage mechanisms were published, improving the understanding on the behavior of the particles when subjected to various types of stressing modes (impact, compression, abrasion). Based on this and with the aim of decoupling the influence of material and comminution environment,

analyzing up the breaking events individually, KING and BOURGEOIS (1993) proposed a model based on the population balance model. This approach has been called modeling in microscale. Subsequently, TAVARES and KING (1998) demonstrated that the particles have a variability of their properties (resistance to fracture, type of fragmentation, etc.), recognizing the importance of the description of this effect into mathematical modeling. A few years later, the authors proposed a model based on continuum damage mechanics applied to the ore particles, which takes account the weakness caused by repeated impacts (TAVARES and KING, 2002).

Combining the recent advances in DEM with the microscale approach and with the mechanical model of the damage, a new modeling approach was proposed which in theory can be applied to any process of particle size reduction. The UFRJ ball mill mechanistic model was developed by researchers from the Laboratório de Tecnologia Mineral (LTM) of the Universidade Federal do Rio de Janeiro (TAVARES and CARVALHO, 2009, 2010). This approach allows describing in much greater detail the effect of operating and design variables since it decouples material from mill contributions in the process, while maintaining the mass balancing capabilities of the population balance model.

As such, the aim of the present work is to make use of traditional and more advanced modeling and simulation techniques in order to reach the best operational performance of a selected closed-circuit ball mill producing fines for pelletizing process. In the case of traditional tools, the aim is to demonstrate the application of the population balance model approach to optimizing ball milling in iron ore grinding for pellet feed preparation, showing how information from batch grinding tests and proper measurements of residence time distributions of a pilot-scale and a continuous mill can describe continuous mill performance. The variables that were investigated using this methodology were solids concentration, top ball size and slurry filling. Further, the mill liners were periodically laser scanned and these measurements provided important data to understand how media motion changes as liners wore. In addition, this provided data for DEM – based simulation of mill and integrating its outcome with the UFRJ ball mill mechanistic model.

This dissertation is structured in five chapters. After this introduction, the literature in the field is reviewed in Chapter 2, including the population balance model and UFRJ mechanistic model description. Chapter 3 presents the methodology and experimental

procedures used to generate data to feed the PBM model and UFRJ mechanistic model. Chapter 4 presents the parameters estimation and simulations conducted for pilot-scale mill and Vale's industrial mill using the PBM and UFRJ mechanistic model approaches. This chapter also presents the PBM model validation and results of application. Chapter 5 finalizes the dissertation with the conclusions.

2. LITERATURE REVIEW

In this chapter, a brief review on the main equipment that can be used in comminution processes is presented. Initially, the classical comminution theories are reviewed. Afterwards, the traditional and more advanced modeling and simulation techniques are analyzed. In this context, the population balance model and the UFRJ mechanistic model approach are briefly described, and their advantages and limitations are highlighted.

2.1 Comminution Overview

Several types of equipment can be employed in comminution processes, each presenting peculiarities in regard to the dominant mode of stressing applied to the ore particles. Generally, comminution in a mineral processing plant takes place as a sequence of crushing and grinding operations. Crushing reduces the particle size of run-of-mine ore to such a size that grinding can be carried out until the mineral and gangue are substantially liberated.

The main difference between crushing and grinding is that while crushing is typically accomplished by compression of the ore particles against rigid surfaces, or by impact against surfaces in a rigidly constrained motion path, grinding is accomplished by abrasion and impact of the ore by the free motion of unconnected media such as rods, balls, or pebbles. Figure 2.1 illustrates a jaw crusher and an industrial ball mill.

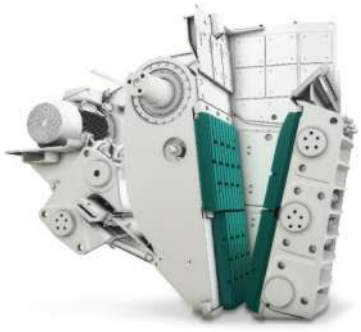

(a)

(b)

Figure 2.1: Jaw Crusher (courtesy of Metso) (a) and industrial ball Mill at Vale's pelletizing plant #8 (b)

Crushing is usually a dry process, and is typically performed in several stages. In most cases, tumbling mills with either steel rods or balls, or pebbles as the grinding media are used after crushing and the grinding process is usually performed wet, although dry grinding has limited, but important, applications.

Stirred mills (Figure 2.2) are now commonly used in mineral processing. This type of mill uses a stirrer to provide motion to the steel, ceramic, or rock media. Both vertical and horizontal configurations exist, and since they can operate with smaller media sizes, they are far more suitable for fine grinding applications than conventional ball mills. Stirred mills are claimed to be more energy efficient (by up to 35%) than conventional ball mills (LISBOA *et al.*, 2014; MAZZINGHY and SCHNEIDER, 2014).

Figure 2.2 Vertical stirred mill (Vertimill® Metso – courtesy of Metso)

Another comminution device that is relatively new in some applications is the high pressure grinding rolls (HPGR) (Figure 2.3). This machine applies compression to the bed of particles, resulting in energy-efficient inter-particle breakage (SCHÖNERT, 1988). Nowadays, green field projects are considering HPGR as an economic alternative in the comminution circuits due to their greater energy efficiency when compared to conventional crushers and mills (AMELUNXEN and MEADOWS, 2011). The HPGR can be installed as primary grinding in replacement of crushers, before or after a ball mill, or can be installed in series in order to replace conventional tumbling mills.

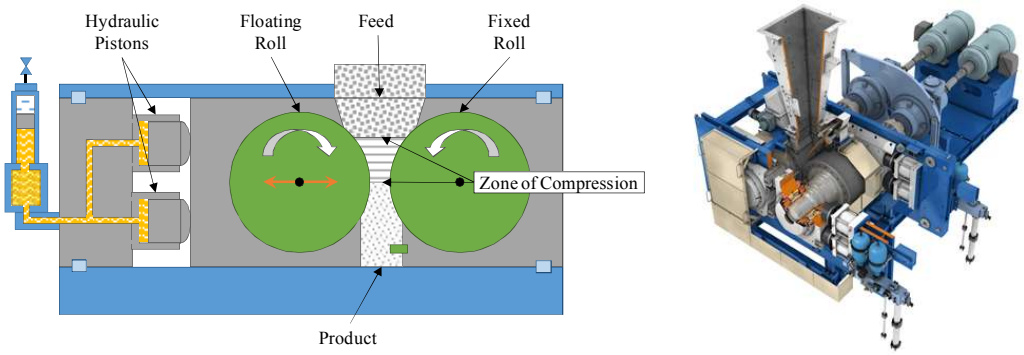

(a) (b)

Figure 2.3 High Pressure Grinding Rolls (adapted from technology.infomine.com (a) and courtesy of FLSmidth (b))

Particulate materials are generally fractured primarily by the imposition of compressive stresses applied fairly rapidly by impact. Subsidiary fracture is caused by high shearing stress particularly at the surface of the particle. The former leads to cleavage and shattering while the latter leads to attrition and wear (KING, 2001). All materials resist fracture to a greater or lesser extent and energy must be spent to break a solid. In this context, comminution equipment utilizes different mechanisms to promote particle fracture, and each of them is associated with an amount of energy necessary to break the material. When a particle is coarse, the energy that is required for its fracture, called particle fracture energy, is usually high, even though the energy per mass unit (specific energy) is comparatively low. As particle sizes become smaller, the specific energy (per mass unit) increases rapidly. This relationship explains the use of different comminution equipment according to the desired particle size reduction. In general, in the minerals industry, the comminution process utilizes different types of tumbling mills: balls, rods, pebbles (autogenous or semi-autogenous) that use the motion of the grinding media (balls, rods, pebbles or cylpebs) to promote particle grinding. This motion results in collisions that result in particle breakage due to impact or attrition (KING, 2001).

According to WILLS and NAPIER-MUNN (2006) comminution theory is mainly concerned with the establishment of relationships between energy input and product particle size from a given feed size. It is also known that the greatest part of the energy input to a grinding machine is absorbed by the machine itself and that only a small fraction of the total energy is available for breaking the material. As such, particle size reduction is a very costly process in terms of energy consumption. From this standpoint,

the pursuit of the optimal operating conditions in the comminution process has always been a major goal in the field. Historically, a series of mathematical models have been developed as tools to assist reaching this goal (CARVALHO, 2009).

A good model of the comminution process should represent how the applied energy on the material will produce its breakage and how this breakage will take place considering the material properties. Hence based on NAPIER-MUNN *et al.* (1996) a comminution model should be defined considering:

- Material breakage properties – essentially the breakage that occurs as a result of the stress application with a given amount of specific energy;
- Comminution equipment characteristics – the magnitude and nature of the energy applied and the transport through the machine.

Bearing in mind the extent of the application of comminution processes in the minerals industry and their impact in energy consumption, several theories and mathematical models based directly or indirectly on the assumptions listed above were developed by several researchers. Each of them demonstrated vantages and disadvantages in some specific application and contributed with some importance to develop and improve the advanced mathematical models currently in use in the comminution circuits' optimization. These theories, expressions and mathematical models are described in the following section.

2.2 Classical Comminution Theories

As mentioned by WILLS and NAPIER-MUNN (2006) it is to be expected that there is a relationship between the energy required to break the material and the new surface produced in the process. Considering the fact that more energy per unit mass is required as particles get smaller, an empirical relationship between comminution energy absorbed per unit mass and the representative size (often the 80% passing size – mass basis) is defined by a differential equation:

$$\frac{dE}{dx} = -\frac{k}{x^{n_e}} \qquad 2.1$$

where E is the energy input, x is the representative size and k and n_e are constants.

It may be demonstrated that the classical comminution theories were developed based on this general equation. The oldest one is that of Von Rittinger (1867), which states that the energy consumed in size reduction is proportional to the area of new surfaces produced, hence Rittinger's law equates to:

$$E = k\left(\frac{1}{x_2} - \frac{1}{x_1}\right) \qquad 2.2$$

where E is the energy input, x_1 is the initial particle size, x_2 is the final particle size, and k is a constant.

The second theory is that of Kick (1885) in which he stated that the work required in comminution is proportional to the reduction in volume of the particles concerned. According to Kick's law, the energy required for comminution is dependent of the reduction ratio:

$$E = k \ln \frac{x_1}{x_2} \qquad 2.3$$

where x_1 is the representative size of the feed particles and x_2 the representative size of the product particles, the reduction ratio R is x_1/x_2.

Extensive work has been done until the 1950s to validate Rittinger and Kick's postulates, until Fred Bond developed a method of great importance, which remains in use in the mineral industry (BOND, 1952a). Bond's law or the third theory of comminution was proposed in 1952 after an intense campaign of laboratory tests and industrial correlations. This postulate states that the total useful work in breakage that has been applied to a stated weight of homogeneous broken material is inversely proportional to the square root of the representative size of the product particles. When the work input, feed size, and product size of a reduction stage are known, the theory allows rapid calculation of the work required for any size reduction and permits direct comparisons of efficiency (BOND, 1952b). Hence, the third theory of comminution can be represented by:

$$E = 10W_i\left(\frac{1}{\sqrt{P_{80}}} - \frac{1}{\sqrt{F_{80}}}\right) \qquad 2.4$$

where P_{80} is the size in microns which 80% of the product passes, F_{80} is the size which 80% of the feed passes, the energy input in kilowatt hours per ton is E and W_i is the

work index. The work index is the comminution parameter which expresses the resistance of the material to crushing and grinding; numerically it is the kilowatt hours per ton required to reduce the material from theoretically infinite feed size to 80% passing 100 μm. Bond developed standard laboratory tests to calculate this parameter.

Equation 2.4 can be used directly to estimate the specific grinding energy and, therefore, the grinding power for the following specific conditions:

- Rod milling: wet, open circuit grinding in a 2.44 meters (8 ft) diameter inside liners;
- Ball milling: wet, closed circuit grinding in a 2.44 meters (8 ft) diameter inside liners;
- Power calculated is the power required at the pinion shaft of the mill, which includes mill bearings and gear and pinion losses, but does not include motor losses or losses in any other drive components, such as reducers and clutches.

Considering those limitations in the applicability of the Bond's equation, ROWLAND (1976) proposed eight efficiency factors that can be applied to calculate grinding power allowing for variations from the specified conditions, such as the grinding circuit and equipment used. The efficiency factors take into account dry grinding, open circuit ball milling, mill diameter, oversized feed, fine grinding in ball mills, high reduction ratio in rod milling, low reduction ratio in ball milling and rod milling. Evidently, since the Rowland factors resulted from industrial practice, they are empirical and arbitrary.

For several years, energy-size reduction relationships were the dominant form of mathematical model used in the description of tumbling mill grinding processes and to design commercial mills. Usually, in these empirical models the single measure of product fineness (the 80% passing size for example) is chosen as the dependent variable and the specific energy (energy input per unit mass of material being ground) acts as the independent variable.

According to HERBST and FUERSTENAU (1980) a scale-up criterion using the specific energy should be based on two important premises:

- Mills of different sizes delivering the same specific energy will yield identical products when fed with the same feed material;
- Existing mill size/power draft relationships are accurate enough to allow the selection of a mill size which will deliver the necessary energy at the design throughput.

Whenever possible the specific energy requirement for a given feed to product transformation is determined in such a way as to minimize the design risk, i.e. the value is determined from an existing full-scale operation or from a pilot-plant circuit which is operated in a similar fashion to that anticipated for the commercial installation. When commercial or pilot-scale data are not available, generally the Bond equation, or its equivalent, is used to estimate specific energy requirements. In some instances these models have been useful for the correlation of experimental data, but, invariably, they have been found to be inadequate for process simulation.

2.2.1 The Use of Power Equations for Tumbling Ball Mills

In order to complete a mill design and calculate the grinding specific energy using the energy-size reduction laws and also phenomenological models, it is necessary to have a mechanical law that relates mill power with mill size and operating conditions. Several power equations were developed with this purpose and some of them are described as follows.

BOND (1960) defined the shaft mill power (P in kW) as a function of mill dimensions (D is the internal diameter and L is the internal length, both in meters) and loading conditions using:

$$m_b = \frac{\pi D^2 L J_b \rho_b (1-\varepsilon)}{4} \qquad 2.5$$

$$P = 7.33 A_B J_b \varphi_c (1-0.937 J_b)\left(1-\frac{0.1}{2^{9-10\varphi_c}}\right)(\rho_b L D^{2.3}) \qquad 2.6$$

where m_b is the mass of grinding media, bed porosity, ε, is taken as 0.4, ρ_b is the true grinding media density (t/m^3), φ_c is the fraction of critical speed ($\varphi_c=N/N_c$; N is the mill rotation speed and N_c is the mill critical speed), J_b is the ball loading fraction and A_B is a constant, equal to 1 is for wet overflow mills; 1.16 is for wet grate discharge mills; and 1.08 for dry grinding.

Another equation that can be used to calculate the mill power is the one established by ROWLAND *et al.* (1982) and BOND (1983):

$$kW_b = 4.879D^{0.3}(3.2 - 3J_b)\varphi_c\left[1 - \frac{0.1}{2^{(9-10\varphi_c)}}\right] + S_s \qquad 2.7$$

where kW_b is the kilowatts per media tons in the mill pinion, D is the mill diameter inside liners in meters, J_b is the fraction of the mill volume that is occupied by balls, φ_c is the fraction of the critical speed and S_s is the factor of the ball size.

This equation is valid for ball mills with overflow discharge and diameter larger than 2.44 m and it calculates the power absorbed per ton of media, then multiplying it by media load results in the power absorbed in the mill pinion.

For mills with diameter inside liners larger than 3.0 meters, the ball size used influences the mill power, and then the factor S_s is added to Equation 2.7:

$$S_s = 1.102\frac{(B - 12.5D)}{50.8} \qquad 2.8$$

where B is the top ball size in millimeters and D is the mill diameter inside liners in meters.

The effectiveness of Equation 2.7 for predicting the power of the industrial mill was demonstrated by DONDA (2003). In his study, the power measured in three different mills was compared with the power calculated by this equation.

For mills with diameters that are smaller than 2.44 m, Rowland made an adjustment in Equation 2.7 as a function of the load rest angle:

$$kW_b = 6.3D^{0.3}sen\left(51 - 22\left(\frac{2.44 - D}{2.44}\right)\right)(3.2 - 3J_b)\varphi_c\left[1 - \frac{0.1}{2^{(9-10\varphi_c)}}\right] \qquad 2.9$$

One simple model described by KING (2001) to establish the essential features of a model for mill power is illustrated in the picture of the mill load shown in Figure 2.4.

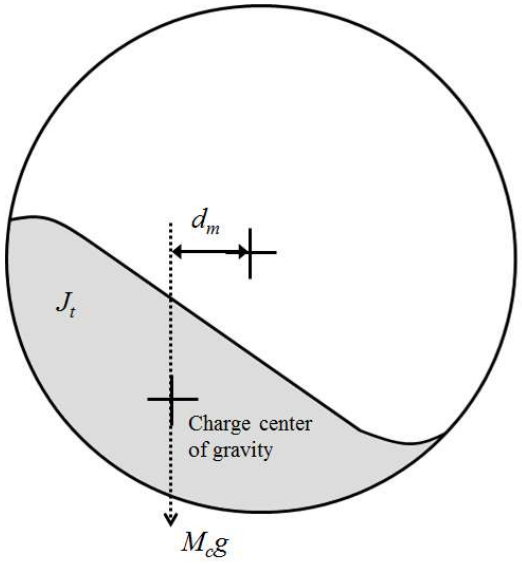

Figure 2.4: Simplified calculation of the torque required to turn a mill (adapted from KING, 2001)

The torque required to turn the mill is given by:

$$T = M_c g d_m + T_f \qquad 2.10$$

where M_c is the total mass charge in the mill and T_f is the torque required to overcome friction.

The mill power can be calculated by:

$$P = 2\pi NT \qquad 2.11$$

N is the mill rotation speed.

According to KING (2001) the mill rotation speed influences the power draft through two effects: the value of N and the shift in the center of gravity with speed. The center of gravity first starts to shift to the left, as the rotation speed increases the critical speed is reached and the center of gravity moves towards the center of the mill while more and more of the material is held against the shell throughout the cycle. Since critical speed (N_c) is larger at smaller radii, the centrifuging layer gets thicker and thicker as the speed increases until the entire charge is centrifuging and the net power draw is zero.

The effect of mill charge is primarily through the shifting of the center of gravity and the charge mass. As the charge increases the center of gravity moves inward.

Considering those influences, a simple equation for calculating net power (kW) draft is:

$$P_{net} = 2\varphi_c D^{2.5} L K_L \qquad 2.12$$

K_L is the loading factor which can be obtained from Figure 2.5 for the popular mill types.

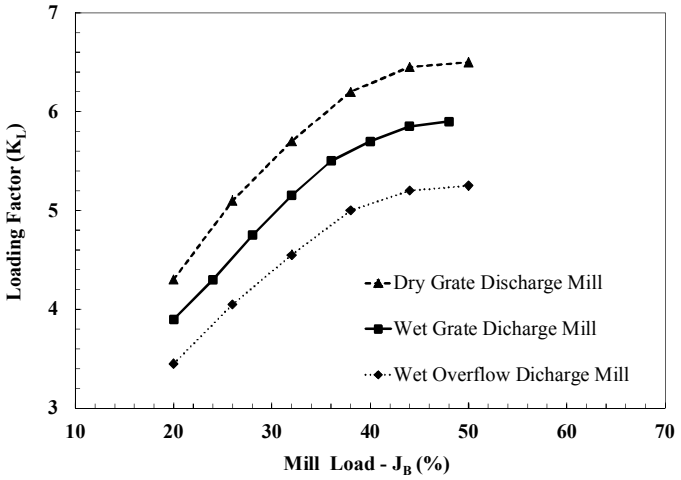

Figure 2.5: Effect of mill filling on power draft for ball mills (adapted from KING, 2001)

KING (2001) also commented that more reliable models for the prediction of the power drawn by ball, semi-autogenous (SAG) and fully autogenous (AG) mills have been developed by MORRELL (1996) and by AUSTIN (1990). The relationship between gross power and net power is given by:

Gross power = No-load power + Net power drawn by the charge

The net power (in Watts) is calculated from:

$$P_{net} = kD^{2.5} L_e \rho_c \theta \xi \qquad 2.13$$

where D is the diameter inside the mill liners, L_e is the effective length of the mill including the conical ends, ρ_c is the charge specific gravity, ξ and θ are factors that account for the fractional filling and the rotation speed, respectively. k is a calibration constant that varies with the discharge type. For overflow mills k = 7.98 and for grate mills k = 9.10. This difference is ascribed to the presence of a pool of slurry that is present on the bottom of overflow-discharge mills but which is not present to the same

extent in grate-discharge mills. This pool is situated more or less symmetrically with respect to the axis of the mill and therefore does not draw significant power. Austin recommends k = 10.6 for overflow semi-autogenous mills, however a value of k = 9.32 gives a better fit between Austin's formula and Morrell's data and this value is recommended (KING, 2001).

The no-load power accounts for all frictional and mechanical losses in the drive system of the mill and can be calculated (in kW) from MORRELL (1996):

$$P_{\text{no-load}} = 1.68 D^{2.05} \left[\varphi_c \left(0.667 L_d + L \right) \right]^{0.82} \qquad 2.14$$

L_d is the mean length of the conical ends and is calculated as half the difference between the centerline length of the mill and the length of the cylindrical section:

$$L_d = \frac{L_c - L}{2} \qquad 2.15$$

The geometry of a mill with conical ends is shown in Figure 2.6. All dimensions are inside liners. L_c = centerline length, L = belly length, D = mill diameter, D_t = trunnion diameter.

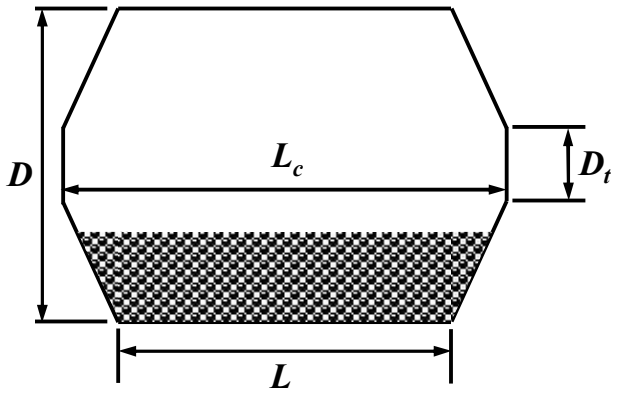

Figure 2.6: Mill geometry with cylindrical ends (adapted from KING, 2001)

The total volume inside the mill is given by:

$$V_m = \frac{\pi}{4} D^2 L + \frac{2(L_c - L)}{L} \frac{1-(D_t/D)^3}{1-D_t/D} \tag{2.16}$$

The charge density must account for all of the material in the mill including the media which may be steel balls in a ball mill, or large lumps of ore in an autogenous mill or a mixture in a semi-autogenous mill, as well as the slurry that makes up the operating charge. Let J_t be the fraction of the mill volume that is occupied by the total charge (media and material), J_b the fraction of the mill volume that is occupied by steel balls and ε the voidage of the balls and media. U is the fraction of the voidage that is filled by slurry and ϕ_v is the volume fraction of solids in the slurry. Let V_B be the volume of steel balls in the mill, V_{Med} be the volume of autogenous media and V_S the volume of slurry.

$$\begin{aligned} V_B &= J_b(1-\varepsilon)V_m \\ V_S &= J_t U \varepsilon V_m \\ V_{Med} &= (J_t - J_b)(1-\varepsilon)V_m \end{aligned} \tag{2.17}$$

The charge density is calculated from:

$$\rho_c = \frac{V_B\rho_b + V_{Med}\rho_m + V_S(1-\phi_v)1000 + V_S\phi_v\rho_s}{J_t} \tag{2.18}$$

where ρ_b is the balls density and ρ_m is the media density and ρ_s is the slurry density.

The effective mill length in Equation 2.13 is dependent on the load and can be calculated by different functions:

$$L_e = L(1+f_3) \tag{2.19}$$

According to Morrell:

$$f_3 = 2.28 J_t(1-J_t)\frac{L_d}{L} \tag{2.20}$$

According to Austin:

$$f_3 = \frac{0.092}{J_t(1-1.03J_t)} \frac{L_d}{L\left(1-\frac{D_t}{D}\right)} \left[\left(\frac{0.625}{0.5-J_t}\right)^{0.1} - \left(\frac{0.625}{0.5-J_t}\right)^{-4.0} \right] \tag{2.21}$$

The functions ξ and θ account for the effects of mill filling and rotation speed, respectively. However each of these factors is a function of both mill filling and rotation speed. Austin recommends the following formulas for those factors:

$$\xi = J_t(1-1.03J_t) \text{ and } \theta = \varphi_c\left[1-\frac{0.1}{2^{(9-10\varphi_c)}}\right] \qquad 2.22$$

Morrell recommends those below:

$$\xi = \frac{J_t(\omega - J_t)}{\omega^2} \text{ where } \omega = 2(2.986\varphi_c - 2.213\varphi^2 - 0.4927)$$
$$\theta = \varphi_c\left[1-(1-\varphi_{max})\exp(-19.42\varphi_{max}+19.42\varphi_c)\right] \text{ where } \varphi_{max} = 0.954 - 0.135J_t \qquad 2.23$$

The formulas proposed by Austin and Morrell give essentially the same estimates of the net power that is drawn by the mill (KING, 2001).

The power equations described previously do not explicitly describe the influence of slurry level on power draw and the relationship between slurry level, slurry flow and pulp lifter design and, according to MORRELL (2014), the slurry level in AG/SAG and ball mills has influence on their power draw, which in some instances can be profound.

Most tumbling mill power draw models (BOND, 1962, HOGG and FUERSTENAU, 1972, AUSTIN, 1990) that have been developed over the last 70 years or so used the charge shape shown in Figure 2.4 in which it was assumed that all particles moved with the same rotational rate and that the slurry phase was not explicitly considered (MORRELL, 2014). Morrell's earlier model (MORRELL, 1993) used a different media charge shape to that in Figure 2.4 and was configured to consider the cases where slurry was contained within the grinding charge as in a typical grate discharge AG/SAG mill (Figure 2.7 a) or where it additionally formed a large slurry pool as occurs in all overflow ball mills (Figure 2.7 b). However, from experience gained with single stage AG/SAG mills it became clear that even grate discharge mills can accumulate slurry at the toe of the charge and this can considerably affect power draw depending on the extent of the slurry pool (MORRELL, 1989, MORRELL and KOJOVIC, 1996). Hence it can be concluded that the extent of the slurry phase can have a significant impact on power draw and therefore should be explicitly described if a model is to be as accurate as possible. Based on this assumption, Citic SMCC Process Technology Pty Ltd (Citic SMCC) has developed a model, from Morrell's earlier published work, that incorporates the slurry phase, considering those influences, described previously, in mill power draw.

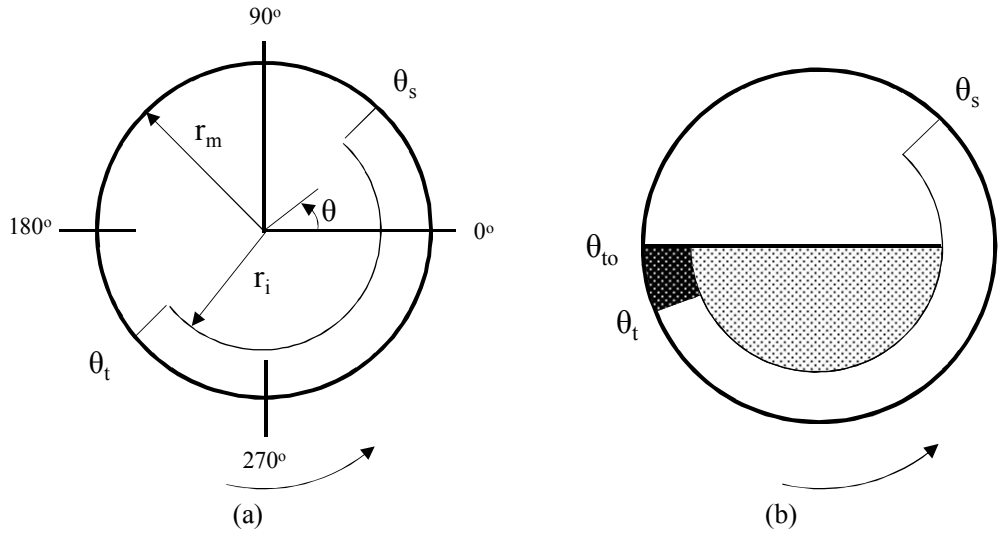

Figure 2.7: Simplified charge shape for grate mills - no slurry pool (a) and simplified charge shape for overflow mills (b) (adapted from MORRELL, 2014)

In order to handle the slurry phase, the Citic SMCC approach adopted to predict its power draw separately to the grinding media phase (balls/rocks) and then to add the powers of each phase to obtain the total power draw. Based on the energy balance, where power is taken to be the rate at which potential and kinetic energy is imparted to the charge, Equation 2.24 was developed for the cylindrical section of the mill. For mills that have conical end-sections, the contribution of the conical ends to the power have to be included using the same approach that Morrell adopted in his original model (MORRELL, 1993):

$$P = kL\int_{r_i}^{r_m}(V_r((rg\rho_m(\sin\theta_s - \sin\theta_{tm}) + V_r^2) + (rg\rho_s(\sin\theta_s - \sin\theta_{tp}) + V_r^2)))dr \qquad 2.24$$

where, P is the power drawn by the charge (net) and excludes all mechanical and electrical losses, k the calibration constant, L the length of cylindrical section of the mill inside liners, r the radial position, r_i the radial position of charge inner surface, r_m the radius of mill inside liners, V_r the tangential velocity of a particle at radial distance r, θ_s the angular displacement of shoulder position at the mill shell, θ_t the angular displacement of toe position at the mill shell, θ_{tm} the angular displacement of the grinding media (rocks and balls) toe position at the mill shell, θ_{tp} the angular displacement of the pulp (slurry) toe position at the mill shell (for overflow ball mills $\theta_{tp} = \theta_{to}$), ρ_m the density of rock/ball charge (excluding pulp), ρ_s the density of pulp phase.

In full scale plants the only power draw that is usually measured is the metered power, i.e. motor input power. Then, in order to validate the model through comparison of measured and predicted values, the power model must also predict motor input power. To do so the Citic SMCC model is configured considering the same relationship between gross power and net power used by MORRELL (1996a, 1996b) and AUSTIN (1990). The proposed model should be applicable to all tumbling mills.

Motor input power = No-load power + Net power

where net power is given by Equation 2.24 and the semi-empirical no-load power equation form proposed by MORRELL (1996a) is used for this purpose, though it has been modified slightly on the basis of additional data:

$$P_{\text{no-load}} = k\left[D^{2.5}\varphi_c\left(0.667L_d + L\right)\right]^{0.82} \qquad 2.25$$

where k = 2.13 for gear and pinion drives and 1.28 for gearless drives, D the mill diameter, L the length of cylindrical section, L_d the length of cone end, φ_c the fraction of critical speed.

However, to apply the model it is necessary to also have relationships which predict values for parameters such as θ_s, θ_{tm}, θ_{tp}, V_r, ρ_s, ρ_m and r_i. All of these relationships, with the exception of θ_{tp}, are provided by MORRELL (1993, 1996a, 1996b). According to MORRELL (2014), in the vast majority of situations mills are operated in a "normal" regime, e.g. the AG/SAG mill does not have a slurry pool or the ball mill slurry flowrate is the result of a recycle load which is not excessive. In such cases good predictive results can be obtained by setting θ_{tp} to the same value as θ_{tm} for AG/SAG mills (this is equivalent to assuming all the interstices are just filled with slurry), and for overflow ball mills a fixed value of θ_{to} can be used as proposed by MORRELL (1993).

For various reasons, there are situations where mills operate under unusual conditions and as a result their power response is atypical. In the case of overflow mills, they can be considered as a special case of a grate discharge mill in which the grates have no holes (or all of the holes are blocked) and slurry builds up until it overflows out of the discharge trunnion. At this point θ_{tp} is referred to as the slurry overflow angle θ_{to}. According to MORRELL (2014), from a power draw modeling viewpoint the position of the slurry pool, as measured by the toe angle θ_{to}, can be calculated theoretically from a knowledge of the trunnion diameter, mill diameter and slurry level within the mill.

The slurry level will vary with flow of slurry into and out of the mill (higher level resulting from a higher flow) and it can be estimated by making the simplifying assumption that the discharge trunnion behaves like a rectangular section, broad crested weir as shown in Figure 2.8.

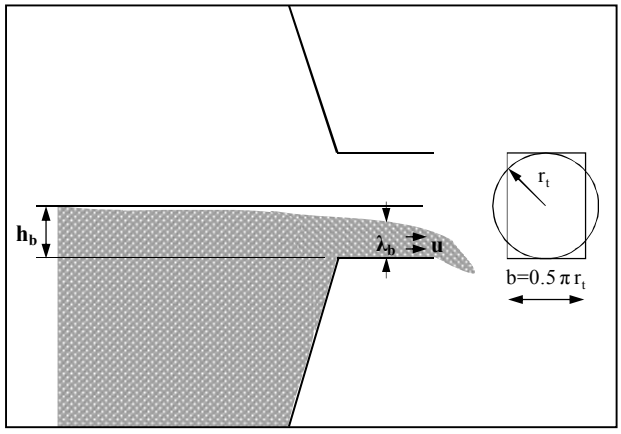

Figure 2.8: Schematic of an overflow discharge (adapted from MORRELL, 2014)

Through Figure 2.9, θ_{to} can be calculated:

$$\theta_{to} = \arcsin\left(\frac{r_t - h_b}{r_m}\right) + \pi \qquad 2.26$$

where r_t is the trunnion radius and h_b is given by:

$$h_b = 0.67\left(\frac{2Q}{\pi r_t g^{0.5}}\right)^{2/3} \qquad 2.27$$

In order to calculate h_b, the Bernoulli equation was applied to such a weir of width b, and then the velocity (u) and the volumetric discharge rate (Q) at the end of the weir can be obtained by:

$$Q = b\lambda_b(2g)^{0.5}(h_b - \lambda_b)^{0.5} \qquad 2.28$$

For maximum discharge rate, h_b is constant and by differentiating $dQ/d\lambda_b = 0$, one obtains $\lambda_b = 0.67h_b$ and setting $b = \pi r_t / 2$ (to maintain the same cross-sectional area and maximum vertical height as the mill discharge trunnion), Q_{max} is obtained:

$$Q_{\max} = 0.5\pi r_t g^{0.5}(0.67h_b)^{1.5} \qquad 2.29$$

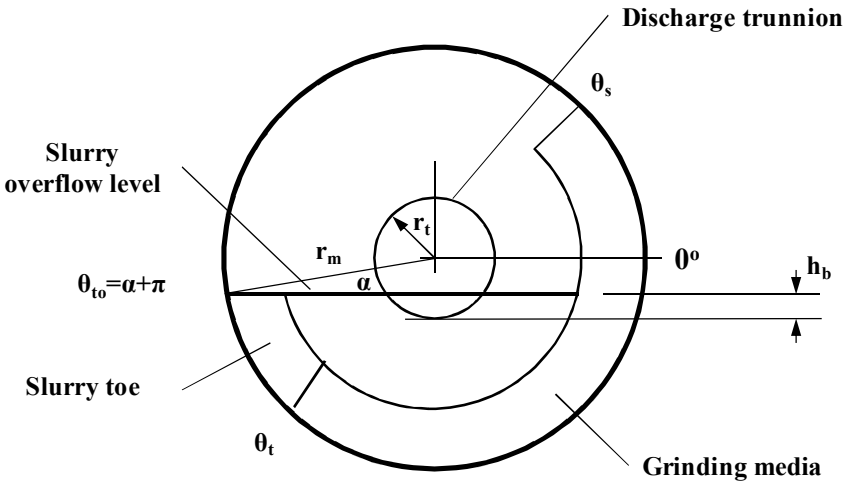

Figure 2.9: Estimation of θ_{to} (adapted from MORRELL, 2014)

Considering that these equations are theoretical and relate to inviscid flow and in practice the slurries are far from inviscid in behavior, a multiplier of the order of 2 is applied to Equation 2.27 in order to reflect slurry behavior.

To conclude, the Citic SMCC model utilizes equations which initially predict the volume of the slurry phase then uses this information to predict its position and motion in relation to the grinding media phase. According to this model, the magnitude of the slurry phase is dictated by the design of the discharge system, the volume of grinding media and the slurry flowrate. The model has been tested using a large volume of operational data and has been demonstrated to provide very accurate results (MORRELL, 2014).

2.2.2 An Energy-Size Reduction Equation Applied to Iron Ore

DONDA (2003) obtained good results using the Equation 2.9 to predict the power in a laboratory mill (0.3048 x 0.3048 m). Through this equation, he developed a method that is based on the use of a laboratory mill, applicable to iron ore from Quadrilátero Ferrífero in Brazil, which allows predicting the specific energy consumption in an industrial ball mill. The method consists in:

- The ore is ground in a batch ball mill during four different times of grinding in standardized operational conditions;

- The particle size analysis of the product from each grinding time, as well as of the feed, is measured;
- With the value of the ball load (in tons), the power of the lab mill is calculated using Equation 2.9;
- Finally, the specific energy consumption (kWh/ton) is obtained by the multiplication of the mill power by the grinding time and divided by the mass load into the mill.

The results are plotted in a graph as percent retained in a desired mesh versus specific energy. From this graph, the energy required to attain a desired product is obtained and compared to the industrial mill specific energy recorded during the processing of the same ore tested in the lab tests. From the example shown in Figure 2.10, in order to obtain a product with 8% retained in 0.149 mm, the specific energy required would be approximately 4.5 kWh/ton.

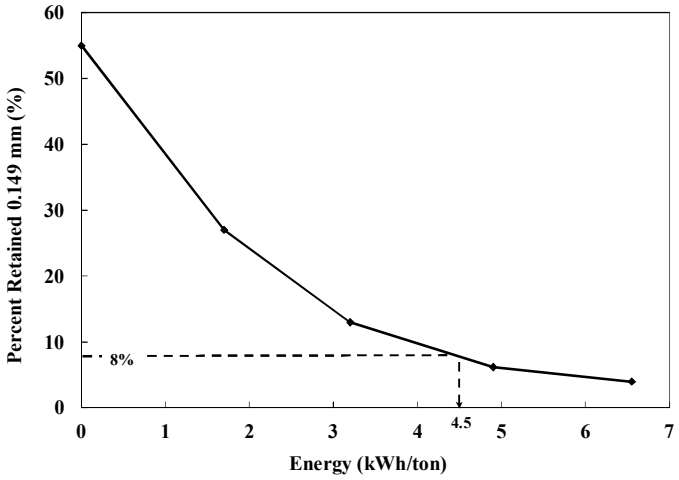

Figure 2.10: Percent retained in 0.149 mm as a function of specific energy obtained from different grinding times (adapted from DONDA, 2003)

For many years, data on the specific energy of Samarco's industrial mills in operation were collected and compared to those obtained from the batch lab tests, demonstrating the effectiveness of the methodology (DONDA, 2003). The values of ratio between the specific energy of the industrial mill and that of the lab mill were lower than 1.1.

This method was tested in three different grinding circuits, each with a different duty. In the case of the secondary grinding circuit, some modifications in the operational

conditions of the lab trial and mill dimensions (0.22 x 0.32 meters), besides a new calibration of the method, were necessary.

In order to demonstrate the validity of the proposed standard conditions adopted in the lab tests for the secondary circuit, the main variables that can affect the test have been studied. The media size distribution, the media shape, the mill liner and the test procedure were fixed and the variables: mill diameter, fraction of critical speed, ratio of slurry volume and void volume (V_s/V_{void}), the ball filling fraction, and the percentage of solids were studied using factorial experiments. The output variables were surface area (Blaine – cm^2/g) and percent passing in 0.044 mm. Based on the factorial design results, the lab test conditions were standardized and, once again, the specific energy of the industrial mills from Samarco was used to compare to the specific energy obtained in the laboratory tests. The relation between both remained below 1.11. In this case, the lab specific energy is obtained from the curve percent retained in 0.044 mm and Blaine as function of specific energy.

The methodology described above is valid for wet overflow mills operating in closed circuit (direct or reverse), mill diameters between 2.44 and 5.49 m, ball as grinding media, iron ore from Quadrilátero Ferrífero and the feed top size below 2 mm for lab tests.

In 2014, DONDA and ROSA stated that: "The specific energy in the ball mill pinion, necessary to promote the size reduction of the iron ore located in Quadrilátero Ferrífero, can be determined by the relationship":

$$E = \frac{1}{K_D} \ln \frac{R_f}{R_p} \qquad 2.30$$

where E is the specific energy of tumbling mills, K_D is a parameter determined from Donda's grindability tests for primary grinding or regrinding (DONDA, 2003), R_f is the percentage retained on the desired mesh of the feed and R_p is the percentage retained on the desired mesh of the product.

Based on the methodology described previously the curve obtained through the relationship between the percent retained in the desired mesh and the specific energy (as exemplified in Figure 2.11) could be described by the exponential equation:

$$R_p = R_f e^{-K_D E} \qquad 2.31$$

where K_D is expressed in ton/kWh and is dependent on grinding conditions.

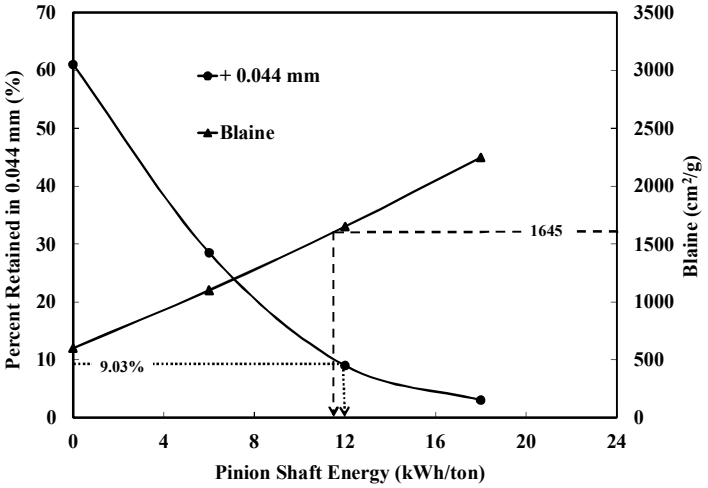

Figure 2.11: Percent retained in 0.044 mm and Blaine as function of specific energy (adapted from DONDA, 2003)

The same validations have been carried out to prove the effectiveness of Equation 2.31 in predicting the industrial mill performance. DONDA and ROSA (2014) compared the K_D obtained in laboratory trials with those from the industrial ball mills. The relation $K_{D\ industrial}/K_{D\ laboratory}$ was lower than 1.1.

The effect of some variables that may affect the K_D value in laboratory and in industrial grinding was also investigated.

According to DONDA and ROSA (2014) the relationship between the batch grinding time and the percentage retained in a specific size, also with exponential behavior, is the specific breakage rate, with a K_D value for each size, normally applied in the mill feed and mill discharge and for so many years incorporated into the population balance model. The authors' finding is that: the relationship represented by Equation 2.31, considering the specific energy, can be applied in the feed and product of the grinding circuit, for iron ore from Quadrilátero Ferrífero, taking as reference for K_D the desired particle size considered into the grinding control.

DONDA (2003) emphasized that through this approach, a grinding circuit in operation in Samarco's plant was improved and another grinding circuit was designed.

In summary, the three comminution theories described above propose relationships between energy and particle size. According to HUKKI (1962, 1975) the probability of breakage in comminution is high for coarse particles and rapidly diminishes for fine sizes. He shows that Kick's law is reasonably accurate in the crushing range above about 1 cm in particle size; Rittinger's law applies fairly well in the fine grinding range of 10-1000 μm and Bond's theory applies reasonably in the range of conventional rod-mill and ball-mill grinding. In fact, despite of its simple implementation and its extensive use, the Bond approach shows a major deficiency when it is applied to autogenous and semi-autogenous mills. The method is based on correlating the specific energy required to change a coarse feed into a finer product in which these materials exhibit a particle size following the Rosin-Rammler distribution. Any feed size distribution that does not follow these characteristics may provide inaccurate results (AUSTIN *et al.*, 1984), characterizing a limitation of the method.

Indeed, work by TAVARES *et al.* (2012) demonstrated that the Bond grindability test and method has important challenges when applied to iron ores from Brazil, in particular owing to the bimodal character of the feed size distribution. Others researchers also demonstrated limitations of the Bond's method (AUSTIN and TANGSATHITKULCHAI, 1987; LO and HERBST, 1986). Further, the Bond method has very limited applicability in optimizing ball mills (AUSTIN *et al.*, 1984, HERBST and FUERSTENAU, 1980).

In the same manner, Donda's methodology has several similarities to Bond's approach and also can be characterized as an empirical energy-size reduction equation, likewise, the breakage kinetics, transport through the mill and classification sub processes have been characterized by a single parameter, the variable K_D. As such, this methodology is not, a priori, useful for circuit optimization.

2.3 Population Balance Model Approach

Considering the limitations of mathematical models developed based on empirical energy-size reduction relationships, some researchers sought new ideas to describe the complex mechanisms involved in the comminution processes. One of these new ideas came up with AUSTIN and GARDNER (1962), followed by REID (1965), where the concepts of first-order breakage kinetics to steady-state continuous grinding in a fully mixed mill were extended. The grinding mill was described as a perfect mixer reactor which is "reacting" large particles to smaller particles, in such a way that the particles feeding the mill would be the reagent and the ground materials the product. However, to apply this idea in practice, a model that took into account the process on populations of particles needed to be developed. In this context, the population balance model (PBM) used as a tool to solve problems of chemical engineering started to be used to describe the grinding process.

Several studies have been carried out in the development of detailed phenomenological grinding models derived from population balance considerations (HERBST and FUERSTENAU, 1968; HERBST *et al.*, 1973, HERBST and FUERSTENAU, 1973, HERBST *et al.*, 1977; AUSTIN *et al*., 1984). In these models the explicit accounting of grinding sub processes (size reduction kinetics, material transport in the mill and size classification) gives them significant advantage over the simpler energy size reduction equations. This type of model, in its complete form, is capable of describing the size distribution in tumbling mill grinding as a function of time in batch grinding or steady state mill discharge in continuous mills, since it takes into account the breakage mechanisms that occur inside the size reduction machine. As such, according to this methodology the plant scale mill can be optimized via laboratory scale grinding mill tests. Thus the PBM became a very useful tool for both the design for tumbling mills and for process optimization.

The breakage process is characterized by two physically interpretable quantities: a selection or breakage rate function, which gives the fractional rate of particles broken in each size interval, and the breakage function or the breakage distribution function, which gives the average size distribution of daughter fragments resulting from primary breakage events. By suitably defining the dependence of these two functions on mill design and operating conditions, the behavior of each size fraction in the mill can be represented mathematically for industrial grinding conditions (HERBST and

FUERSTENAU, 1980). For these reasons, the more detailed models allow, in principle, to reduce the risk associated with traditional mill scale-up design methods (HERBST *et al.*, 1983).

Some investigators followed different lines of thought in their comminution models based on the population balance model. Two well-known approaches of ball mill scale-up were proposed by HERBST and FUERSTENAU (1980) and AUSTIN *et al.* (1984). The authors have attempted to develop a relationship that accurately predicts the value of parameters in functions that are part of the population balance model as a function of mill design and operating variables. HERBST and FUERSTENAU (1980) proposed a scale-up procedure in which the specific breakage rate varies with the specific power input to the mill, whereas, at first, AUSTIN (1973) proposed correlating the selection and breakage functions with mill diameter. In a second approach, AUSTIN *et al.* (1984) proposed empirical expressions to account for the effect of design and operating variables on the specific breakage rates. As such, the breakage distribution function in both methodologies is considered mostly material-dependent whereas the breakage rate function is influenced by both material and operational conditions.

2.3.1 Model Framework for Ball Mills

The phenomenological model chosen by HERBST and FUERSTENAU (1968) to represent tumbling mill behavior is a deterministic model (as opposed to a stochastic) which is formulated in terms of a continuous time variable and a discretized size variable, since the size-discretized form is especially convenient for application to experimental data. Then the development of the PBM considering this approach is briefly described.

Consider a material mass in a ball mill to be divided into n narrow size intervals with maximum size x_1 and minimum size x_{n+1}.The ith size interval, bound by x_i above and x_{i+1} below, contains a mass fraction of material $m_i(t)$ at time t. A differential mass balance for ith size interval yields the kinetic model:

$$\frac{d\left[H\, m_i(t)\right]}{dt} = -S_i(t) H\, \mathrm{m_i}(t) + \sum_{j=1}^{\mathrm{i\text{-}1}} \mathrm{b_{ij}} S_j(t) H\, \mathrm{m_j}(t) \qquad 2.32$$

where: $m_i(t)$ is the mass fraction of the material in the ith size interval at any time t, H is the total mass of material to be ground, also known as hold-up, $S_i(t)$ is the size

discretized selection function for each *i*th size interval that denotes the fractional rate at which material is broken out of the *i*th size interval, b_{ij} is the size discretized breakage distribution function that represents the fraction of primary breakage fragments of material from the *j*th size interval which appear in the *i*th size interval (HERBST and FUERSTENAU, 1980).

The following assumptions are associated with the development of Equation 2.32 (HERBST, 1971, KIM, 1974):

- The size interval *i* is sufficiently narrow to ensure that the behavior of all particles in the interval can be described by the interval average parameters $S_i(t)$ and b_{ij};
- The size discretized breakage distribution functions do not depend on the size consist in the mill, i.e., $b_{ij} \neq b_{ij}$ (H, $m_i(t)$, i=1, 2,..., n);
- Agglomeration of particles is non-existent and attrition is negligible.

The distinct advantage of Equation 2.32 is that the parameters $S_i(t)$ and b_{ij} can be obtained directly from single size fraction experimental data using simple graphical procedures (HERBST and FUERSTENAU, 1968, AUSTIN and LUCKIE, 1971, 1972). Further, when the selection functions are environment and time independent, Equation 2.32 is linear with constant coefficients and admits an analytical solution for batch grinding (HERBST and FUERSTENAU, 1968, 1980). Estimation of both the selection and breakage function parameters of a linear model is made possible by a combination of an efficient modified Gauss-Newton non-linear regression routine and a reduced parameter set obtained from flexible functional forms for selection and breakage functions (HERBST *et al.*, 1977). The extension of this model to the description of continuous grinding using residence time distribution information is straightforward for the linear case.

Since population balance models are phenomenological in nature, various attempts have been made to correlate kinetic parameters to mill dimensions, mill speed, ball load, ball density, ball diameter, and hold-up mass of material. According to findings first reported by HERBST and FUERSTENAU (1973), the S_i is, to a good approximation, proportional to the specific power input to the mill (P/H):

$$S_i = S_i^E(P/H) \text{ or } S_i^E(ton/kWh) = \frac{S_i(hours^{-1})H(ton)}{P(kW)} \qquad 2.33$$

where S_i^E, termed the specific selection function for the ith size interval, is essentially independent of mill design and operating conditions. In addition the breakage functions b_{ij} has been demonstrated to be to a good approximation, invariant in respect to design and operating variables over a wide range of conditions (SIDDIQUE, 1977). Incorporating these findings into Equation 2.32, yields the energy normalized form of the batch grinding model:

$$\frac{d\left[m_i(\overline{E})\right]}{d\overline{E}} = -S_i^E \, \mathrm{m_i}(\overline{E}) + \sum_{j=1}^{\mathrm{i-1}} \mathrm{b_{ij}} S_j^E \, \mathrm{m_j}(\overline{E}) \qquad 2.34$$

where $\overline{E}$ is the specific energy input to the mill and is equal to the product of specific power, P/H, and grind time, t. The implication of such a formulation is that the evolution of particle size distribution depends only on the specific energy input to the mill. In this sense, Equation 2.34 and its solution represent a detailed energy-size distribution model that has proved to be very useful for scale-up design.

To simplify the task of estimating all of these kinetic parameters (S_i^E and b_{ij}) from experimental data, frequently a log-polynomial of adjustable order is used to represent the size dependence of the specific selection function (HERBST *et al.*, 1977):

$$S_i^E = S_1^E \exp\left(-\sum_j^J \zeta_j \left[\ln\left(\frac{\sqrt{x_i x_{i+1}}}{\sqrt{x_1 x_2}} \right) \right]^j \right) \quad \mathrm{J} = 1, 2, 3 \, \mathrm{etc} \qquad 2.35$$

Where S_1^E is the feed size specific selection function determined from a feed disappearance plot, and ζ_j are adjustable parameters.

To represent the cumulative breakage function, three parameters in functional form are used $\left(B_{ij} = \sum_{k=i}^{n} b_{kj} \right)$:

$$B_{ij} = \alpha_1 \left(x_i / x_{j+1} \right)^{\alpha_2} + \left(1 - \alpha_1\right)\left(x_i / x_{j+1} \right)^{\alpha_3} \qquad 2.36$$

Thus the usual number of parameters required to describe the breakage and selection functions using these functional forms is three for the breakage (α_1, α_2 and α_3) and two or three for the selection function (S_1^E, ζ_1 and ζ_2). Equation 2.36 implies that the

breakage distribution is a function of the ratio of daughter fragment size to parent fragment size only and does not depend on the absolute size of the parent fragment. This assumption, known as normalizability condition, has been confirmed to be valid for many ore types (HERBST *et al.*, 1985).

The normalized form of the model can be extended to continuous grinding. In this case a description of a continuous tumbling mill requires not only a description of the breakage kinetics, but also a mathematical description of material transport through the mill:

$$m_{i,MP} = \int_0^\infty m_{i,BATCH}(t)E(t)dt \qquad 2.37$$

where: the continuous response, $m_{i,MP}$, is considered to be an average of batch responses, $m_{i,BATCH}(t)$, weighted according to the amount of material that resides for various times in the mill, $E(t)dt$.

As briefly mentioned, a mill can be described as a perfect mixer. Consequently the residence time distribution in a mill, $E(t)$, can be represented with a highly flexible mixers-in-series model, i.e.,

$$E(t) = \frac{n^n (t/\tau)^{n-1}}{\tau\,\Gamma(n)} \exp\left(-\frac{nt}{\tau}\right) \qquad 2.38$$

where n is the mixing parameter which gives the equivalent number of equal mixers-in-series and τ is the mean residence time for material in the mill.

According to AUSTIN and CONCHA (1994) to represent the residence time distribution (RTD) in a mill, found by experiments, several models have been proposed, some of which are presented as follows.

A model that has been very successful to represent the RTD function is that one that considered one larger perfect mixer with average time τ_1, followed by two perfect and equal mixers-in-series with average time τ_2. The RTD function for this model is:

$$E(t) = \frac{\tau_1}{(\tau_1 - \tau_2)}\left[\exp(-t/\tau_1) - \exp(-t/\tau_2)\right] - \frac{t}{(\tau_1 - \tau_2)\tau_2}\exp(-t/\tau_2) \qquad 2.39$$

where $\tau = \tau_1 + 2\tau_2$

For n perfect and equal mixers-in-series:

$$E(t) = \frac{1}{\tau'^{n}} \frac{t^{n-1}}{(n-1)!} \exp(-t/\tau') \qquad 2.40$$

For $\tau = n\tau'$; τ' is the mean residence time of each mixer.

For three perfect and different mixers-in-series:

$$E(t) = \frac{\tau_1(\tau_2 - \tau_3)\exp(-t/\tau_1) + \tau_2(\tau_3 - \tau_1)\exp(-t/\tau_2) + \tau_3(\tau_1 - \tau_2)\exp(-t/\tau_3)}{(\tau_1 - \tau_2)(\tau_3 - \tau_1)(\tau_2 - \tau_3)} \qquad 2.41$$

where $\tau = \tau_1 + \tau_2 + \tau_3$

For two perfect and different mixers-in-series:

$$E(t) = \frac{\exp(-t/\tau_1) - \exp(-t/\tau_2)}{(\tau_1 - \tau_2)} \qquad 2.42$$

where $\tau = \tau_1 + \tau_2$

HERBST and FUERSTENAU (1980) briefly described the steps required for the scale-up design:

1. Perform batch grinding experiments in a reference ball mill:

The monosize determination and test conditions (ball load, ball top size, amount of material to be ground, mill speed) need to be set according to requirements of the study. The grinding times should follow a geometric progression, i.e., 0.5, 1, 2, 4, etc., minutes. After each grinding period, the particle size distribution is required and the net mill power should be calculated from a torque measurement.

2. Estimate the feed-size breakage rate function:

From the linear model for batch grinding, the behavior of the top size fraction is predicted to follow the relationship:

$$m_1(t) = m_1(0)\exp(-S_1 t) \qquad 2.43$$

Therefore, a semi-logarithmic plot of $m_1(t)/m_1(0)$ versus grinding time will yield a straight line with negative slope equal to S_1 provided that the breakage kinetics are linear. Experiments with limestone have shown that the linear model accurately describes dry grinding of the feed size material (Figure 2.12).

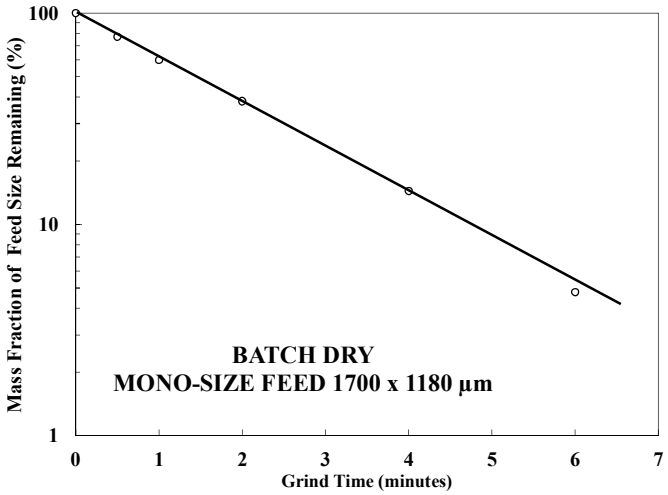

Figure 2.12: Determination of feed size selection function for 1700 x 1180 µm (10 x 14 mesh) feed at 25.4 cm mill (adapted from SIDDIQUE, 1977)

3. Estimate the feed-size breakage distribution function:

It has been shown that the feed-size breakage distribution function can be estimated from linear-linear production rate plots for the material contained in size fractions finer than the feed. Equivalently, the cumulative breakage distribution function $\left(B_{i1} = \sum_{k=i}^{n} b_{k1} \right)$ can be estimated by plotting the cumulative fraction finer than size x_i versus time, where the zero order production rate constants, F_i, measured at short grind times, is determined from the slope. Then, B_{i1} is calculated according to:

$$B_{i1} = F_i / S_1 \qquad 2.44$$

and the individual breakage distribution function is obtained by difference:

$$b_{i1} = B_{i1} - B_{i+1,1} \qquad 2.45$$

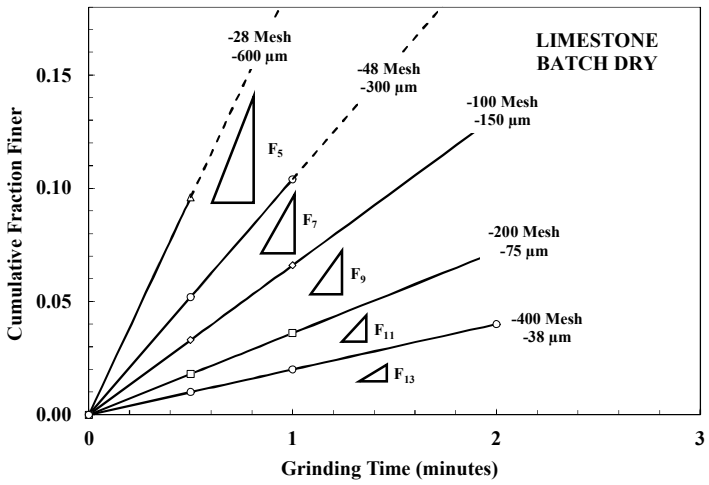

Figure 2.13: Determination of "production rate constants" for the grinding of 2360 x 1700 µm (8 x 10 mesh) limestone at 25.4 cm mill (adapted from HERBST and FUERSTENAU, 1980)

The estimated cumulative breakage distribution function for a limestone sample is shown in Figure 2.14.

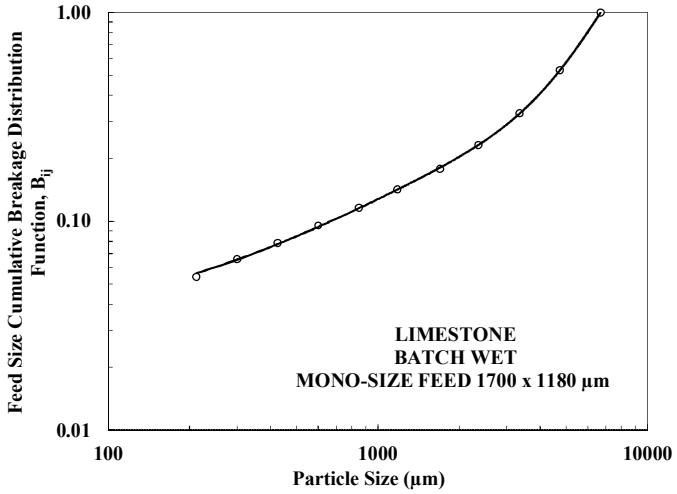

Figure 2.14: Estimated feed size cumulative breakage distribution function for 1700 x 1180 µm (10 x 14 mesh) limestone in 25.4 cm mill (adapted from SIDDIQUE, 1977)

4. Estimate the nonfeed-size kinetic parameters:

In principle, the breakage rate and distribution functions for the other size fractions can be obtained by performing experiments with each size as a feed material. Alternatively,

an estimation scheme based on experimental observations from grinding other materials can be used. First, it is often observed that the breakage distribution functions for homogeneous materials can be normalized with respect to the feed-size material, i.e. for j=2, n; i=j, n

$$B_{ij} = B_{i-j+1,1} \tag{2.46}$$

and therefore all breakage distribution functions can be defined from the estimated feed-size breakage distribution function.

Secondly, it has been observed that the breakage rate function size dependence frequently follows a power-law relationship:

$$S_i = S_1 \left(\frac{\sqrt{x_i x_{i+1}}}{\sqrt{x_1 x_2}} \right)^{\zeta_1} \tag{2.47}$$

with a slope, ζ_1, that is approximately equal to the slope of the cumulative breakage distribution function plot in the fine size range. Thus the nonfeed-size breakage distribution function can be assumed to be given by Equation 2.45, and S_1 and ζ_1 found according to these steps in conjunction with Equation 2.47 provide the initial estimates of S_i (i=2, n) for the batch mill.

5. Calculate the specific breakage rate function:

Initial estimates of this function can be calculated from Equation 2.33, i.e.,

$$S_i^E = \frac{S_i \mathrm{H}}{\mathrm{P}} \tag{2.48}$$

using the initial estimates of S_i from step 4 and P/H as determined from the batch experiments.

In turn, these initial estimates can be improved by using an appropriate nonlinear regression. The Gauss-Newton estimation algorithm referred to earlier (HERBST *et al.*, 1977) can be used to obtain values of S_i^E and ζ_1 (in Equation 2.47) which resulted in the "best fit" (in the sense of least squares) of the linear model to batch data. The initial and final estimates of the specific breakage rate functions for limestone are plotted in Figure 2.15.

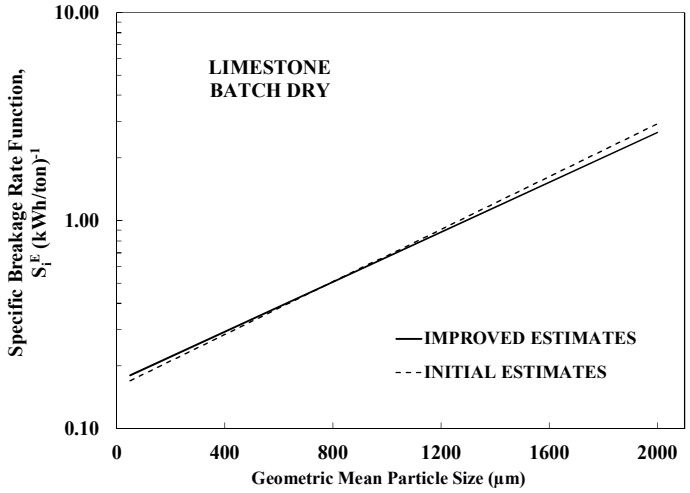

Figure 2.15: Dependence of the initial and improved estimates of the specific breakage rate function on particle size (adapted from HERBST and FUERSTENAU, 1980)

6. Calculate specific energy to satisfy design conditions:

The specific breakage rate and breakage distribution functions, transport model, classifier constants and feed-size distribution are input to a computer program (HERBST *et al.*, 1977) which simulates the grinding circuit behavior. An initial estimate for the specific energy, P/M_{MF} (M_{MF} is the mass flow rate of feed to the mill), is introduced into the program and the corresponding circulating load obtained from the simulation. Since a log-log plot of circulating loads versus specific energy is approximately linear over a wide range of circulating loads (Figure 2.16), the approximate specific energy required to obtain 250% circulating load is easily determined by linear interpolation between the first simulation and another simulation selected such that the 250% circulating load point is bracketed. By repeating this procedure the exact specific energy is quickly obtained.

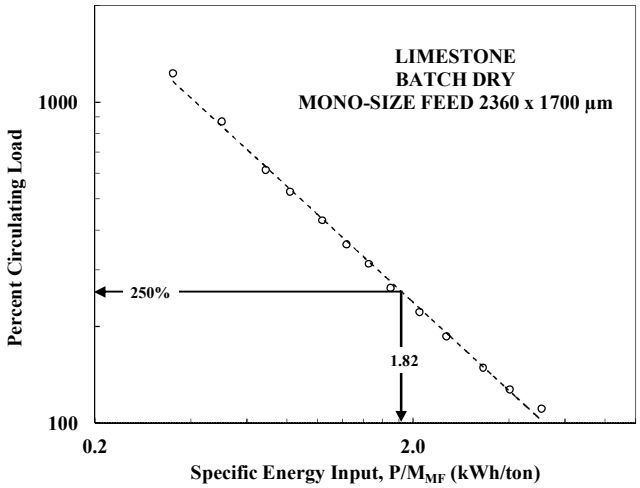

Figure 2.16: Estimation of the specific energy input required to reach a 250% circulating load from simulations of the grinding circuit (adapted from HERBST and FUERSTENAU, 1980)

7. Calculate the mill size from the specific energy:

The scale-up relationship for the breakage rate function, given by Equation 2.33, can be expressed directly in terms of mill dimensions and operating variables by recognizing that the net power draft of a mill can be obtained from an equation of the form (ROSE and SULLIVAN, 1958, BOND, 1962, MORRELL, 1993):

$$P = \phi_1(\varphi_c, J_b, U, Q^*) L D^{(2.5+\gamma)} \qquad 2.49$$

where D is the mill diameter, L is its length and ϕ_1 is function of dimensionless mill speed = φ_c, dimensionless ball load = J_b, dimensionless particle load = U, and dimensionless ball size and lifter geometry variables = Q^*. The parameter γ is zero by dimensional analysis (ROSE and SULLIVAN, 1958) as demonstrated by Equation 2.12 (KING, 2001), but values ranging from -0.1 to +0.1 are generally used in empirical correlations (BOND, 1962, ROWLAND, 1976).

Once the specific energy is known, the mill dimensions can be determined in the usual way. For example: if M_p is 100 ton/h, which means that M_{MF} is 350 ton/h (250% circulating load), then the mill power is calculated from the specific energy obtained by Figure 2.16, therefore 1.82 x 350 or 637 kW. Thus the mill dimension can be calculated from Equation 2.50 written in the form:

$$D = \left[\frac{P}{\phi_1(\varphi_c, J_b, U, Q^*)[L/D]} \right]^{\frac{1}{3.5+\gamma}} \qquad 2.50$$

where L/D is chosen to be the same as the batch mill, $\gamma = 0$ and ϕ_1 can be determined from the power measurement for the batch mill:

$$S_i = S_i^E \left[\frac{P}{H} \right] = S_i^E \frac{\phi_1\left(\varphi_c, J_b, U, Q^*\right) LD^{(2.5+\gamma)}}{H} \qquad 2.51$$

8. Evaluate the sensitivity of mill capacity to deviations from the design assumptions:

Once the mill size and the power requirements have been determined, the effect of deviations from the assumed classifier performance, RTD model (residence time distribution model) and feed-size distribution as well as deviations from the measured kinetic parameters can be readily determined by simulation. The same procedure can be used to optimize an already existing industrial mill.

The computer program named Estimill, used for the computations presented in these steps, was developed by HERBST *et al.* (1977) and it is a Fortran program with the purpose of estimating the required model parameters from experimental data and simulating tumbling mill grinding behavior for a specified set of grinding model parameters.

The program, which is based on a linear-kinetic grinding model, is capable of carrying out simulation and/or parameter estimation for batch grinding and steady state grinding in a continuous mill for several circuit configurations (open circuit, standard and reverse closed circuit). Residence time distribution for continuous mills can take on a variety of forms according to a mixers-in-series model. Circuit simulations are made rapidly and accurately by using analytical rather than numerical solutions. Also the breakage rate and distribution functions from data obtained with an arbitrary feed size distribution can be simultaneously estimated, and then the design procedure described earlier can be simplified by eliminating the need for performing single feed size fraction experiments to determine breakage distribution functions.

According to HERBST and FUERSTENAU (1980), the design procedure mentioned not only yields information on mill and drive size requirements but also complete circuit size distribution. Perhaps most importantly, it provides an opportunity to evaluate the effect of deviations from the design risk associated with a new installation.

The primary motivation for developing an alternative to Bond approach to mill design was the potential improvement in design accuracy achievable by introducing the kinetics of breakage, material transport and size classification behavior - in an explicit manner – into the design equations.

In fact, several investigators have presented convincing cases for the appropriateness of population balance models for use in scale-up design and ball mill optimization (AUSTIN, 1973, SIDDIQUE, 1977, HERBST and FUERSTENAU, 1980, HERBST *at al.*, 1983, 1985, ALVES, 2006, AUSTIN *et al.*, 2007, FARIA *et al.*, 2013, 2014a, 2014b, MAZZINGHY and SCHNEIDER, 2014), however some limitations of this approach should be considered.

In most cases, the results confirmed the validity of the linear population balance model for dry grinding and the specific power correlation previously observed by HERBST and FUERSTENAU (1973). Generally, the breakage function has been found to be invariant over the range of operating variables for different mill sizes and the specific selection functions has been found to be independent of the operating conditions and mill design variables.

On the other hand, unlike dry grinding, wet grinding is inherently nonlinear, so that the spatial distribution of material in the mill plays an important role. Apparently in wet grinding systems the fine particles tend to suspend in the water while the coarse particles are settled in the ball mass resulting in an increased probability of breakage of the coarse particles (HERBST, 1971, KIM, 1974). This phenomenon termed as "preferential breakage" implies that as the grind is extended more and more fine particles are produced resulting in the increased rate of breakage of coarse particles while the rate of breakage of fine particles decreases. It demonstrates that the breakage and specific selection functions generally depend on the size distribution existing within the mill (Figure 2.17) as well as operating conditions.

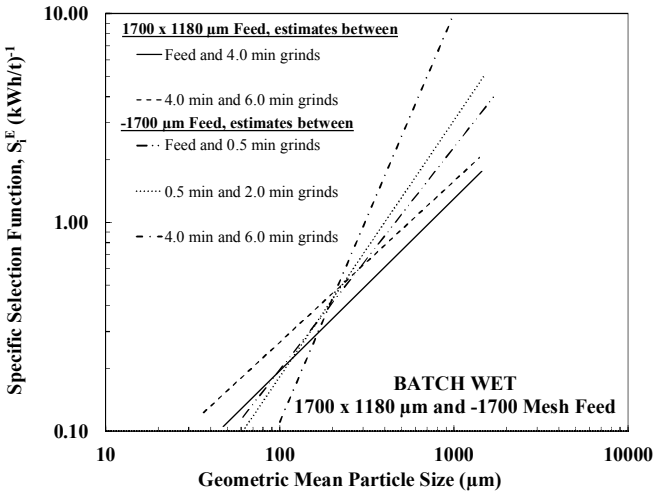

Figure 2.17: Dependence of specific selection functions on the particle size distribution in 25.4 cm ball mill, for 1700 x 1180 µm (10 x 14 mesh) feed and -1700 µm (-10 mesh) feed in wet grinding of limestone (adapted from SIDDIQUE, 1977)

The dependence of specific selection functions on the size consist in the mill generated some problems in the application of the linear population balance model (SIDDIQUE, 1977). Nevertheless, the problem was overcome, to a good approximation, by estimating the specific selection functions based on the so-called "similar fineness of grind procedure" for wet grinding scale-up, which encompassed the product size distribution from the larger mill. This is a type of linearization over product fineness (HERBST and MIKA, 1973), which assumes that, for the same fineness, the breakage and the specific selection functions will be approximately the same in different size mills.

2.3.2 The Influence of Operating and Design Variables on Breakage Rates

Since batch grinding tests in laboratory mill can focus solely on the factors which affect breakage without the complicating effect of mass transfer that occurs in continuous pilot-scale or large-scale mills, batch tests have been a very good tool to examine quantitatively the influence of design and operating variables on breakage rates. A large number of papers has been published showing how ball mills respond to changes in mill speed, mill diameter, configuration of the lifters, ball filling, ball size, powder and slurry filling and solids concentration.

The effect of mill speed and ball load (at constant interstitial filling) on the parameters of the batch grinding model was examined for the dry ball milling of macro-crystalline dolomite by HERBST and FUERSTENAU (1972). Certain generalizations regarding the form of selection and breakage functions have begun to emerge from these studies. The authors assume that for normal operating conditions in a dry batch ball mill, the selection function is to a good approximation independent of the size distribution within the mill. As such, the set of breakage functions is little affected by operating conditions for a given material and mill combination and the breakage function for homogeneous materials is normalizable, that is, it is completely determined by the size ratio of daughter to parent fragments.

From their studies, it was found (Figures 2.18 and 2.19) that the selection function is essentially constant down to less than 5% of the feed remaining and therefore independent of environment for all except for the two slowest speeds of rotation and the largest ball load.

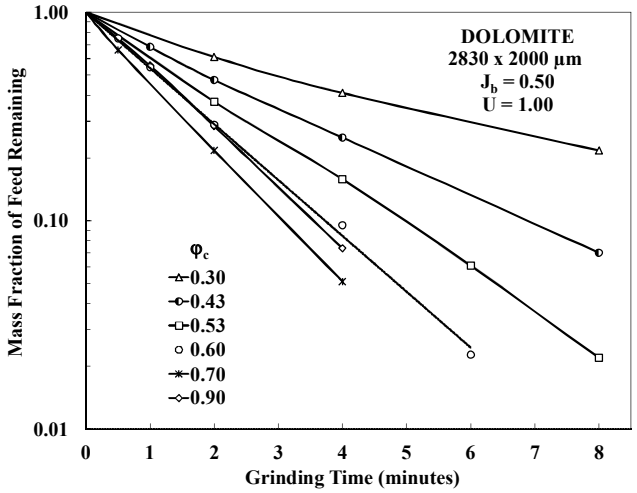

Figure 2.18: Feed disappearance plot for various mill speeds at constant ball load for 2.83 x 2.00 mm (7 x 9 mesh) feed of dolomite (adapted from HERBST and FUERSTENAU, 1972)

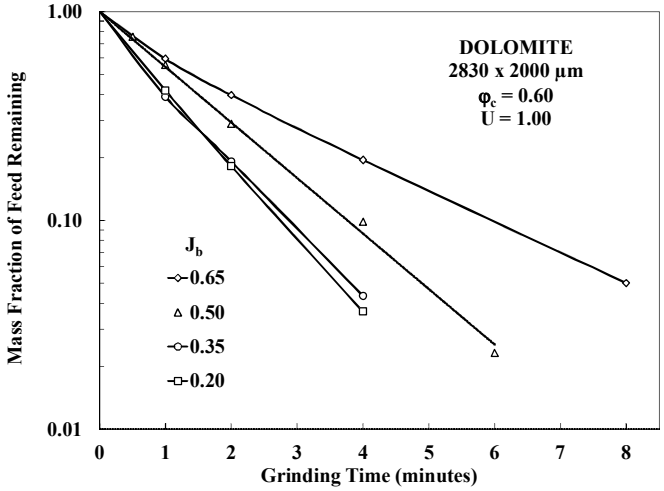

Figure 2.19: Feed disappearance plot for various ball loads at constant speed (adapted from HERBST and FUERSTENAU, 1972)

HERBST and FUERSTENAU (1972) demonstrated that the selection function increases with increasing speed of rotation, attains a maximum at about 80% of the critical speed, and then decreases sharply as the mill speed approaches 100% of the critical speed. These conditions observed experimentally are in accordance with ROSE and SULLIVAN (1958): at slow speeds of rotation, the dynamic configuration of the ball mass changes little with increasing speed, thus the fractional rate of breakage on a per revolution basis would expected to remain essentially constant. At higher speeds, the balls no longer cascade down the surface of the charge, but rather at a certain point are projected into space and thereafter describe approximately parabolic paths before again meeting the ball mass. Apparently under these conditions the reduction in ball-ball contacts results in an increase in the rate of breakage per revolution.

The experimental dependence of the selection function on ball load is shown in Figure 2.20. When the ball load in the mill is small, the selection function is essentially independent of the load; this corresponds to a condition for which a large number of balls are projected into free flight (HERBST and FUERSTENAU, 1972). As the ball load is increased to values in excess of J_b = 0.40, the selection function decreases, presumably as a result of significant ball-ball interactions. These results are in agreement with the findings of AUSTIN *et al.* (1967) for variable ball load, but fixed particle load (U). To make this comparison, it is necessary to account for differences in

interstitial filling of particles. AUSTIN *et al.* (1967) and MIKA *et al.* (1967) considered in their studies the relationship between particle load and the selection function:

$$US_1 = \text{constant for fixed speed and ball load for U} \geq 1.0$$

Austin's work indicates that US_1 increases approximately linearly with ball load for small loads and attains a maximum at $J_b = 0.5$, as observed in Figure 2.20.

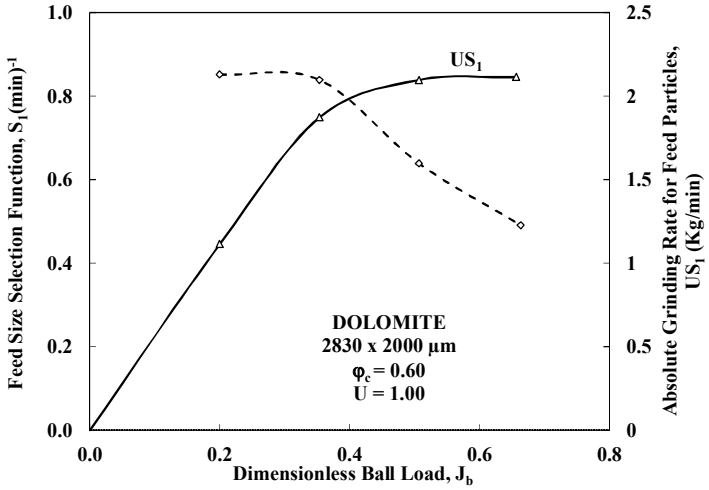

Figure 2.20: Feed size selection function vs. ball load for the batch dry ball milling of dolomite (adapted from HERBST and FUERSTENAU, 1972)

In summary, the results obtained by HERBST and FUERSTENAU (1972) showed that the selection function is independent of environment over a wide range of mill speeds and ball loads (the exceptions occur at very low speeds of rotation and large ball loads); depends strongly on the speed of mill rotation, exhibiting a maximum at approximately 80% of the mill critical speed (with $J_b = 0.5$); and with its mass dependence removed, i.e., US_1, increases linearly with ball load attaining a maximum at $J_b = 0.5$ (with $\varphi_c = 0.6$).

In the case of breakage function, the studies demonstrated that the sets of feed size breakage functions were essentially identical. For higher speeds of rotation the form of the distribution of fine sizes remained unchanged, but the primary breakage product became slightly but progressively coarser. Turning to ball load, the breakage function was found to be independent of the ball load in the mill for the range of loads examined.

The implication is that although the frequency of occurrence of breakage events changes with changes in ball load, the nature of the average stress application event changes very little. This finding is also consistent with the results of AUSTIN *et al.* (1967).

The results presented by SIDDIQUE (1977), in his studies with limestone in batch wet grinding, demonstrated that the breakage and the specific selection functions are independent of mill diameter, ball load and lifter configuration.

The influence of top ball size on breakage and selection functions was studied by HERBST *et al.* (1982). Batch wet tests were performed in a 25.4 cm diameter mill with different monosize fractions and with natural size (as received -1180 µm) of iron ore (magnetite and about 4% of quartz). The percent solids was 76 by weight and the ball filling was 50%. The speed of the mill for all monosize grinding tests was kept at 70% of the critical speed and for natural size feed was 65%. Three different ball sizes (38, 25 and 19 mm) were used in these experiments. It was found that the breakage functions are normalized for all size fractions, except for the 1180 x 850 µm fraction (Figures 2.21 and 2.22).

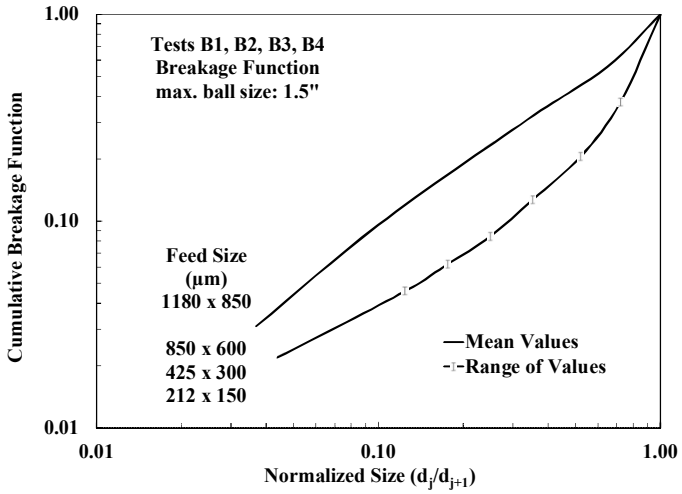

Figure 2.21: Breakage functions for monosize feeds obtained in wet grinding with 38 mm of ball top size (adapted from HERBST *et al.*, 1982)

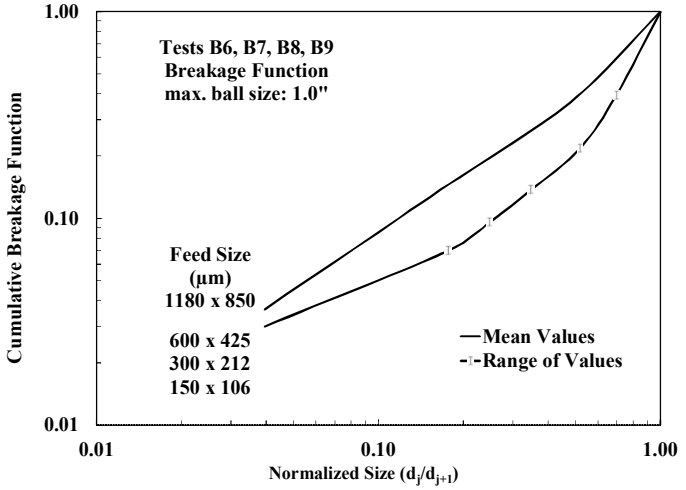

Figure 2.22: Breakage functions for monosize feeds obtained in wet grinding with 25 mm of ball top size (adapted from HERBST *et al.*, 1982)

The studies demonstrated that the specific selection function depends upon the size distribution in the mill as depicted in Figures 2.23 and 2.24. According to the authors, the nonlinearity appears to occur as a result of "preferential breakage" of coarse particles which are classified due to suspension of finer particles in the water and settling of coarse particles onto grinding surfaces in the ball mill. This phenomenon results in an increased probability of breakage of coarse particles and decreased probability of breakage of fine particles (SIDDIQUE, 1977). When the fineness of the product in the mill increases, the top size specific selection functions increase and the very fine size specific functions decrease. It is observed from extrapolated specific selection functions in Figure 2.23, that geometric mean size of about 10 microns (about 14 microns in Figure 2.24) was a pivoting point indicating that particles finer than that size presented higher probability of suspension in water.

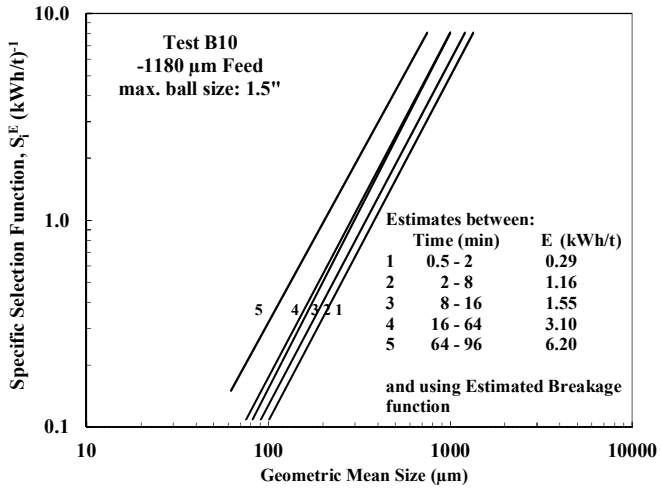

Figure 2.23: Specific selection functions for -1180 µm (-14 mesh) feed in wet grinding with 38 mm balls (adapted from HERBST *et al.*, 1982)

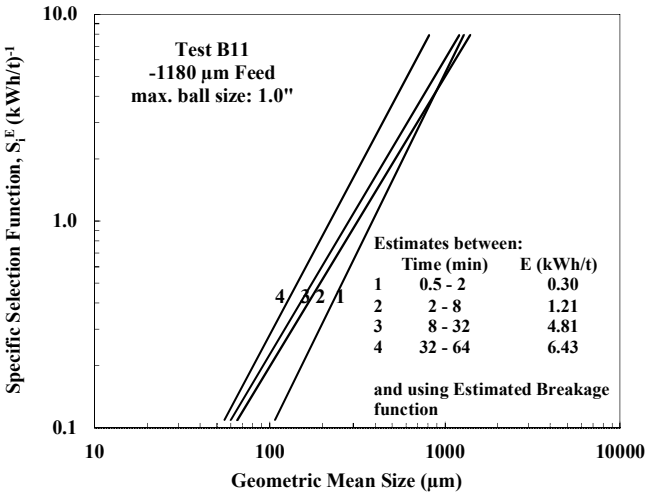

Figure 2.24: Specific selection functions for -1180 µm (-14 mesh) feed in wet grinding with 25 mm balls (adapted from HERBST *et al.*, 1982)

Considering the comparison between the specific selection functions determined for the top ball sizes of 38, 25 and 19 mm using monosize feed, it can be observed in Figure 2.25 that the breakage rates are higher for 25 mm balls than 38 mm balls for finer size fractions (below 450 microns). Thus starting from the same coarser feed the 25 mm balls will produce a finer product than the 38 mm balls.

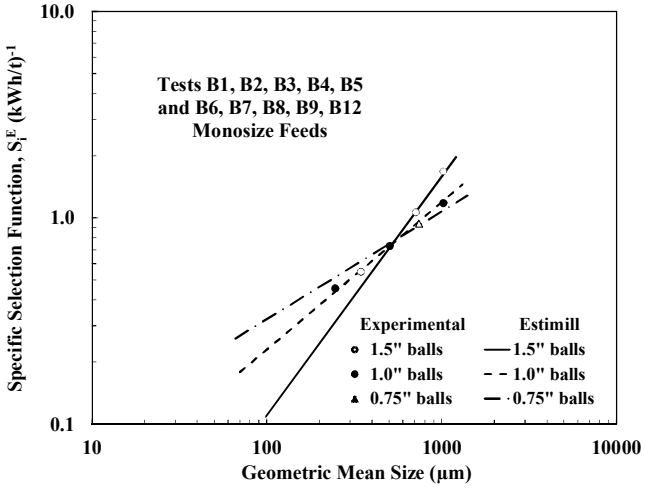

Figure 2.25: A comparison of specific selection functions determined for the top ball sizes of 38, 25 and 19 mm using monosize feeds in wet grinding (adapted from HERBST *et al.*, 1982)

HERBST *et al.* (1983) conducted detailed experimental work by wet and dry grinding of two homogeneous materials, namely limestone (soft) and quartz (hard), and one heterogeneous material, a complex molybdenite ore. They demonstrated that breakage functions for those ores are invariant with the size distribution existing within the mill, but that selection functions vary with the extent of grinding (Figure 2.17 and 2.26).

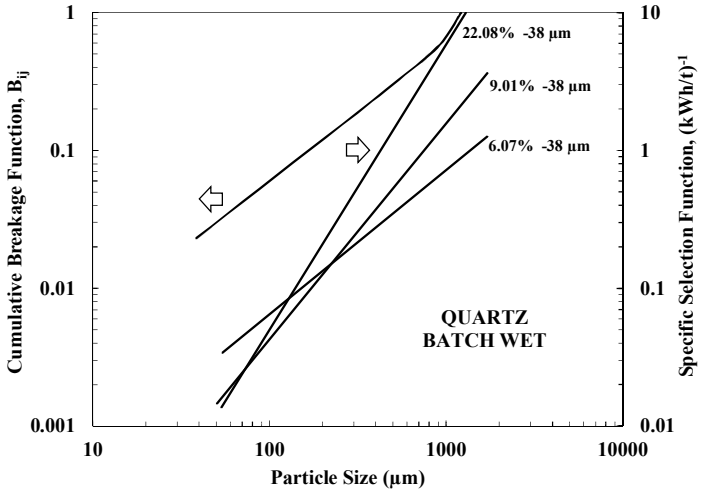

Figure 2.26: Breakage function and dependence of specific selection functions on the particle size distribution (percent -38 µm) in the 25.4 cm mill for wet grinding of quartz (adapted from HERBST *et al.*,1983)

In spite of the known effect of size, shape, and number of lifters in the mill on the ball motion, HERBST *et al.* (1983) demonstrated that the effect of lifter configuration on breakage kinetics can be considered insignificant. In other words, they concluded that different lifter configurations did not affect the energy normalized breakage kinetics significantly. In their investigations, the breakage functions were found to be, to a good approximation, independent of lifter configuration and the specific power relationship for selection functions was found to be valid for each of the configurations (square and ramp lifters were used). This means that configurations that resulted in less lift drew less power but the grinding rate was reduced in the same proportion. This is illustrated in Figure 2.27 where the normalizability of top size disappearance kinetics with specific energy input is shown for both wet and dry grinding. They also conclude that the specific power scale-up relationship, the invariance of breakage functions and the "similar fineness" hypothesis were all found to be applicable for lifter configurations ranging from sharp edge to smooth.

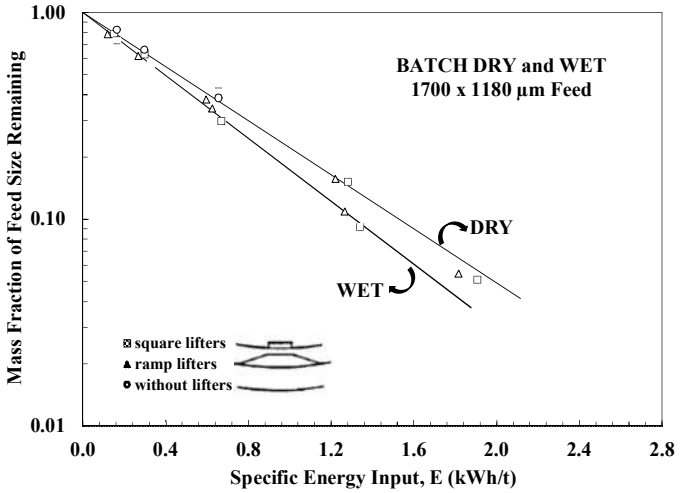

Figure 2.27: Normalized feed size disappearance plot for dry and wet grinding in 25.4 cm mill diameter with square, ramp and without lifters configuration (adapted from SIDDIQUE, 1977)

MARTINOVIC *et al.* (1990) also studied the effect of top ball size on specific selection functions. Batch wet grinding experiments were carried out with plant feed samples of iron ore concentrate prior to pelletizing. The top ball sizes used in the experiments were 38, 25, 22 and 19 mm.

The specific selection function dependence on ball size is shown in Figure 2.28. In the cases examined, it was found that the overall grinding efficiency could be improved by appropriately decreasing the ball sizes. Similar behavior was observed by HERBST *et al.* (1982), where the breakage rates showed to be faster for small balls.

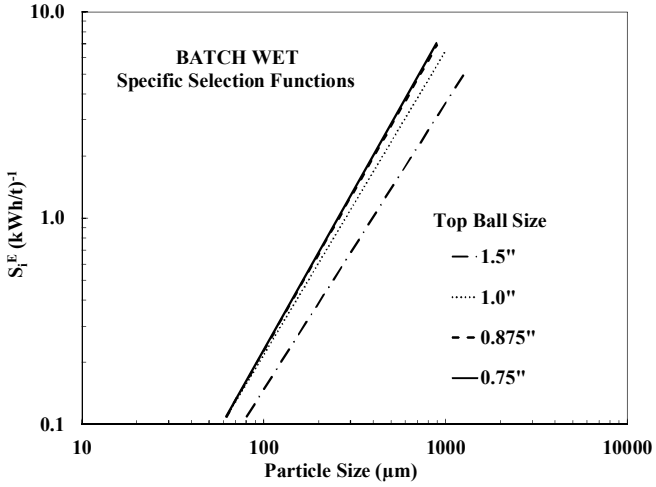

Figure 2.28: Specific selection functions of wet grinding with different top size balls: 38, 25, 22 and 19 mm (adapted from MARTINOVIC *et al.*, 1990)

The influence of solids concentration on specific selection function was also studied by MARTINOVIC *et al.* (1990). In this case the tests were performed with the optimum, 19 mm ball size, previously determined. The specific selection functions estimated for 72%, 77% and 82% solids of slurry are shown in Figure 2.29. The results indicate that the breakage rates are faster for 72% solids than 82% solids for finer size fractions (below 450 microns).

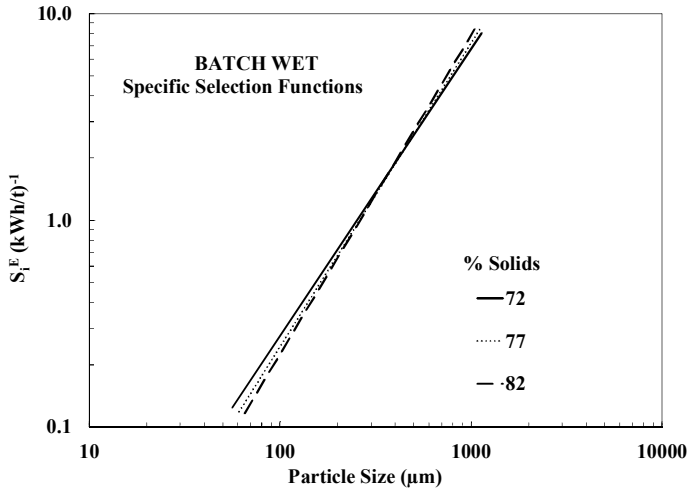

Figure 2.29: Comparison of specific selection functions of wet grinding at different percent solids (adapted from MARTINOVIC *et al.*, 1990)

SAMSKOG *et al.* (1990) found different behavior on the effect of top ball size on specific selection functions in comparison to Martinovic's studies, when iron ore (magnetite) with -25 mm and -10 mm of top size feed was ground. Previous research has shown that in a wet grinding system, breakage rates for different particle sizes is often a strong function of the ball size distribution in the mill (LO and HERBST, 1986). This phenomenon was clearly demonstrated in Samskog's studies, where the relationship between specific selection functions and particle size was not linear, presented a parabolic function, i.e. S_i^E passes through a maximum at a certain size, x_i. The existence of a maximum is quite logical because large lumps obviously will be too strong to be broken in the mill (AUSTIN *et al.*, 1984). This parabolic behavior was observed in the specific selection function estimated for -25 mm feed with 63, 76 and 88 mm of top size balls and for -10 mm feed grinding with 38, 50 and 63 mm balls.

According to AUSTIN *et al.* (1984) it is found that the disappearance of material from a given top size intervals is often not first order for coarser particle sizes. It may be rather described as an initial faster rate followed by a slower rate. Some of the particles are too coarse and tough to be properly nipped and fractured by the balls, so they have low rates of breakage. In addition, the accumulation of finer material appears to cushion the breakage of these larger sizes. The authors refer to the first-order breakage of smaller sizes as normal breakage and to the non-first order breakage of larger sizes as the

abnormal breakage region. Indeed, the abnormal breakage in a given mill situation could represent direct inefficiency.

SAMSKOG *et al*. (1990) also studied the influence of solids concentration and mill speed on specific selection functions. In the study of the effect of percent solids, pebbles were prepared as grinding media and for comparison, one test was performed using 63 mm of steel balls as media. The speed of the mill was kept at 78% of the critical speed and the specific selection functions were estimated for 65, 70 and 75% solids (Figure 2.30).

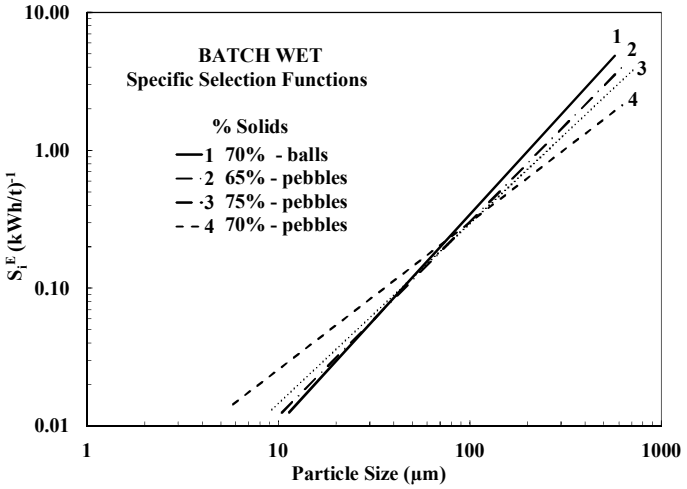

Figure 2.30: Comparison of specific selection functions for different percent solids (adapted from SAMSKOG *et al*., 1990)

Observing Figure 2.30, the results indicate that the breakage rates are faster for 70% solids for finer size fractions (below 100 microns, approximately). Comparing pebbles with balls as grinding media, the specific selection function estimated with balls presented higher breakage rates for coarse size fractions (above 100 microns, approximately).

In order to investigate the effect of mill speed on breakage rates for pebble grinding, the batch mill was operated at 73, 78 and 83% of critical speed. The percent solids in the mill was maintained at 70% for all speeds. The specific selection functions estimated for different mill speeds are shown in Figure 2.31. According to the results obtained, the

breakage rates for pebble grinding (for coarse size fractions) are higher at high mill speeds (78-83%).

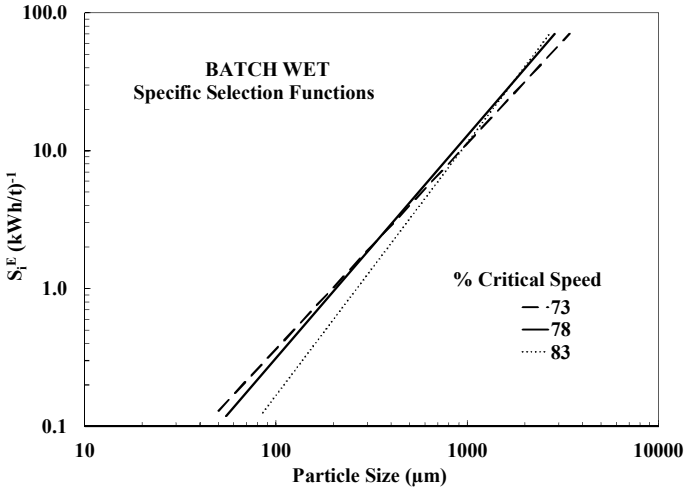

Figure 2.31: Comparison of specific selection functions for different mill speed (adapted from SAMSKOG *et al.*, 1990)

The effect of slurry filling or powder filling on specific selection function was studied by AUSTIN *et al.* (1984). It was found that for a given ball loading J_b it is undesirable both to underfill and to overfill the mill with powder. At low powder filling much of the energy of the tumbling balls is taken up in the steel-to-steel contact giving low values of Sf_c (absolute rates of breakages that has the physical meaning of the volume of powder broken per unit time per unit mill volume if all of the power is of size i and f_c is the fractional volume filling). On the other hand, at high powder fillings, the powder cushions the breakage action and Sf_c is again lower than normal. This also gives rise to non-first-order breakage, with the rate slowing down as fines accumulate in the bed. The optimum filling condition for the maximum breakage rates at all ball loads is with U ($U=f_c/0.4J_b$ - fraction of voidage that is filled by powder) around 0.6 to 1.1. However, mills will normally operate at the higher end of this range to avoid the excess ball wear caused by lower powder fillings.

The effect of high slurry density on the optimum filling level is demonstrated in Figure 2.32 (KATZER *et al.*, 1981). It appears that the optimum filling level at a given slurry density shifts to higher values of U as slurry density increases.

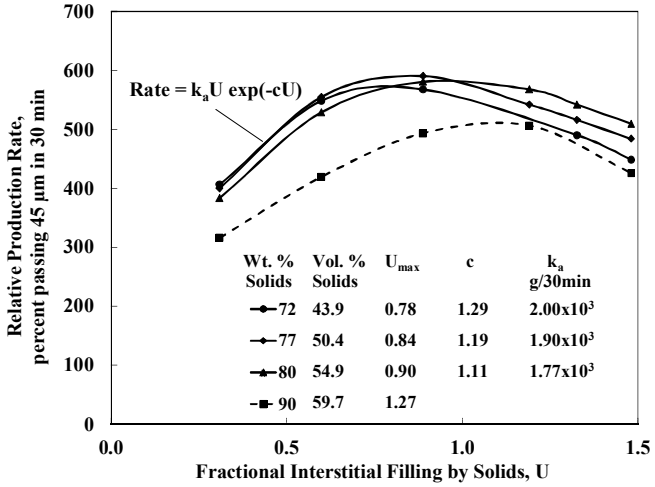

Figure 2.32: Variation of breakage rates with mill filling and slurry density (adapted from AUSTIN *et al.*, 1984)

Figure 2.33 shows that the slight maximum also occurs at constant slurry volume, so that the slurry is sufficient to fill the interstitial ball voids. It is concluded that the maximum production rate obtained at each optimum filling condition increases slightly to an optimum slurry density. After that the rate drops very significantly at high slurry density (AUSTIN *et al.*, 1984).

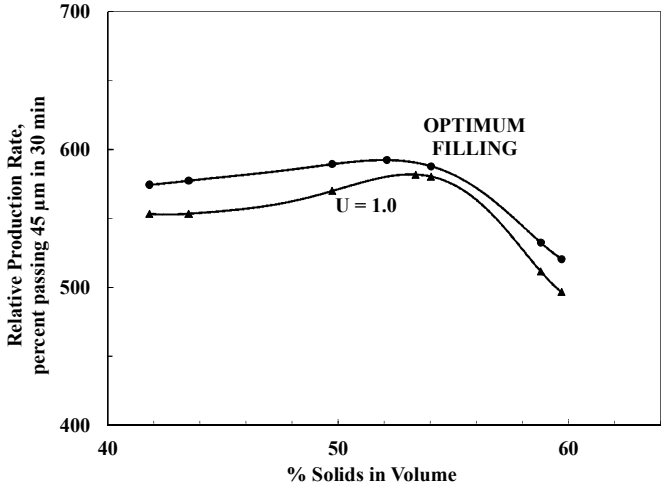

Figure 2.33: Variation of breakage rates with slurry density at: (a) optimum filling levels; (b) a hold-up of $U = 1$ (adapted from AUSTIN *et al.*, 1984)

2.3.3 PBM Approach to Ball Mill Optimization in Iron Ore Grinding

Grinding process optimization consists in identifying the specific values of the critical operating variables that result in the minimum specific energy consumption (kWh/ton), maintaining the product size in the range required by the processes that follow it.

According to LO *et al.* (1996) the critical operating variables that affect performance in steady state optimization of ball mill grinding are ball size, mill percent solids and cyclone classification efficiency.

The considerable improvement that has been made in phenomenological models to describe grinding circuit behavior makes these detailed models well suited for simulation and optimization of tumbling mill grinding circuits. Indeed, the population balance model has been used in the optimization of full-scale ball mill circuits grinding iron ore by some researchers (MARTINOVIC *et al.*, 1990; SAMSKOG *et al.*, 1990; LO *et al.*, 1996; AUSTIN *et al.*, 2007).

MARTINOVIC *et al.* (1990) demonstrated that the overall grinding efficiency can be improved by appropriately decreasing the ball sizes and percent solids. Predictions for mixture of ball sizes (19 mm/25 mm) also were conducted, but the simulation of mill operation with 19 mm top size balls resulted in the highest efficiency grinding. On the other hand, Figure 2.34 shows that lowering percent solids in the mill from 77% to 72% increased mill capacity by about 6%.

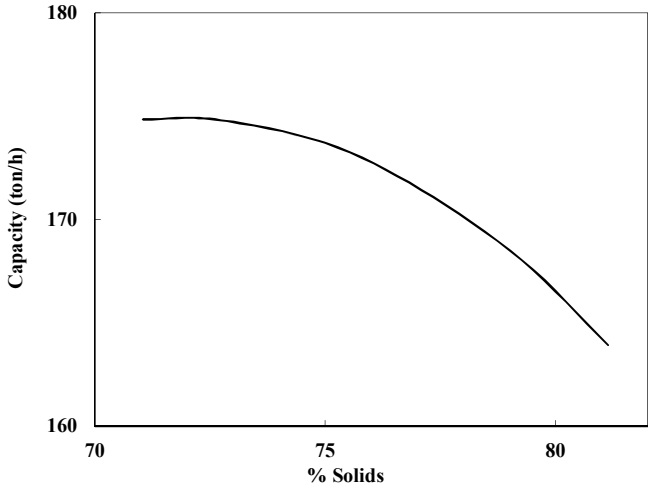

Figure 2.34: Predictions of mill capacity with percent solids adapted from (adapted from MARTINOVIC *et al.*, 1990)

Considering the energy consumption, the simulation results indicated that in the feedrate variation of +4% for a given product size, the energy requirement decreases with decreasing percent solids in the mill (Figure 2.35).

From the tests results, the authors also observed that when the mill was operated at a feedrate of 180 ton/h and 81% solids, the mill power dropped, indicating that the mill has probably entered an incipient overload condition. Indeed, when the mill overloads, the rate of breakage decreases significantly in the fine size range. At the same feedrate of 180 ton/h, lowering percent solids from 81.1% to 75.6% allowed the mill power to reach normal values, indicating that overload will not occur until higher feedrates when the mill is operated at lower percent solids.

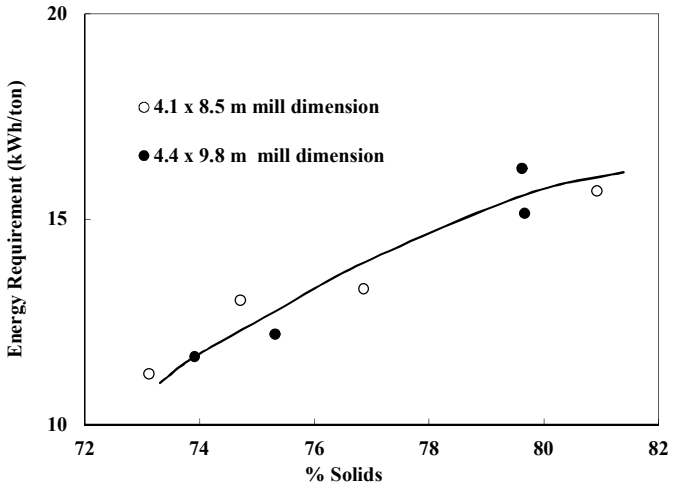

Figure 2.35: Prediction of energy requirements with percent solids at a product size of 67.5% passing 53 μm (adapted from MARTINOVIC *et al.*, 1990)

Based on the findings of Martinovic's study, a 12-15% increase in capacity was predicted to be possible with a proper combination of ball size charge and optimum percent solids. These predictions have been confirmed by plant tests in which the recommended operating changes have been made.

The rod mill/pebble mill circuit at the Kiruna Plant of LKAB was also optimized using the population balance model (SAMSKOG *et al.*, 1990). In this case a model for the pebble mill process was developed by modifying the specific population balance energy formulation of HERBST and FUERSTENAU (1980). A series of laboratory tests was

conducted to investigate the effect of ball size, percent solids and mill speed on iron ore grinding efficiency. The specific selection functions previously shown in Figure 2.30 and 2.31 were used to predict the continuous performance of the rod mill if it were converted to a ball mill producing a ground product size of 83% passing 295 microns.

The simulation results indicated that:

- The alternative of converting the rod mill to a ball mill with the correct top size balls can increase the open circuit capacity significantly;
- An additional capacity increase in excess of 10% was predicted to be available, if the ball mill is operated in closed circuit;
- The 63 mm balls are optimal for the grinding of -10 mm feed;
- By reducing the feed size from -25 mm to -10 mm, a capacity increase over rod milling of up to 50% was expected if ball mill grinding is used;
- The percent solids in the mill should be maintained at 70%;
- The similarity of results obtained using pebbles and balls as grinding media supports the assumption that the pebble mill can be modeled as a ball mill with low density, irregularly shaped media;
- The grinding efficiency (ton/kWh) for grinding with steel balls is only about 2% higher than that for pebble milling (this difference can probably be attributed to the non-spherical character of the pebbles (HERBST and LO, 1989));
- The grinding efficiency increases with increasing mill speed, but beyond a certain speed (78-80%) almost no difference is observed in the grinding efficiency.

The relationship between percent of increase in mill capacity and mill speed is shown in Figure 2.36.

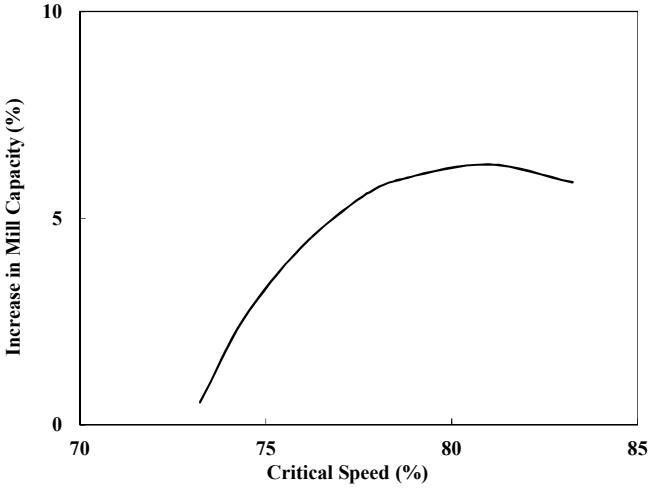

Figure 2.36: Relationship between percent of increase in mill capacity and mill speed (adapted from SAMSKOG *et al.*, 1990

Another study involving iron ore was carried out by AUSTIN *et al*. (2007). Laboratory-scale batch wet grinding tests were performed with hematite-rich ore mined at Vale's Carajás mine and the population balance model according to Austin's approach was used to simulate the full-scale mill. In this work, unlike many other studies, the primary breakage distribution functions were not normalizable. According to the authors, this behavior occurred possibly due to internal porosity of the ore, once smaller particles produce proportionally more fines on primary breakage, although this has not been proved. In spite of this anomaly, batch grinding tests showed excellent first-order breakage kinetics and reasonably good simulations of the product size distributions were obtained.

The studies implemented in the iron ore grinding previously mentioned have provided additional proof of the applicability of the population balance model methodology for simulation and optimization of an industrial scale mill.

In summary, generally, the following assumptions are adopted in the population balance model as it is used as an alternative to Bond equation for scale-up design or as a tool for process optimization:

- In dry and wet grinding systems:

- ✓ The breakage functions are considered as a good approximation to be independent of mill diameter, particle load, ball load, lifter configuration and the size distribution existing within the mill;
- ✓ The selection functions are considered to be proportional to the specific power draft of the mill, according to HERBST and FUERSTENAU (1973) approach;

- In dry ball milling:
  - ✓ The specific selection functions are considered independent of mill diameter, lifter configuration, particle load and the size consist in the mill;
  - ✓ The kinetics is considered linear, so usually the linear normalized model is adequate for scale-up predictions for larger mills using the data obtained from a lab-scale mill;
- In wet ball milling:
  - ✓ Due to the inherent nonlinearity, the specific selection functions use to be strongly dependent on the particle size distribution in the mill but are considered to be independent of mill diameter, particle load, ball load and lifter configuration;
  - ✓ The linear model is considered to be valid only if the predictions are made for a narrow range of the specific energy input to the larger mills using parameters obtained in the laboratory scale mill for the corresponding energy range and similar fineness of feeds;
- In predicting the performance of a ball mill operation in open circuit, the linear model should be valid with the same restrictions as applied to the wet batch grinding case using parameters obtained in a laboratory scale batch test.

Despite the proven track record of PBM in mill scale-up design and grinding circuit optimization, this approach has important limitations. Some of them have already been mentioned before and another one highlighted by PRATHY (2005) is that the PBM technique does not account the mode of breakage (impact and abrasion) and liner design, as known both concepts affect significantly the grinding performance.

CARVALHO and TAVARES (2013) also mentioned that this approach itself has no intrinsic capabilities to allow simulating the process under conditions that are different from those that were used to fit its parameters. The reason is that the population balance

model is essentially a mass balance over a range of sizes, having no direct information on the underlying physics of the process.

According to WEERASEKARA *et al.* (2013) the existing power-based and semi-empirical/phenomenological models suffer inadequacies in accuracy, application to multi-component ores, ability to incorporate liberation, and inability to predict the performance of new or novel equipment.

2.4 Discrete Element Method

In the mineral processing industry where the size reduction of particles is a key focus, the chase for advanced techniques to model comminution has been increased with the necessity for more accurate and sophisticated models. In this context, the introduction of computational models like the discrete element method (DEM) has started to solve some of the complex problems in comminution.

According to PRATHY (2005) the discrete element algorithm is a numerical technique, which solves engineering problems that are modeled as a large system of distinct interacting general shaped (deformable or rigid) bodies or particles that are subjected to bulk motion. It accounts for complex linear and nonlinear interaction between bodies. Essentially, DEM solves Newton's equations of motion to resolve particle motion and uses a contact law to resolve inter-particle contact forces. Forces are typically integrated explicitly in time to predict the time history response of the material using an appropriate quadrature method. DEM includes a family of techniques (contact model, bonding model, energy logging) that use radically different treatments for the element geometry and the form of the contact forces (WEERASEKARA *et al.*, 2013).

CUNDALL and STRACK (1979) were the pioneers in the development of the discrete element method to describe the motion of particulate material. They used it to analyze soil behavior by using two-dimensional disk elements. Since then, DEM has been used to study many applications in the processing industries. One of the first applications of DEM in minerals industry was the simulation of grinding media motion in ball mills developed by MISHRA and RAJAMANI (1992). Other applications are in simulating flow of granular media in chutes, particle mixing in blenders and mixers, blast furnace hearth flow, particle stratification in jigging and charge motion in tumbling mills (CLEARY, 2001).

The results obtained from MISHRA and RAJAMANI (1992) and CLEARY (1998) showed that the numerical technique produces results that are close to measured values when DEM is applied in predicting mill power draw. In terms of power draw and visual snap shot comparison of charge motion, CLEARY and HOYER (2000) demonstrated good agreement between the experimental and two dimensional DEM simulation of a centrifugal ball mill. AGRAWALA *et al.* (1997) and RAJAMANI *et al.* (2000) presented similar comparison between experimental tumbling mills and DEM simulations.

Many simulation studies using DEM reveal that lifter bar shape and profile greatly influence the charge profile (PRATHY, 2005; TOOR *et al.*, 2011; POWELL, 2011). As a consequence of wear of liners, liner-bar shape changes cause change in ball trajectory. These liner profile changes result in changes in power draft of the mill and also in changes in the size distribution of the product of the grinding mill. The modification in charge profile in terms of its cataracting and cascading zones due to wear of the liners is clearly observable in DEM simulations.

Findings that come up with DEM simulations have made possible for researchers to better understand the nature of breakage events that occur in each type of comminution equipment. The better understanding of these events allows the description and separation of mechanisms that are involved in particle fracture, enabling the description of comminution processes as distinct as those that occur during handling, transport and grinding, contemplating the breakage by impact grinding media, autogenous impact and abrasion.

According to the overview provided by WEERASEKARA *et al.* (2013) about the application of computational techniques to the science of comminution, DEM now plays an important role in understanding comminution fundamentals and in the design and optimization of comminution equipment. The main advantages of DEM application are:

- The nature of the collision energy spectra and their dominance by vast numbers of weak collisions has been revealed, leading to development of the concept of incremental breakage, where a particle fails by accumulation of damage over many weak collisions, impacting in more energy consumption than the same degree of breakage produced by a single high energy impact;

- DEM is now able to predict the nature of the particle flows for coarse and mid-sized particles within most comminution machines. It can predict and give insight into the nature of how the energy supplied by the machine is used for particle breakage;
- Liner stress and wear can be predicted through the evolution of the liner and the change in performance over the liner life cycle.

Although the DEM and accompanying computational techniques are providing an essential contribution to elevating the study of comminution process from a semi-empirical basis to an engineering science, based on the underlying mechanics of the processes, there are still many questions to be resolved, such as:

- How to relate specific wear patterns to operating conditions;
- The transport and classification can also be studied effectively when the finer particulate material can be included in the DEM models;
- Major challenges still remain in relation to the inclusion of fine particles and slurry in mills;
- The development of new generations of ore breakage characterization (nowadays the ore characterization testing techniques are impact damage, surface damage and fine particle breakage), including the investigation of much lower energies and of repeated collisions.

Despite the increase in computer processing capacity, the time consumed and the computation power needed to calculate the forces and positions of all the particles present in the system is still a limitation of DEM. According to WEERASEKARA *et al.* (2013) some DEM software provides a GUI based data analysis environment, however their techniques either require a considerable amount of processing power or are not capable of delivering the required inputs for a fully mechanistic comminution model. Therefore, a data logging system is required to fulfill the following objectives: provide flexibility in handling huge data sets generated by typical DEM code; extract particle collision information from the DEM output database; and summarize data to provide more useful information for further comminution modelling processes. To this end, considerable effort has been directed into data extraction and analysis dedicated to providing the outputs required for comminution modelling, as in the work of WEERASEKARA *et al.* (2008, 2010) and POWELL *et al.* (2010).

2.5 Mechanistic Model Approach to Ball Mill

2.5.1 Background and Examples of Applications

Given the limitations presented by the classic population balance model and considering the evolution of the discrete element method, in the late 1980s some researchers have already argued that major advances in comminution modeling would only occur through the development of mechanistic models. These models would allow describing how ball mills respond to changes in a number of design and operating variables, including mill diameter, mill speed, ball filling, ball size, ball density, and powder filling from knowledge of particle breakage characteristics.

During the last 30 years or so a large number of papers have been published about:

- The breakage mechanisms of the individual particles when they were impacted on flat surfaces or on beds, in order to simulate the events occurring within mills and crushers (CHO, 1987);
- The application of discrete element method (DEM) to the grinding environment, considering a ball mill as a set of circular slices (MISHRA and RAJAMANI, 1992);
- The characterization of the breakage mechanisms of the individual particles, that improved the understanding about the particle behavior when it is subjected to different types of breakage mechanisms (impact, compression, abrasion) (KING and BOURGEOIS, 1993; TAVARES and KING, 1998; TAVARES, 2007);
- Microscale modeling based on the population balance model, where the influences of the material and the comminution environment were decoupled by analyzing the breakage events individually (KING and BOURGEOIS, 1993);
- The variability in particles properties (fracture toughness, type of fragmentation, etc.), recognizing the importance of the description of this effect in mathematical modeling (TAVARES and KING, 1998);
- The modeling of particle breakage by repeated impacts using continuum damage mechanics, also called incremental breakage (TAVARES and KING, 2002).

In 2009, a mechanistic and generalized mathematical model was developed, based on concepts of modeling at the micro-scale (CARVALHO and TAVARES, 2009). This "generalized model of the comminution" and later called "UFRJ mechanistic model" describes the breakage process that occurs in size reduction equipment, decoupling the effects of materials and equipment. As such, it allows adapting and formulating the

model to selected applications such as the breakage of individual particles, in beds, degradation by handling, grinding in ball mills, autogenous and semi-autogenous and crushers such as the hammer mill.

According to CARVALHO (2009) the model applied to batch grinding described reasonably well the breakage products over time when compared to the experimental data. An improvement of the model can be obtained by the development of models for capture of particles and the distribution of impact energy on beds. Furthermore, the modeling of continuous grinding in ball mills for a multicomponent material indicated a change in the particle size distribution of the mill product when the mill was fed with a higher proportion of a less tough (softer) component.

The use of the discrete element method in the UFRJ mechanistic model allows describing appropriately the effects related to physical construction and working principle of comminution equipment. An example is the new approach proposed by ME Elecmetal and UFRJ to improve the design of mill liners using elements from mechanistic modeling of grinding (COLLINAO *et al.*, 2014). The results of simulations and analyzes obtained by using these tools allowed to support the new design proposal applied to liners of the 38' SAG mill. The new configuration of liners resulted in:

- Better charge liberation as it used 50% less lifters in number, and thus more space between lifters;
- Increased in lifters' face angle from 20° a 35° allowed improving the particle trajectory, transforming the milling movement from "cataract" to "cascade" thus achieving a better concentration of the charge and also eliminating the failures due to broken liners;
- The new design yielded a higher throughput between 6% and 12% when comparing to the old lifter design.

A methodology for quantifying the influence of liner wear has been provided by TOOR *et al.* (2011). According to the researchers this methodology could be used for optimizing liner design and reline scheduling. In the case of liner design it is possible to define a favorable shape for the majority of liner life, yielding desirable production parameters such as lower specific energy consumption and higher throughput, while at the same time maintaining practical liner life cycles. A description of this process of liner life cycle optimization and initial results from the first of two life cycles being studied for a 32' SAG mill has been presented. A preliminary analysis of fully worn and

new liners was carried out as this represented the greatest step change in the mill operating conditions. The results indicated that the worn mill is more suitable at producing fines at a higher rate resulting in increased throughput. The increased throughput is achieved at a lower power, possibly due to a decrease in high impact energy collisions occurring in a worn mill due to the reduction in lift. This is based on findings from JKSimMet breakage rates which show that the worn mill has increased breakage rates for particles with size below 30 mm.

2.5.2 Description of the UFRJ Mechanistic Model

A general scheme of the principles of the UFRJ mechanistic model developed by TAVARES and CARVALHO (2009) and described in CARVALHO (2009) is illustrated in Figure 2.37.

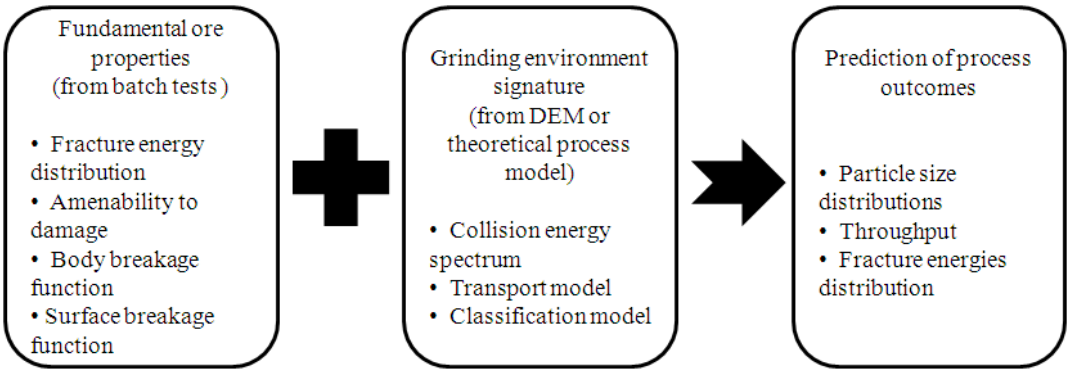

Figure 2.37: Framework of the UFRJ mechanistic model as proposed by CARVALHO (2009)

This model considers as input the ore breakage fundamental properties and can be used in modeling of different equipment mainly due to its ability to completely decouple the effects of grinding material and the environment, unlike the classic models based on the traditional population balance models and, more so, the Bond method. This characteristic puts it in good standing when it is compared to the traditional PBM approach.

As mentioned by CARVALHO (2009), the mechanical environment inside comminution machines is characterized by the collision energy spectrum, which gives the input on how the energy dissipated in the charge is applied to the particles to be

ground. In most grinding processes the collision energy spectrum can be estimated using the discrete element method. For materials handling and transport the collision energies may be estimated using analytical equations.

The model also requires that the mixing and transport properties are informed. For example, it is necessary to inform if the mill can be considered as a perfect mixer with or without internal classification, as well as mass transfer relationships, that is, the relationship between the mill hold up and the discharge. For the sake of simplicity, the proposed mechanistic model considered the ball mill as a perfect mixing reactor, although the approach can be extended to other cases such as plug flow regime or by considering a distribution of residence times in the case of continuous mills.

The population balance model discretized in particle size classes is the base of the mechanistic model approach. This first simplification is important since it keeps the modeling approach consistent to the current methodology of measuring particle sizes, which is sieving.

The UFRJ mechanistic model is also formulated in a way that allows accounting for composition or mineralogical classes. Thus, it is possible to model processes that involve the differential breakage of distinct minerals that compose an ore. An example is the case of iron ore which is composed of iron minerals, mainly magnetite and hematite, which typically present comparatively low strength (low fracture energies/high breakage probability) and silicate minerals such as quartz which present higher strength. Thus, in the same mill, when the materials are subjected to impact energies of similar magnitude, different products could be obtained. This may become a challenge when the mill operates in closed circuit, since the tougher unbroken particles would return from the classifier to the mill, so that the recycle stream will present a different composition than the fresh feed. This type of situation, however, should be considered in PBM formulations.

A complete description of the mechanistic model of the ball mill was presented by CARVALHO and TAVARES (2013) and this approach is described only briefly as follows:

At the microscale level, the model considers that a number of outcomes may result from each collision event in the mill. It considers that when particles suffer an impact, some of them undergo catastrophic breakage and some do not (Figure 2.38). If stresses are

insufficient to cause catastrophic (body) fracture, particles will undergo surface breakage (abrasion/chipping) and will also become progressively weaker (incremental breakage - damage).

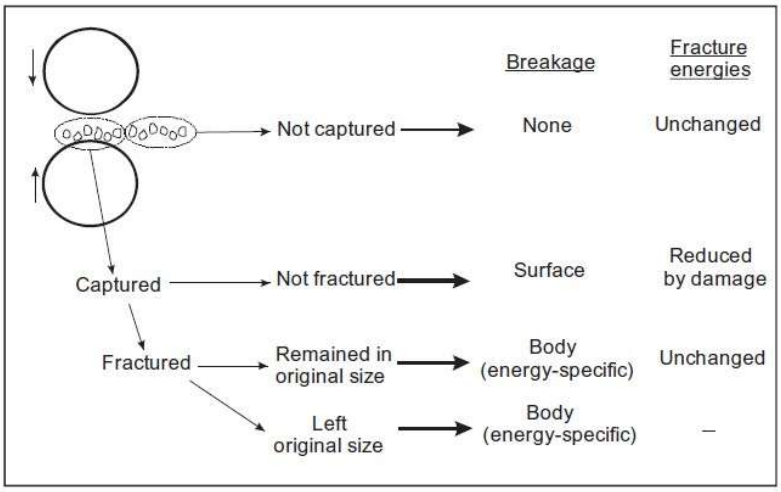

Figure 2.38: Schematic diagram of the structure of the mechanistic model at the microscale (TAVARES and CARVALHO, 2009)

A general formulation of the traditional population balance model applied to the microscale description of size reduction processes has been used to derive the batch grinding process equation (CARVALHO and TAVARES, 2009). Then the rates of changes in mass of material contained in size class *i* can be described by Equation 2.52:

$$\frac{dm_i(t)}{dt} = \frac{\omega}{H}\left[-D_{i,b}(t) - D_{i,s}(t) + A_{i,b}(t) + A_{i,s}(t)\right] \qquad 2.52$$

where H is the mill hold-up, $m_i(t)$ is the mass fraction of particles contained in size class i in the mill and ω is the frequency of stressing events in the comminution machine. Functions A and D represent the rate of appearance and disappearance of material in class i due to fracture, being defined in Table 2.1, whereas subscripts b and s stand for body and surface breakage mechanisms, respectively.

Table 2.1: Definition of terms in Equation 2.52

Breakage Mode	***Rate of Appearance (A)***
Body (b)	$A_{i,b}(t) = \sum_{j=1}^{i-1} m_j(t) \int_0^{\infty} m_j(E) p(E) \int_0^1 b_{ij}(eE,t) F_j(eE,t) p(e) de dE$
Surface (s)	$A_{i,s}(t) = \sum_{j=1}^{i-1} m_j(t) \kappa_j \int_0^{\infty} m_j(E) p(E) \int_0^1 a_{ij}(eE,t) \left[1 - F_j(eE,t)\right] p(e) de dE$
	Rate of Disappearance (D)
Body (b)	$D_{i,b}(t) = m_i(t) \int_0^{\infty} m_i(E) p(E) \int_0^1 \left[1 - b_{ii}(eE,t)\right] F_i(eE,t) p(e) de dE$
Surface (s)	$D_{i,s}(t) = m_i(t) \kappa_i \int_0^{\infty} m_i(E) p(E) \int_0^1 \left[1 - F_i(eE,t)\right] p(e) de dE$

In the equations listed in Table 2.1, $p(E)$ is the distribution of stressing energies E in the mill, m_j is the mass of particles contained in size class j captured in each stressing event and $p(e)$ is the function that represents the energy split among particles. a_{ij} and b_{ij} are the breakage functions in density form, corresponding to the mechanisms of surface and body breakage, respectively, the later dependent on stressing energy (TAVARES and CARVALHO, 2009). κ_i is the first order surface breakage rate. The density distribution of stressing energies in the mill $p(E)$ is calculated from the cumulative distribution, from $P(E) = dp(E)/dE$. The product eE is the fraction of the impact energy that is absorbed by each particle captured in an impact event.

The body breakage function is described on the basis of expressions that account for the effect of particle size and stressing energy on the size distribution of the progeny fragments. The reduction in size of the progeny with increasing applied energy has been described very successfully using the t_{10}-procedure, originally proposed by NARAYANAN and WHITEN (1988). The size distribution from impacts at a specific energy E on particles contained in size class j is calculated by first estimating the fraction of material passing 1/10th of the original particle size, called t_{10}, using the expression proposed by TAVARES (2009):

$$t_{10j} = A\left[1 - \exp\left(-b' \frac{E}{E_{50b,j}}\right)\right] \tag{2.53}$$

where A and b' are model parameters and $E_{50b,j}$ is the median mass-specific particle fracture energy that are broken as a result of the impact of magnitude E. When the collision energy is higher than the fracture energy of the toughest particle contained in size class j, then $E_{50b,j} = E_{50,j}$, otherwise it should be calculated numerically (TAVARES and CARVALHO, 2009).

From the t_{10} value calculated using Equation 2.53, it is then possible to estimate the proportions passing (t_n values) of different fractions of the original parent size for each stressing energy and particle size investigated. This is done with an additional model that is based on the incomplete beta function, given by (CARVALHO, 2009):

$$t_n(t_{10}) = \frac{100}{\int_0^1 x^{\alpha_n - 1}(1-x)^{\beta_n - 1} dx} \int_0^{t_{10}/100} x^{\alpha_n - 1}(1-x)^{\beta_n - 1} dx \tag{2.54}$$

where each t_n is the percent passing in a d^*/n size, in which d^* is the original size of the particle. α_n and β_n are parameters that are fitted to the experimental data. The size-normalizable and energy-specific breakage function is then obtained by interpolating the various t_ns, so that the elements of the breakage matrix are calculated by $B_{ij}(E)$ = interp(t_{10},t_n) . The breakage function in density form may then be calculated by:

$$\begin{aligned} b_{ii}(E) &= 1 - B_{ii}(E) \\ b_{ij}(E) &= B_{i-1,j}(E) - B_{ij}(E) \end{aligned} \tag{2.55}$$

Finally, surface breakage is modeled using data from the JKMRC tumbling test (NAPIER-MUNN *et al.*, 1996) assuming that breakage follows first-order kinetics and a size-independent surface breakage rate ($\kappa_i = \kappa$), being independent of collision energy. Its breakage function in the cumulative form is given by $A_{ij} = (d_i / d_A)^{\lambda}$, where d_A and λ are model parameters and d_i is the representative size of particles contained in the ith class.

Equation 2.52 should be solved simultaneously with the equation that describes how the fracture probability distribution of each component varies with time, which may be calculated by:

$$F_i(E,t+\Delta t)=\frac{G_i F_i^*(E,t+\Delta t)+H_i F_i(E,0)+I_i F_i(E,t)}{G_i+H_i+I_i} \quad 2.56$$

where $G_i(t)$ is the fraction of material in the class i that has been damaged but remained in the original size range, $H_i(t)$ is the fraction of material that appeared due to body and surface breakage, and $I_i(t)$ is the fraction of material that was not captured in the time interval. All these equations are described in CARVALHO and TAVARES (2013).

$F_i(E,0)$ is the fracture probability distribution of the original material and can be, generally, described well using the upper-truncated lognormal distribution, given by TAVARES and KING (1998):

$$F_i(E,0)=\frac{1}{2}\left[1+\mathrm{erf}\left(\frac{\ln E^*-\ln E_{50,i}}{\sqrt{2\sigma_i^2}}\right)\right] \quad 2.57$$

where

$$E^*=\frac{E_{\max,i}E}{E_{\max,i}-E} \quad 2.58$$

$E_{50,i}$ is the median particle fracture energy, σ_i^2 is the variance and $E_{max,i}$ is the upper truncation value of the distribution.

Typically, as particles become finer, they become tougher and their specific fracture energy increases. An expression that can be used to describe that variation is given by:

$$E_{50,i}=E_\infty\left[1+\left(\frac{d_o}{d_i}\right)^\phi\right]\overline{m}_{p,i} \quad 2.59$$

where E_∞, d_o and ϕ are model parameters that should be fitted to experimental data. The mean weight of particles contained in size class i may be estimated by:

$$\overline{m}_{p,i}=\rho_{ore}\beta d_i^3 \quad 2.60$$

where ρ_{ore} is the material specific gravity and β the volume shape factor.

In analogy to Equation 2.59, the standard deviation of the lognormal distribution of particle fracture energies can vary with size, often increasing as particle sizes decrease. An expression that can be used to describe this variation is:

$$\sigma_i = \sigma_\infty \left[1 + \left(\frac{d'}{d_i} \right)^{\theta'} \right] \tag{2.61}$$

where d' and θ' are fitting parameters.

In Equation 2.56, $F_i(E,\ t)$ is the distribution of fracture energies of the material contained in size class i that did not suffer any impact event during the time interval, whereas $F_i^*(E,\ t+\Delta t)$ is the distribution of fracture energies of the particles in size class i that were captured in an impact event, but which did not fracture, being given by:

$$F_i^*(E, t+\Delta t) = \frac{\int_0^{E_i^*} p(E_k) \int_0^1 \left[\frac{F_i[E/(1-D), t] - F_i(eE_k, t)}{1 - F_i(eE_k, t)} \right] p(e)\, de\, dE_k}{\int_0^{E_i^*} p(E_k)\, dE_k} \tag{2.62}$$

and

$$D = \left[\frac{2\gamma(1-D)}{(2\gamma - 5D + 5)} \frac{eE_k}{E} \right]^{\frac{2\gamma}{3}} \tag{2.63}$$

where E_i^* is the maximum fracture energy of particles contained in class i, which is equal to E_{max} in the first time interval and $F_i(E_i^*) = 1$ as comminution progresses (TAVARES and CARVALHO, 2009).

Considering all formulations, the model is able to account for the fact that particles that are stressed but do not fracture in a stressing event, may become progressively weaker.

Furthermore, the mass of material captured between two grinding media elements (w_i) may be estimated from the product of the number of particles caught between the media elements ($N_{cap,i}$) and the average weight of the particles ($\overline{m}_{p,i}$),

$$w_i = \overline{m}_{p,i} N_{cap,i} \tag{2.64}$$

Given the evidence from earlier work (HÖFLER, 1990), that particles in an unconfined bed normally only break when they are typically squeezed down to a monolayer between grinding media, it is assumed that particles are modeled as a packed monolayer bed. If particles had spherical shapes, and if they were arranged according to a dense hexagonal packing arrangement, then the number of particles captured as a function of radius could be estimated by BARRIOS *et al.* (2011):

$$N_{cap,i} = \frac{1}{4} + \frac{3}{4}\left(\frac{2r_c}{d_j}\right)^2 \quad \text{for } r_c \geq d_j/2$$
$$= 1 \quad \text{for } r_c < d_j/2 \tag{2.65}$$

where r_c is the radius of the bed, also called radius of capture, and d_j is the mean size of the particles caught by the colliding steel ball, estimated from the geometric mean of sieves containing the narrow size fraction.

The radius of capture can be calculated by adding the radius of contact due to geometry (r_g) and the radius of contact due to the elastic deformation in the vicinity of contact (r_e), giving $r_c = r_e + r_g$ (BARRIOS *et al.*, 2011).

The radius of the elastic deformation zone, resulting from the collision of two bodies, is given by Hertz contact theory as:

$$r_e = \left(\frac{15E}{8K_e}\right)^{1/5} K_g^{2/5} \tag{2.66}$$

where K_g is the geometric constant of the contact, given by:

$$K_g = \frac{r_{c1}r_{c2}}{r_{c1} + r_{c2}} \tag{2.67}$$

and the elastic constant of the contact is given by TAVARES and KING (2004):

$$K_e = \frac{K_1 K_2}{K_1 + K_2} \tag{2.68}$$

where r_{ci} and K_i are the radius of curvature and the elastic stiffness of each of the bodies in contact, respectively.

It is then necessary to account for the fact that the radius of the zone in which particles are captured increases, due to the influence of their height and to the degree of penetration of the striking ball in the bed resulting from breakage. According to this BARRIOS *et al.* (2011) proposed a model in which the radius of contact due to geometry is calculated by:

$$r_g = \sqrt{K_g^2 - \left[K_g - h\left(\frac{\Delta}{h}\right)\right]^2} \tag{2.69}$$

in which Δ is the maximum deformation of the bed during impact. In the case of a monolayer bed, the initial bed height (h) may be considered equal to d_j, although it is certainly influenced by particle shape.

The term Δ / h, called ''maximum relative deformation of the bed'' has been modeled by BARRIOS *et al*. (2011) using the empirical expression:

$$\frac{\Delta}{h} = a_c \left[1 - \exp\left(-b_c \left(\frac{E}{E_{50b,i}} \right)^c \right) \right] \qquad 2.70$$

in which a_c, b_c and c are constants that must be fitted to the data.

In the description of the energy split function in the bed $p(e)$, it is considered that the stressing energy is split equally among particles positioned within the active breakage zone in the mill. In this case the energy distribution function may be given by:

$$p(e) = \delta(e - 1/N_{cap,i}) \qquad 2.71$$

where δ is the Dirac delta function.

The UFRJ mechanistic model can also be extended to continuous grinding. In this case the model was used to simulate the continuous milling of a copper ore in a laboratory scale mill without internal classification purposes (CARVALHO, 2009).

In summary, the assumptions that are included in the mechanistic model of the ball mill have been described by CARVALHO and TAVARES (2013):

- The mechanical collision environment is determined exclusively by the motion of grinding media and the energy available for breakage is given by the energy loss in the collision;
- Breakage results only from the normal component of the collisions;
- Balls and powder are perfectly mixed within mill charge;
- Powder particles are involved in every collision event within the mill, and particles are stressed as packed monolayer particle beds;
- The fracture strength of a particle does not vary if it was produced as a progeny of a low-energy or a high-energy stressing event.

The mechanistic model has shown to be a very suitable as a tool of batch mills simulation. This statement can be proved by the studies made by CARVALHO and

TAVARES (2013) where they applied the mechanistic model of the ball mill in the simulation of batch mills operating under a range conditions. In these studies, the first-order breakage rates have been estimated using data from these simulations, and used to investigate the effect of operating and design variables in milling. The effects of particle size, mill speed, mill filling, mill diameter, ball size, and mill liner configuration on specific breakage rates were investigated.

The authors also compared the predictions using the mechanistic model to those using the scale-up relationships proposed by AUSTIN *et al.* (1984) and HERBST and FUERSTENAU (1980). This comparison showed that the trends predicted using the mechanistic model are in general agreement with these empirical models. Good correlation has also been observed between the simulated specific breakage rates and the specific mill power, which is in agreement with the scale-up method proposed by HERBST and FUERSTENAU (1968, 1980). Furthermore, unlike the traditional scale-up methods, the mechanistic ball mill model is able to predict synergic effects between material and milling variables.

There is a challenge that should be considered in UFRJ mechanistic model framework as proposed. This model allows the incorporation of better models, however, there is a need for understanding how particles behave when hit in slurry beds. This study is ongoing at LTM (Laboratório de Tecnologia Mineral), Universidade Federal do Rio de Janeiro, and the aim is to improve the particle interaction model.

3. MATERIALS AND METHODS

The experimental work consisted of detailed experimentation carried out in a batch mill and in a pilot scale ball mill. Two batch wet experiments using the mono-size feed and seven using natural feed (-2360 μm) were conducted in the batch mill and five continuous tests using natural feed (-2360 μm) were carried out in the pilot mill. These two scale mills are installed in the Mineral Processing Laboratory (MPL) at the University of Utah. They were in good working condition and had been calibrated before the experiments were performed.

In addition to those, three sampling campaigns and four laser scan surveys of the mill internals were executed in Vale's industrial ball mill.

3.1 Material

The material used was iron ore pellet feed acquired from Vale's facility in Vitória. A sample of about 2.5 ton was collect in the iron ore pile and constituted the ore blend chosen for this study.

The specific gravity was found to be 4.34 g/cm^3. The F_{80} was about 540 μm, with a top size of 9.5 mm. The size distribution was analyzed at Vale's laboratory and at MPL (in duplicate) by dry and wet screening. Both curves are presented in Figure 3.1 and the data are presented in Appendix I. The samples used to measure the particle size distribution at MPL were collected following the sampling methodologies in order to guarantee the representative composition of the whole material.

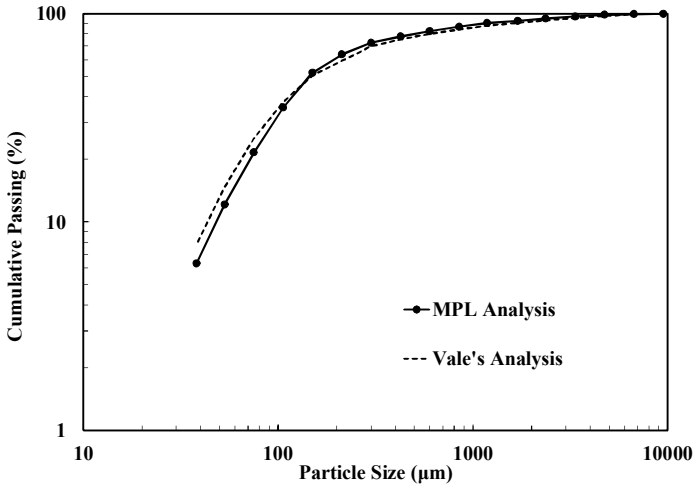

Figure 3.1: Size distribution of the iron ore sample

3.2 Sample Preparation

When the bulk sample of iron ore sent from Brazil arrived at the University of Utah, it was necessary to dry, to homogenize and to reduce it to a sample size suitable for processing in the laboratory.

Seven drums of this bulk sample were spread on the floor in order to have the ore dried in open air (Figure 3.2) and a manual homogenization was made using a shovel.

Figure 3.2: Iron ore drying outdoor

In order to assess the particle size effect on the breakage function, experiments with particles contained in narrow-size ranges were carried out with two size fractions: 3.35 x 2.36 mm (6 x 8 mesh) and 150 x 106 µm (100 x 150 mesh). With the aim of preparing these narrow-size samples, the "as received" iron ore was initially sieved through a set

of Sweco screens as showing Figure 3.3. The +6, -8, +100 and -150 mesh fractions were stored in different buckets. The product was further sieved for ten minutes through Tyler $\sqrt{2}$ interval screens to obtain the narrow size (here called mono-size) fractions of 6 x 8 and 100 x 150 mesh. Afterwards, these samples were washed with water in order to remove fines.

Figure 3.3: Preparation of narrow-size fractions using the Sweco screen

3.3 Equipment

Three different kinds of mills were used in this investigation: the batch mill, the pilot mill and Vale's selected closed-circuit ball mill.

3.3.1 Batch-Scale Mill

The laboratory-scale mill installed at the Mineral Processing Laboratory (MPL) where the wet batch tests were carried out, consisted of a 25.4 cm diameter by 29.2 cm long cylindrical steel shell fitted with eight 2.0 cm width and 0.5 cm thickness square lifters (Figure 3.4 a).

The batch mill was disposed in a steel frame and was equipped with a Graham variable speed transmission coupled with a Futek torque sensor (FUTEK Advanced Sensor Technology) connected to a computer (Figure 3.4 b). Hence, the power draft (torque) measured directly from the drive shaft between the transmission and the mill was recorded each second. Figure 3.5 illustrates one example of the torque recorded during a batch experiment.

(a) (b)

Figure 3.4: Batch mill on steel frame and torque display (a) and the squares lifters inside the mill (b)

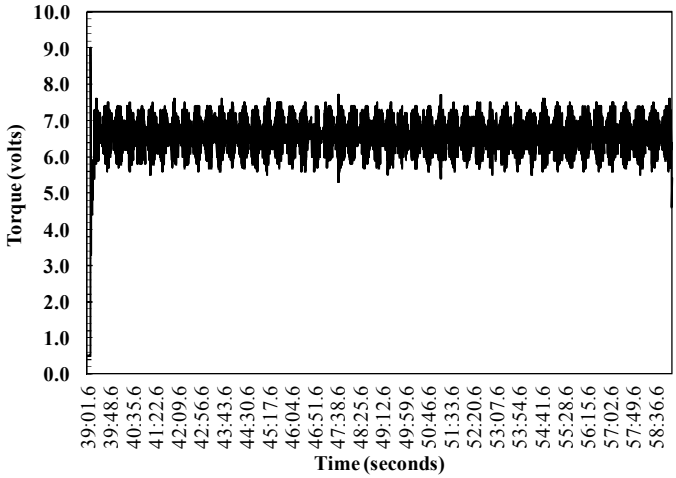

Figure 3.5: Torque recorded during the natural size batch wet experiments

3.3.2 Pilot-Scale Mill

The pilot-scale mill consisted of a 41.6 cm diameter by 64.1 cm long cylindrical steel shell fitted with eight 13.0 cm width and 6.0 cm thickness lifters bars. The mill was designed to be a component of a continuous system and two different types of discharge end-plates can be used for studying mass transport: overflow discharge and grate discharge. In the case of overflow discharge a coarse steel grid was fitted to the overflow opening to prevent balls from rolling out of the mill. Figure 3.6 shows the mill lifters bars, the overflow and the grate discharge, respectively.

(a) (b) (c)

Figure 3.6: Pilot mill with its components: lifters bar (a); overflow discharge (b) and grate discharge (c)

A conveyor belt with variable speed control was part of the system and it was responsible for transporting the dry feed ore from the storage bin to mill feeder. The speed calibration was necessary in order to achieve the feed rate desired in the experimental tests.

The mill and the gearbox were supported by an L-shaped steel frame. Another steel frame next to the L-shaped frame supported the motor, the system of pulleys and the torque sensor. Underneath these two frames was a triangular steel frame and a Rice Lake^{TM} weighing system, which comprised three Paramount^{TM} load sensors that were anchored to the supporting concrete block located in the corners of the triangular frame. Hence, the triangular frame rests on the load sensors responsible for measuring the weight of the whole system.

The torque sensor was located between the motor and the gearbox, and measured the torque at the drive side of the gearbox and sent its electrical signal to a digital indicator. The power input to the mill was obtained by multiplying the recorded torque by the gear ratio and applying the appropriate corrections for losses. During the experiments the torque and the reading on the load sensor (slurry hold-up) were recorded every two minutes and the data was viewed in a computer screen.

The mill electronic speed controller, which had a scale expressed in relative values, was calibrated and the calibration curve was constructed by setting the controller at a given value and measuring the mill speed by counting the number of mill revolutions for a given time period. Provided the reduction ratio of different pulleys and gearbox

combinations, the frequency of rotation of the mill was checked by measuring the speed of any of the gears or pulleys by means of an electronic stroboscope.

A feed water system, composed by a fixed tank near the mill, pump and a flow meter was also part of the pilot mill circuit. Water from the tank was fed to the mill by Masterflex I/P Easy Load pump with maximum flow rate of 13 l/min and minimum capacity of 0.01 l/min. The pump output was connected to a Masterflex I/P digital modular drive. The water rate is constant and adjustable according to the solids concentration required for each pilot test.

In summary, the pilot mill open circuit is composed of speed controller, torque, weight and water display and a computer that collects all data from torque and load sensors (Figure 3.7).

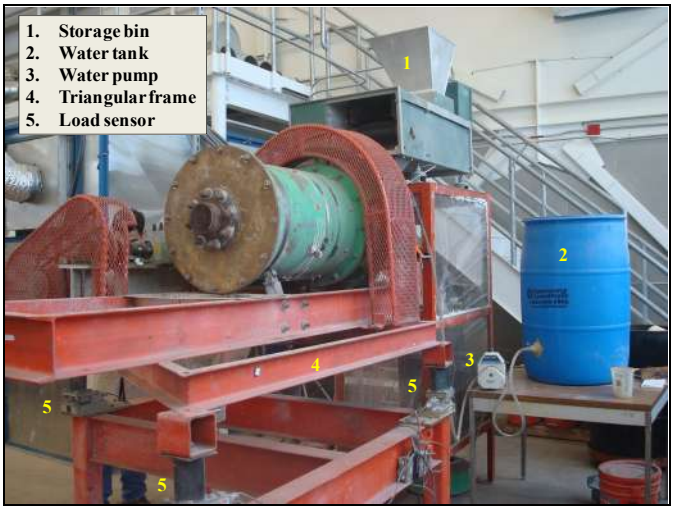

Figure 3.7: Pilot continuous mill circuit

3.3.3 Vale's Industrial Mill

The closed grinding circuit at Vale's pelletizing plant located in Vitória (Espírito Santo State, Brazil) chosen for optimization was composed of six hydrocyclones in a direct circuit with one ball mill with 5.2 m (17.1 ft) internal diameter, 10.6 m (34.8 ft) length, with two motors of 4.5 MW of power. The mill liners were made of rubber and the liners profile were known as bar-plate. Figure 3.8 illustrates the industrial ball mill and liners profile.

(a) (b)

Figure 3.8: Vale's industrial closed-circuit ball mill (a) and bar-plate lifters inside the mill (b)

There was a control system in this mill where the feed rate was controlled according to the surface area and the percentage passing 45 μm of the hydrocyclones overflow. The instrument used to measure the particle size and the surface area was PSI 500 (particle size analyzer from OUTOTEC). The online analysis method is based on laser diffraction and provided continuous measurements.

The ball filling was controlled based on mill power set point and the mill density was maintained in a fixed value previously determined to give the best mill performance.

The pressure in the feed to the classification system was controlled in a range required to achieve the desired partition curve. Table 3.1 shows the hydrocyclones dimensions and the range of operational pressures.

Figure 3.9 illustrates Vale's grinding circuit flowsheet.

Table 3.1: Hydrocyclones dimensions and operational pressure

Diameter	***Free Hight***	***Inlet Diameter***	***Vortex***	***Apex***	***Pressure***
500 mm	2100 mm	150 mm	170 mm	80 mm	0.8 – 1.1 kgf/cm^2
19.7 in	82.7 in	5.9 in	6.7 in	3.1 in	13.70 psi

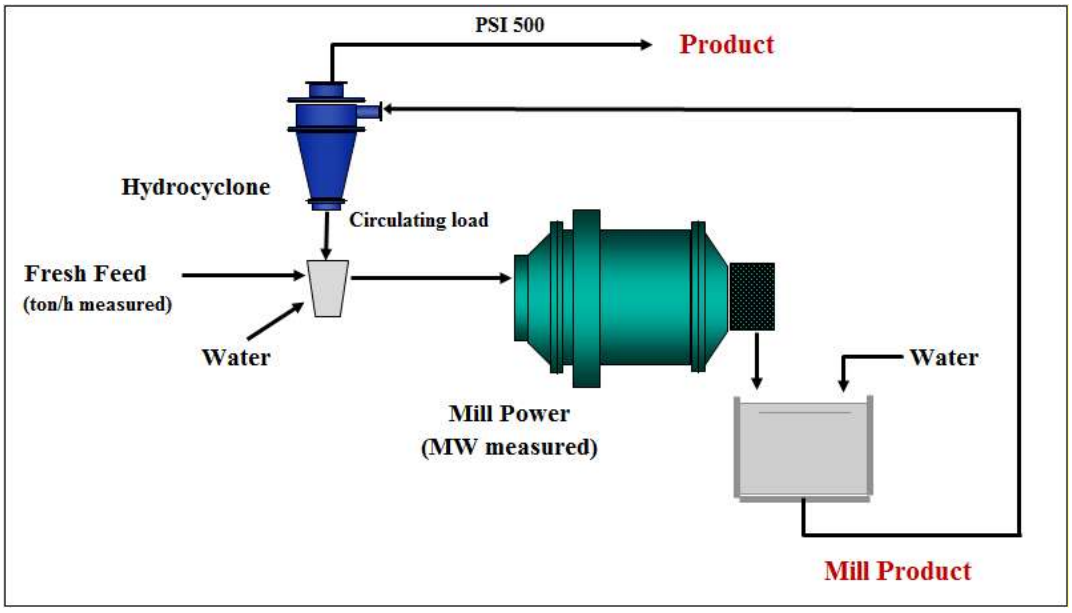

Figure 3.9: Vale's grinding circuit flowsheet

3.4 Experimental Procedures

3.4.1 Wet Batch Grinding Experiments

The wet batch grinding experiments were designed for scale up and plant mill optimization using the predictive capability of the population balance model formulation based on HERBST and FUERSTENAU (1980) approach. The variables that were investigated using this methodology were: solids concentration, top ball size and slurry filling. The solids concentration varied in a range from 72 to 80% and two top ball sizes were considered in this study: 30 mm and 25 mm. The values used to study the influence of slurry filling were 100% and 260%. The initial plan to use these values was to represent the extreme conditions that can occur in a continuous mill.

The ball filling was kept constant at 40% and the speed of the mill for all experiments was maintained at 68.3% of the critical speed. This percentage of critical speed was set to match the one used in Vale's industrial mill.

Narrow-size experiments were carried out with material contained in two size ranges: 3.35 x 2.36 mm (named test B1) and 150 x 106 μm (test B2) and seven experiments (tests B3, B4, B5, B6, B7, B8 and B9) were carried out using the "natural" feed (-2.36 mm). Details of operating conditions and experimental product size distributions of each experimental test are described in Appendix I.

The ball size distribution was determined according to SEPÚLVEDA (2006). He described that the ball size distribution, $F_3(d)$, corresponding to total ball charge weight m_b whose size is lower that a given size "d", is derived from:

$$m_b F_3(d) = \int_{d^S}^{d} \rho_b (\pi d^3 / 6x10^9)\, n_b\, f_0(d)\, d(d) \qquad 3.1$$

where n_b represents the total number of balls in balls charge, d is an intermediate ball size, d^S is the scrap ball size and ρ_b is ball density.

The relationship (m_b/n_b) is derived from the integration of Equation 3.1 in the size interval $[d^S, B]$, imposing the condition that, by definition, $F_3(B) = 1.0$, to obtain:

$$(m_b / n_b) = \left(\frac{\rho_b \pi}{24x10^9}\right) \frac{\left[(B)^4 - (d^S)^4\right]}{\left[B - d^S\right]} \qquad 3.2$$

where B is the ball top size.

Then, through substitution and integration Equation 3.1 becomes:

$$F_3(d) = \frac{\left[d^4 - (d^S)^4\right]}{\left[(B)^4 - (d^S)^4\right]}; \text{ for } d^S < d < B \qquad 3.3$$

The scrap ball size (12.7 mm) and intermediate ball size (25.4 and 17 mm) were selected according to Vale's industrial mill.

Finally, a detailed description of the procedure used for the batch experiment in the 25.4 cm mill using the mono-size and natural feed is given as follows:

1. First of all, the batch mill speed was adjusted with variable speed arrangement provided on the shaft to achieve 68.3% of critical speed, corresponding to 61.3 rpm. The mill speed was calculated according to $\varphi_c = 100\frac{N}{N_c}\varphi_c$, where φ_c is the percentage of critical speed, N the mill speed, N_c the critical speed of mill in revolutions per minute at which the first layer of the balls will centrifuge ($N_c = \frac{42.3}{(D-B)^{1/2}}$ rpm, D the mill diameter in meters and B the maximum ball diameter in meters).
2. The no-load torque was recorded and corresponded to 1.12 N.m.

3. The ball size distribution was calculated according to Equation 3.3 and the percentage by weight of each ball size and the ball mass calculation are represented in Tables 3.2 and 3.3. The ball density was measured and the value of 7.77 g/cm^3 was considered in calculations.

Table 3.2: Ball size distribution for experiments with 30.0 mm of ball top size

Ball Size (mm)	*Percentage (% by wgt)*	*Ball Mass (kg)*	*Number of Balls*
30.0	37.0	10.2	78
25.4	47.0	12.9	194
17.0	14.0	3.9	195
12.7	2.0	0.6	69
Total	**100**	**27.6**	**536**

Table 3.3: Ball size distribution for experiments with 25.4 mm of ball top size

Ball Size (mm)	*Percentage (% by wgt)*	*Ball Mass (kg)*	*Number of Balls*
25.4	59%	16.3	244
17.0	36%	9.9	495
12.7	5%	1.5	175
Total	**100%**	**27.6**	**913**

4. The mass of solids and water and the slurry filling for each experiment were calculated according to equations shown at Table 3.4 and the test conditions are summarized at Appendix I.

Table 3.4: Batch experiments calculation

Mass of solids calculation	
Mill $_{\text{volume}} = V_m = \frac{\pi D^2}{4} * L$	Ball $_{\text{volume}} = V_b = J_b * V_m$
Void $_{\text{volume}} = V_{void} = 0.40 * V_b$	Bulk volume of solids = $V_{bulk} = U * V_{void}$
Solids $_{\text{mass}} = M_{\text{ore}} = \rho_{bulk} * V_{bulk}$	
Water mass calculation	
Water $_{\text{mass}} = M_{water} = \frac{(100 - \%Sd)}{\%Sd} * M_{ore}$	
Slurry filling calculation	
Slurry $_{\text{mass}} = M_{slurry} = M_{ore} + M_{water}$	Slurry $_{\text{volume}} = V_s = \frac{M_{slurry}}{\rho_s}$
Slurry filling (%) = $\frac{V_s}{V_{void}} * 100$	

where D is mill diameter; L is mill length; J_b is ball filling; ρ_{bulk} and ρ_{ore} are the ore bulk density and ore specific gravity, respectively, both densities were determined experimentally; $\%Sd$ is the percentage of solids by weight; ρ_s is the slurry density calculated according to solids concentration $\rho_{slurry} = \frac{100}{(\%Sd / \rho_{ore}) + (100 - \%Sd)}$.

$U = \frac{H}{m_p}$ is the relationship between H that is the mass hold-up (mass of solids) and m_p is the mass of particles that completely fill the interstices between the balls under static conditions.

5. Considering the amount of ore and water specified for each experimental condition, the mill was charged with balls and feed material in a layer-loading manner, that is, alternating layers of ball, ore and water, to ensure thorough mixing at the beginning of each test. Figure 3.10 demonstrates this step-by-step process.

(a) (b) (c)

Figure 3.10: Batch mill charged with only balls (a), ore and balls (b) and ore, balls and water (c)

6. The mill was allowed to run for a preset time. The mill revolutions were checked by a stroboscope and the torque (in volts) was recorded.

7. After achievement of a particular grind, the mill lid was removed and the mill was gently discharged over a grizzly. The material was washed with water through the grizzly (Figure 3.11) and was collected in buckets for further filtration and drying.

Figure 3.11: Batch mill during its unloading

8. The slurry was filtered using a pressure filter. The cake obtained was dried in an oven for approximately 12 hours, and before proceeding with the size analysis, the cake was disaggregated in order to eliminate the flakes that can interfere in the size analysis by sieving as showing in Figure 3.12.

Figure 3.12: Iron ore cake and flakes disaggregation

9. The dry product was weighed and split using a Rotary Sample Splitter (SEPOR) to obtain two representative samples of about 500 grams each (Figure 3.13 a). One of the samples was then sieved using a set of Tyler $\sqrt{2}$ series interval screens from 3.35 mm down to 150 µm (from 6 mesh down to 100 mesh) for 20 minutes on Retsch AS 200 sieve shakers (Figure 3.13 b). The other one was kept in order to check the result, if necessary.

(a) (b)

Figure 3.13: Rotary Sample Splitter (a) and Retsch AS 200 sieve shakers (b)

10. The -150 µm product was wet screened using Retsch AS 200 sieve shakers from 106 µm down to 38 µm (from 150 mesh down to 400 mesh) for 8 minutes (Figure 3.14). The -38 µm slurry was dewatered using a pressure filter. The cake obtained was dried in an oven set to the temperature of 100º Celsius.

Figure 3.14: Retsch AS 200 sieve shaker fitted with the wet screening rig

11. Finally, an AE ADAM HighlandTM scale was used to weigh each size fraction in order to determine the particle size distribution after each grinding time. Then each screen was carefully cleaned to ensure the recovery of all the material sieved (Figure 3.15).

Figure 3.15: AE ADAM Highland^{TM} scale

12. In the case of mono-size experiments, after sieve analysis, the total sample was weighed and additional -38 µm material was added to make up for any weight loss (typically less than 0.4%) presuming the losses in handling were of very fine particles. Then, the entire charge returned to the ball mill for the next grinding interval.

13. In the case of experiments of feed with natural size distribution, the total amount of material used for each test condition was previously weighted and, using the rotary sample splitter, the samples for each grinding time were kept separately and no subsequent grinds were carried out. The feed particle size distribution was determined before each batch test.

3.4.2 Pilot Mill Experiments

The pilot mill was used to validate the use of population balance model approach from HERBST and FUERSTENAU (1980) as a predictive model. The experiments were carried out at a fixed feed rate at 1 kg/min, a ball load of 35%, with a top ball size of 30 mm, at 68.3% of critical speed and in a range of solids concentration (74, 76, 77, 79 and 85%). Details of operating conditions and experimental product size distributions of each experimental test are also presented in Appendix I.

The procedure adopted in each pilot-scale mill test consisted of:

1. Initially, an inspection was carried out on all the equipment for any loose parts or anything that could lead to circuit failure, including slurry leakage at mill shell.
2. The mill speed was set to achieve 68.3% of critical speed, corresponding to 46.5 rpm.
3. The no-load torque was recorded and corresponded to 31.38 lbf-in, or 3.55 N.m.
4. The ball size distribution was calculated according to Equation 3.3 and the percentage by weight of each ball size and the ball mass calculation are represented in Table 3.5. The ball density considered was 7.77 g/cm^3.

Table 3.5: Ball size distribution for pilot mill experiments

Ball Size (mm)	*Percentage (% by wgt)*	*Ball Mass (kg)*	*Number of Balls*
30.0	37.0	52.6	404
25.4	47.0	66.6	999
17.0	14.0	20.1	1005
12.7	2.0	3.0	355
Total	**100**	**142.2**	**2763**

5. The water flow rate was calculated so as to achieve the desired slurry solids concentration.

6. The solids and water flow rates were properly calibrated and were set to achieve the desired experimental condition.

7. The torque and weight of the slurry (hold up) contained in the mill were recorded at successive intervals of time. Once the weight recorder displayed values that did not show a consistent decreasing or increasing trend, the steady-state flow condition was identified (see an example at Figure 3.16).

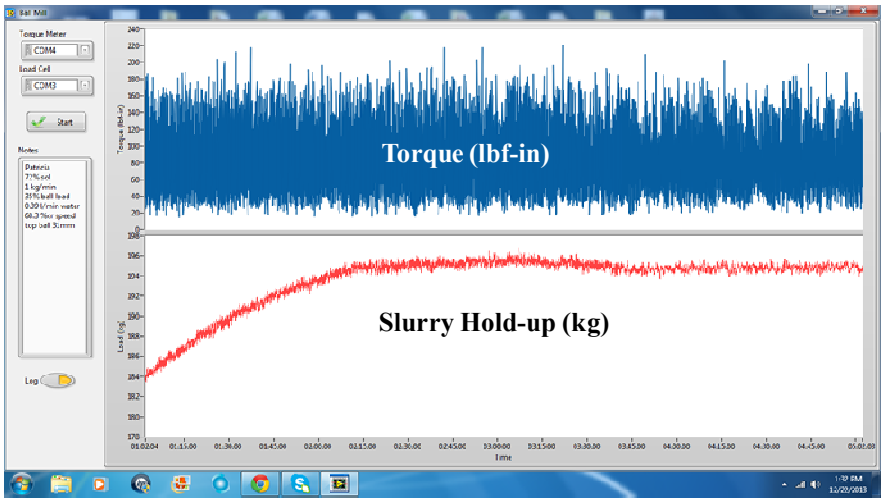

Figure 3.16: Example of torque and weight of the slurry recorded during a pilot mill experiment

8. During steady state conditions, three or more samples were collected, each of which in a time interval of one minute, with the aim of checking the solids flow rate and, therefore, whether or not steady-state conditions were reached. Once it was demonstrated that steady states conditions were reached, those samples were analyzed for particle size distribution and solids concentration. The feed particle size distribution was determined before each pilot test according to the procedure described previously (dry and wet sieve analysis).

3.4.2.1 Residence Time Distribution (RTD) Measurement on the Pilot Mill

In wet grinding, the mean residence time of the solid material in the mill is larger than that of water. As a result, the slurry percent solids inside the mill is supposed to be

higher than the percent solids in the mill feed or discharge (DAVIS, 1946; SONGFACK, 1996). Nevertheless, in this study, the assumption that the slurry density in the mill is the same as the slurry density of the mill feed and discharge was considered. Therefore the residence time of the solids is assumed to be the same as the residence time of water.

The experimental determination of the residence time distribution functions was accomplished through stimulus-response technique using a sort of tracer material in the inlet-fluid stream. The injection is the stimulus and the response is the tracer concentration measured in the outlet stream. The tracer can be a radioactive compound, a colored dye, an electrically conducting salt solution, or another material depending on the particular situation. It should preferably present approximately the same density, viscosity, and other properties as the process stream in order to be a representative measure of the prevailing mixing conditions. Tracer is injected into the inlet stream in some known fashion, such as a step or sudden jump, a pulse, a sine wave or other cycling signal, or even a random signal with known properties.

In the present study, lithium chloride was used as a tracer material for performing the measurement of the residence time distribution. The experimental work was conducted as follows:

1. Approximately 20 grams of lithium chloride was used in each pilot experiment.
2. The tracer material was dissolved in 200 ml of water and once the steady state condition was reached the tracer was injected in the feed stream near the feed end of the mill.
3. The times of tracer injection and sample collection were synchronized.
4. The duration of sample collection was estimated to be at least three times the average retention time, estimated on the basis of mill hold-up and feed flowrate.
5. Subsequently the mill discharge was sampled following a specified time interval.
6. The slurry sample collected was kept in rest to allow the solids to settle and the filtrate conductivity was then analyzed using a conductivity analyzer (Figure 3.17). After that, the filtrate conductivity was converted to parts per million of lithium chloride concentration according to a calibration curve (lithium chloride concentration versus conductivity), determined previously (see Appendix IV).

Figure 3.17: Filtrate conductivity analysis

3.4.3 Vale's Industrial Mill

3.4.3.1 Sampling Campaigns

The closed grinding circuit at Vale's pelletizing plant chosen for the optimization study was sampled using Vale's standard procedure and the mass balance was carried out in order to calculate the classification curve.

Vale's standard procedure used during the sampling campaigns consists of:

1. Firstly, the mill operational conditions (feed rate, percent of solids, number of cyclones in operation) are set according to the desired experimental condition.
2. After 2 hours of process stability, the sampling campaign is started.
3. During additional 2 hours, the samples are collected in four points: fresh feed conveyor, cyclone feed, cyclone underflow and overflow.
4. In order to compose the sample of each point, the samples are collected every 15 min.
5. The slurry density inside the mill is also measured during the sampling time and the feed rate, mill power and hydrocyclones inlet pressure are recorded by automation system.
6. Finally, the size analysis and solids concentration measurements are carried out in each composed sample.

Three sampling campaigns were carried out and the operational conditions of the ball mill circuit and the solids concentration measured during these samplings are summarized in Tables 3.6 and 3.7, respectively. The top ball size, ball filling and the

percentage of critical speed were maintained constant at 30 mm, 31% and 68.3%, respectively.

Table 3.6: Operational conditions of the ball mill circuit during the sampling campaigns

Campaign	*Net Power (kW)*	*Fresh Feed (ton/h) (dry basis)*	*Cyclone Pressure (kgf/cm^2)*
# 1	3405	220	0.96
# 2	3378	237	0.86
# 3	3463	236	1.07

Table 3.7: Solids concentration (% by wt) measured during the sampling campaigns

Process	*Campaign # 1*	*Campaign # 2*	*Campaign # 3*
Fresh Feed	91.0	91.0	91.0
Cyclone Feed	59.7	64.2	61.0
Cyclone Overflow	31.4	35.5	30.4
Cyclone Underflow	83.1	84.5	84.1
Mill Discharge	82.8	83.5	84.6

The RTD was measured according to the same procedure described above. In this case 9.9 kg of lithium chloride was dissolved in 5 liters of water. The Figure 3.18 illustrates the lithium chloride addition point and the sampling point where the slurry with tracer was collected. The figure also shows the sampling points for mass balance calculation.

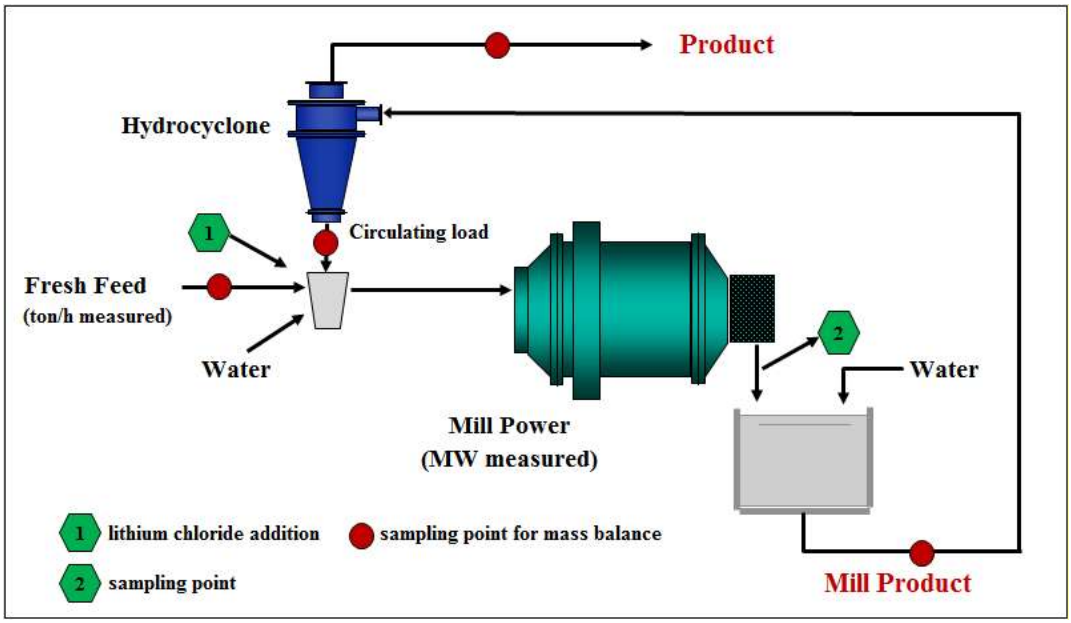

Figure 3.18: Sampling points at Vale's industrial mill circuit

3.4.3.2 Laser Scan of the Mill Internals

In order to provide data to understand how media motion changes as liners become worn and, in addition, provide data for DEM simulations with the purpose of integrating its outcome with the UFRJ mechanistic ball mill model, the mill liners were periodically laser scanned.

The mill internals were laser scanned by a technical expert from Outotec and the liner shape information was provided by the MillMapper® software, also from Outotec.

The methodology used for quantifying the liner wear was the same as the one applied and demonstrated by TOOR *et al.* (2011). The measurements were scheduled for one full liner life cycle (considering bar-plate design) and one measure was carried out considering a new design (symmetric or simple wave). For each laser scan survey, the liner shape, the liner wear and the ball filling were provided by MillMapper® software. The survey protocol and the average of the mill power recorded in the period of the laser scan measurements are presented in Table 3.8.

Table 3.8: Survey protocol and the mill power

Date	*Survey*	*Liners Design*	*Mill Power (kW)*	*Notes*
11/13/2012	# 1 (worn)	bar-plate	3419	Data collection at the end of previous liner life
12/04/2012	# 2 (new)	bar-plate	3403	Data collection immediately prior to reline
06/11/2014	# 3 (mid life)	bar-plate	3353	Data collection at approximately mid life.
11/10/2014	# 4 (new)	simple wave	3222	Data collection immediately prior to reline

Before each measurement the mill was "washed" for approximately 20 min in order to clean its internals (liners and balls). This washing consists in reducing the mill slurry density from 3.0 to 1.7 ton/m^3 approximately, through a high flow of process water that comes from the overflow of the thickener (unit operation that follows grinding), while the mill remains in operation.

After mill washing and cooling, the technician from Outotec centralized the laser scanner in the middle of the mill to collect the measures. After less than 20 minutes the high-quality scan images were completely generated.

The results obtained by laser scan surveys provided very good information about the wear trend of the liner/lifters, ball filling and also an estimate of the probable date that the liners could fail. Those information are important in the operational routine of liners monitoring. Figure 3.19 shows an example about the information that was provided by MillMapper® software using the laser scan data. This figure demonstrates the thickness of the liner in a cross sectional profile at mill shell, showing the difference between the liner wear trend from the beginning of the life cycle to its mid life.

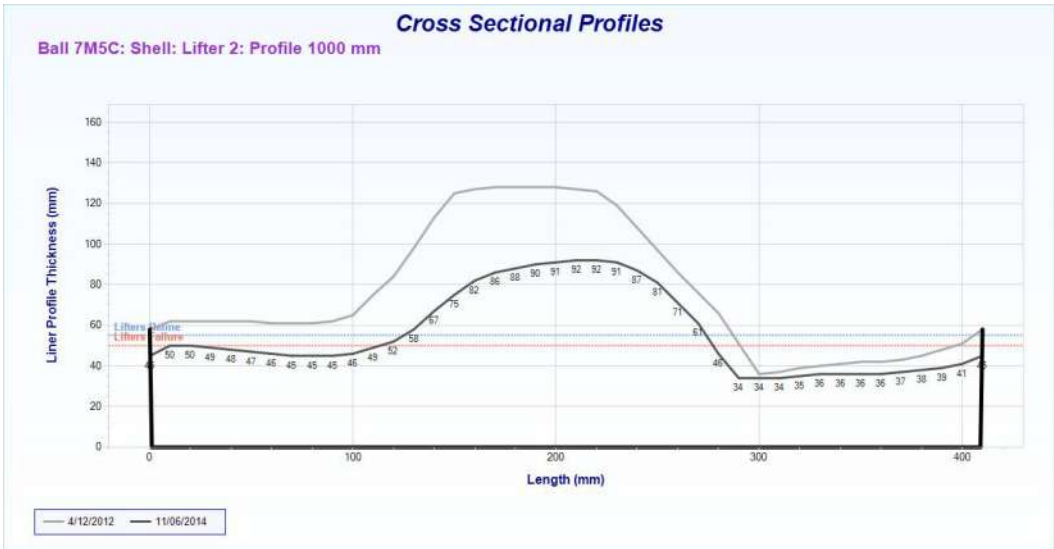

Figure 3.19: Thickness of the liner in a cross sectional profile at mill shell

Figure 3.20 shows the thickness of the inner liner in a cross sectional profile at mill discharge. As expected, the wear in this part of the mill is higher than in the mill shell. Generally, the liner in this area needs to be changed with greater frequency than the whole mill. For the same region, mill discharge, Figure 3.21 illustrates in 3D the liner thickness, showing in red the damaged lining region.

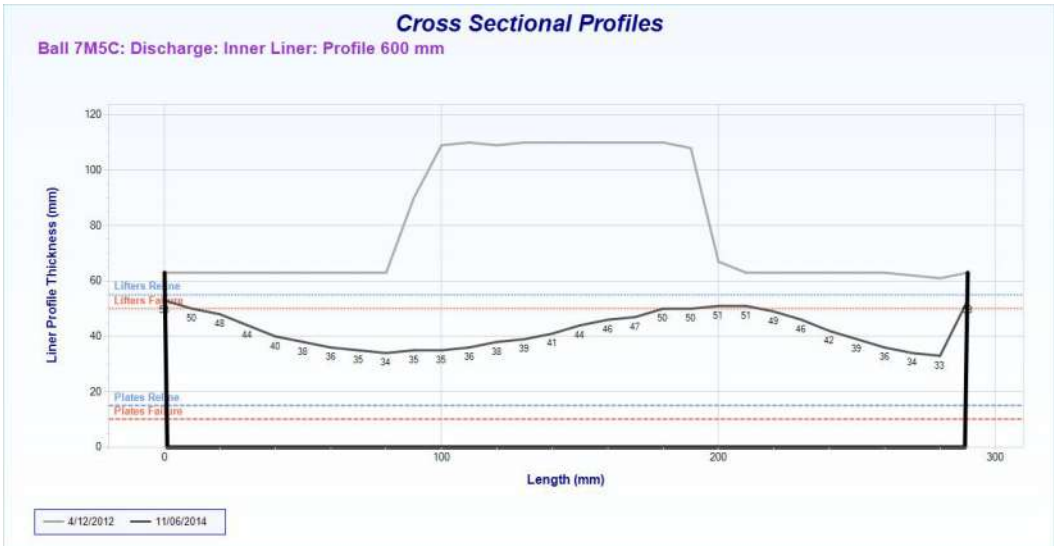

Figure 3.20: Thickness of the inner liner in a cross sectional profile at mill discharge

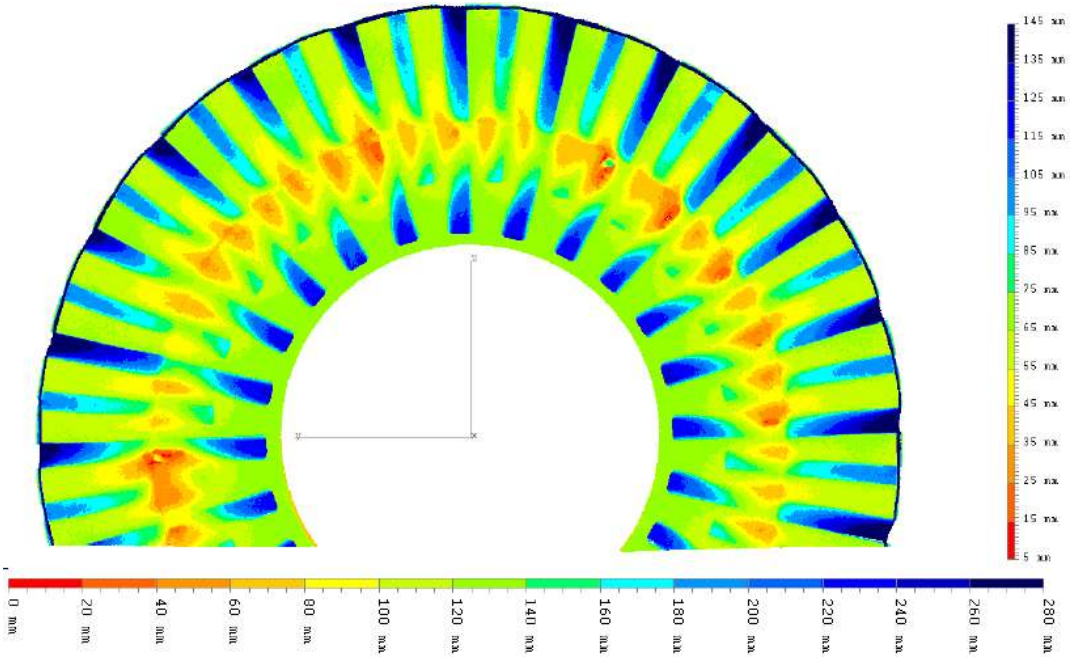

Figure 3.21: Mill discharge – 3D graphic of the liner thickness showing in red the damaged lining region (survey 3)

The values of ball filling measured at the moment of laser scan surveys are listed in Table 3.9. These values were in close agreement with the values collected from the manual measurement that is carried out periodically by Vale's technicians.

Table 3.9: Ball filling at the moment of laser scan survey

Date	***Survey***	***Ball Filling (%)***
11/13/2012	# 1 (worn)	33.4
12/04/2012	# 2 (new)	31.7
06/11/2014	# 3 (mid life)	29.8
11/10/2014	# 4 (new)	29.3

In order to integrate the information from the laser scans and the mechanistic mill model, only two scans were considered, corresponding to the extreme conditions throughout the life of a set of liners: new liners (#2 survey) and nearly fully worn liners, after about 12,000 hours of operation (#1 survey) (Figure 3.22). Wear along the mill is not homogeneous, being more severe in the central longitudinal portions. As such, in order to generate realistic geometries that would lead to useful collision energy spectra

from DEM simulations, it was opted to consider the average profile along the longitudinal length of the mill.

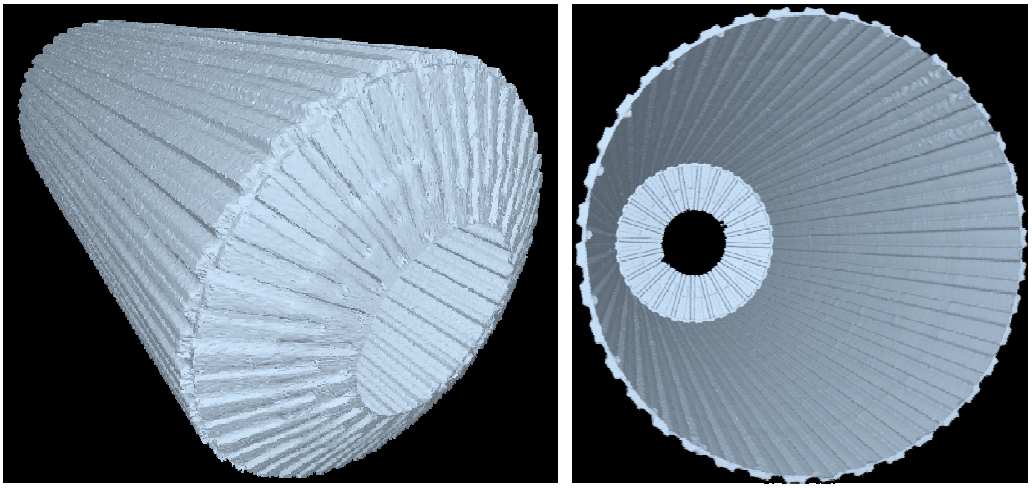

Figure 3.22: 3D laser scan of the mill

The cross section of this average profile is illustrated in Figure 3.23, which superimposes the average profiles in the beginning and the end of the service life. It is evident that the magnitude of the wear is not as significant as in the case of SAG mills (TOOR *et al.*, 2013), suggesting that the change in collision energy spectra during the life of liners will likely be limited.

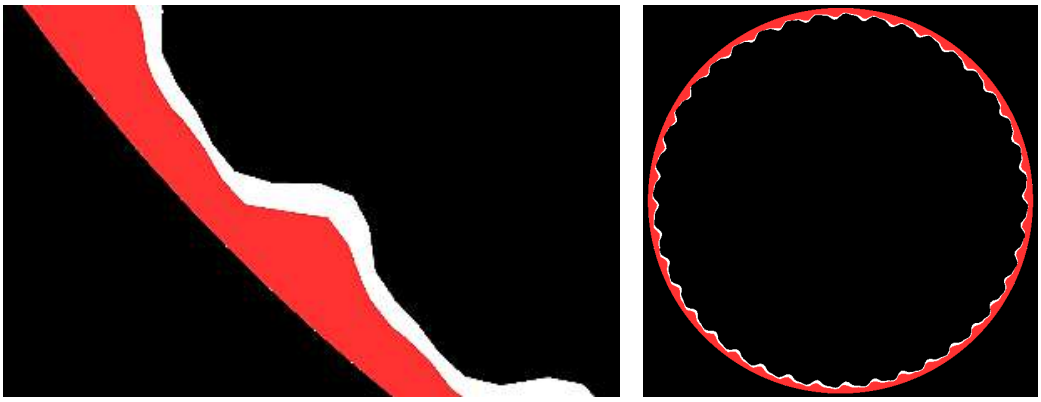

Figure 3.23: Superimposed average liner profile for Vale's industrial mill: white is the new liner and red represents the liner in the end of service life

3.5 UFRJ Mechanistic Model Approach

3.5.1 Particle Breakage Characterization

Unfortunately, material was not available for single-particle breakage testing, which is the basis for applying the UFRJ mechanistic mill model. Nevertheless, earlier work by CARVALHO and TAVARES (2013) contained data from an iron ore with similar characteristics, so it was used as a starting point for the simulations. These results are presented in Table 3.10. These parameters were estimated on the basis of drop weight, impact load cell and tumbling mill tests (TAVARES, 2007).

Table 3.10: Summary of particle breakage parameters of an iron ore (CARVALHO and TAVARES, 2013)

Breakage parameters	***Iron ore #1***
σ_∞	0.46
σ_0 **(mm)**	1.00
σ^*	0.00
$\alpha_{1.2}/\beta_{1.2}$	0.98/5.99
$\alpha_{1.5}/\beta_{1.5}$	1.01/5.01
α_2/β_2	1.36/3.80
α_4/β_4	1.22/2.17
α_{25}/β_{25}	0.95/0.67
α_{50}/β_{50}	0.89/0.48
α_{75}/β_{75}	0.92/0.41
γ	3.00
ρ_{ore} **(g/cm³)**	4.35
β **(-)**	0.62
A **(%)**	60.40
b' **(-)**	0.051
t_a **(%)**	1.60
d_A **(mm)**	0.21
λ **(-)**	0.30

Figure 3.24 shows the appearance function modeled using the incomplete beta function for iron ore #1 from CARVALHO and TAVARES (2013), whereas Figure 3.25 shows the relationship between the ratio between the impact energy and median fracture energy and the resulting t_{10} used to estimate the single particle breakage function.

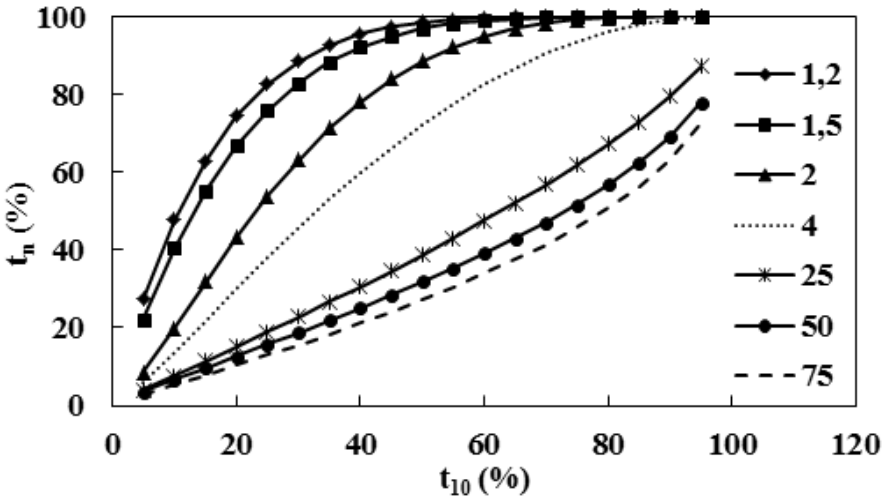

Figure 3.24: t_{10} versus t_n (for n values of 1.2 to 75) relationship for iron ore #1 (CARVALHO and TAVARES, 2013)

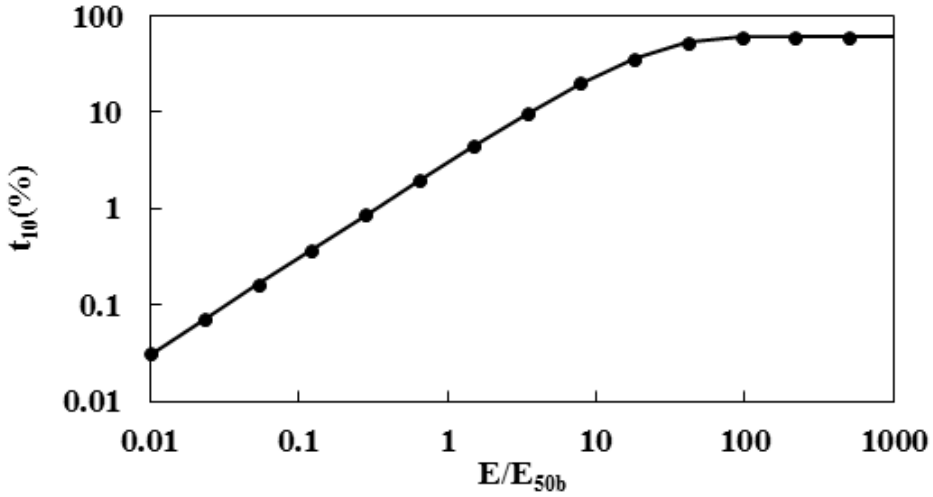

Figure 3.25: t_{10} versus impact energy for iron ore #1 (CARVALHO and TAVARES, 2013)

The approach used in the present work consisted of back-calculating the parameters of the particle fracture energy model (E_∞, d_o and ϕ) as a function of size (Equation 2.59), given by TAVARES and KING (1998), on the basis of data from batch grinding tests, while assuming that the remaining parameters for the reference iron ore (Table 3.10) remain valid for the sample from the present study.

3.5.2 Discrete Element Method

Simulations of the charge motion were carried out using the software EDEM provided by DEM Solutions (2014). EDEM allows importing the CAD geometry generated either from drawing software or from the 3D laser scanning. The contact parameters were selected from a previous study (CARVALHO, 2013) describing the interactions of grinding media with liners and fine iron ore particles (Table 3.11).

The energies dissipated in each of the collisions during 5 seconds of analyzes were registered and post-processed using the software LTM Analyst (CARVALHO, 2013) to generate the collision energy spectra.

Table 3.11: Material and contact parameters for DEM simulations

Parameter	***balls and liner***		
Poisson's ratio	0.30		
Shear modulus (Pa)	$70x10^8$		
Density (kg/m³)	7770		
Contact	***Restitution coefficient***	***Static friction coefficient***	***Rolling friction coefficient***
Ball-ball / Ball-liner	0.35	0.32	0.28

4. RESULTS AND DISCUSSIONS

In this chapter the parameter estimation procedure used for predictive simulation using the population balance model is outlined and the application of the non-normalized breakage function to mill discharge prediction is discussed.

A scheme to predict the behavior of grinding in the industrial mill from the data obtained in the 25.4 cm batch mill is presented.

The back-calculation of the fracture energy distribution from the batch data as well as DEM and mechanistic ball mill model simulations of the industrial mill are presented.

4.1 Batch Grinding: Mono-size Tests

Results from the mono-size grinding experiments (3350 x 2360 µm and 150 x 106 µm) carried out at 72% solids, 100% of slurry filling, 40% of ball load (filling) and 68.3% of critical speed are presented in Figures 4.1 and 4.2.

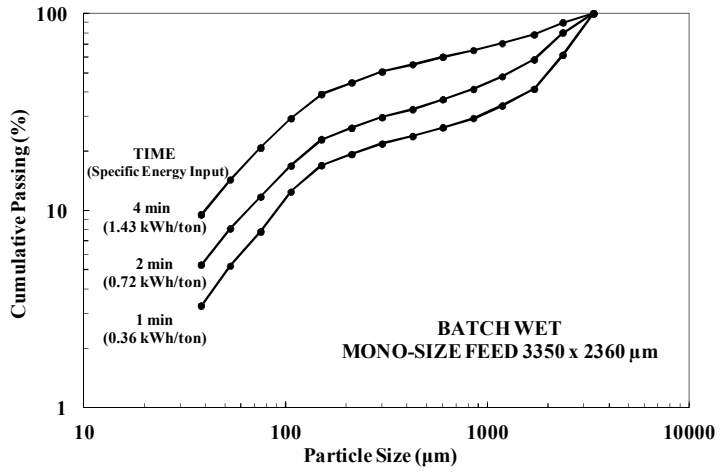

Figure 4.1: Experimental product size distributions for mono-size test 3350 x 2360 µm

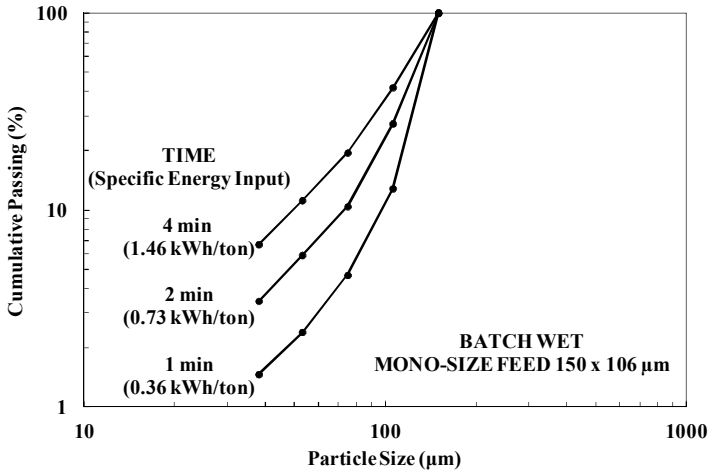

Figure 4.2: Experimental product size distributions for mono-size test 150 x 106 µm

In order to estimate the feed size breakage rate function according to the relationship described by Equation 2.43, the mass fraction retained versus grind time for each mono-size test was plotted (Figures 4.3 and 4.4). In the figures, a deviation from first order breakage rate behavior after about 2 min of grinding can be observed. This behavior was expected once those experiments were carried out wet. Indeed, as mentioned in Chapter 2, the first-order kinetic model has its limitations in wet grinding systems and it should only be applied over narrow ranges of specific energy input where the kinetics would be regarded as "nearly linear". In this case, the initial estimate of feed size breakage rate was obtained from the slope of the curve considering the first two grind times (1 and 2 min), which constitute the coarse grind or "nearly linear" region in the wet grinding system. The values of S_1 from each mono-size experiment are summarized in Table 4.1.

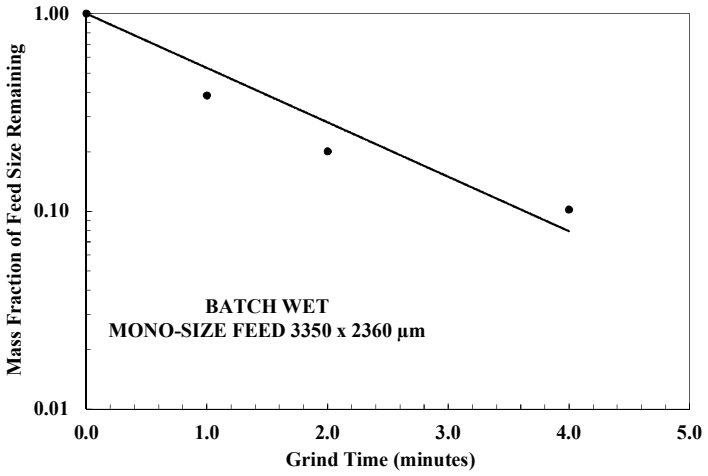

Figure 4.3: Feed disappearance plot for mono-size feed 3350 x 2360 µm

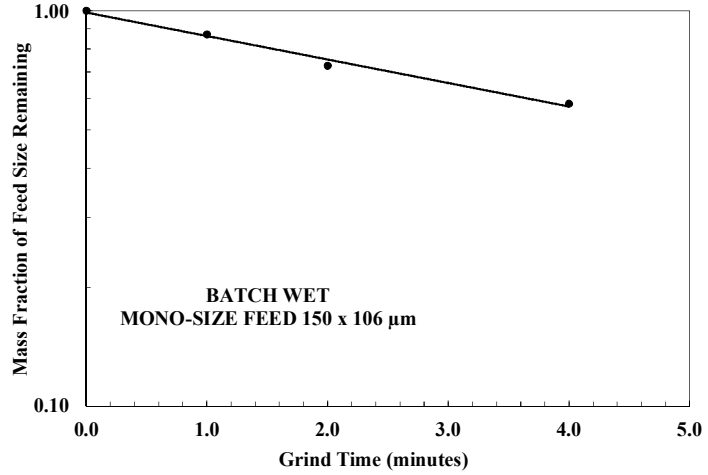

Figure 4.4: Feed disappearance plot for mono-size test 150 x 106 µm

Table 4.1: Initial estimates of feed size breakage rate in mono-size grinding tests

Mono-size Feed (µm)	S_1 ***(min^{-1})***
3350 x 2360	0.6512
150 x 106	0.1544

The feed size breakage function (B_{i1}) was calculated according to Equation 2.44, where the slope, F_i, measured at a short grind time (1 min) was estimated by plotting the cumulative fraction finer than size x_i versus time. The wet grinding nonlinearity also becomes evident through this relation, as illustrated in Figures 4.5 and 4.6.

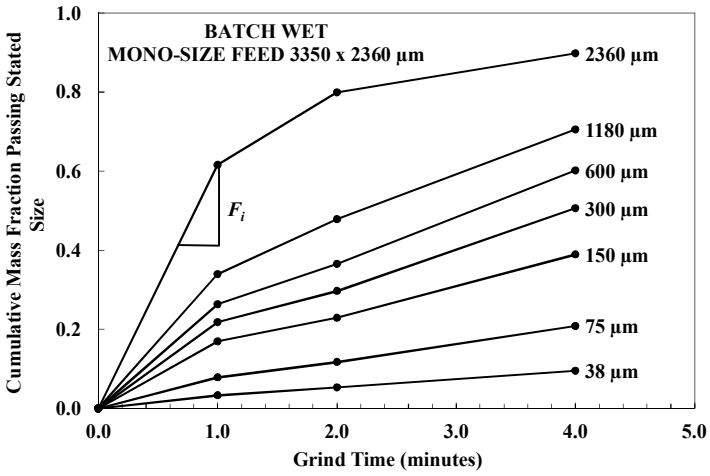

Figure 4.5: Zero order production rate plot for mono-size feed 3350 x 2360 µm

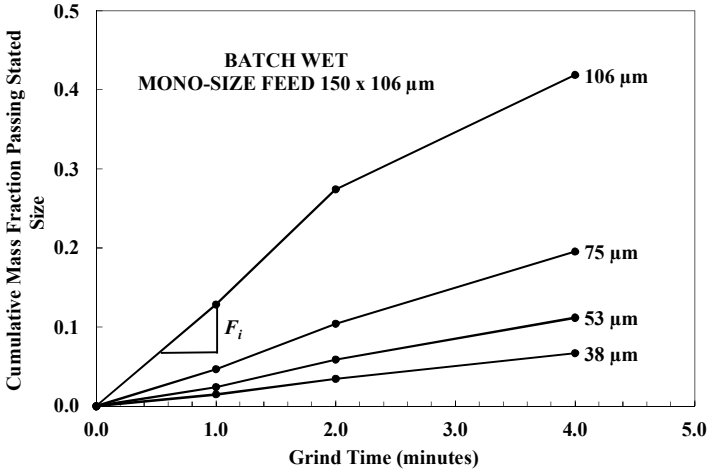

Figure 4.6: Zero order production rate plot for mono-size feed 150 x 106 µm

The estimated cumulative breakage distribution function for the two sizes analyzed is shown in Figure 4.7, which demonstrates the non-normalizable nature of the ore breakage pattern.

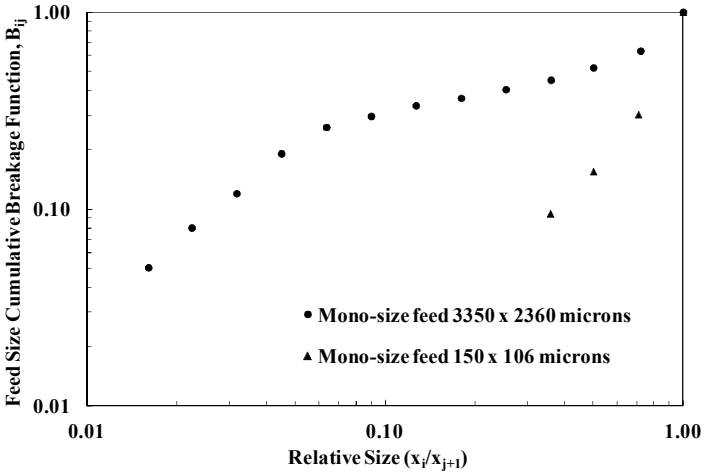

Figure 4.7: Feed size cumulative breakage function for the two sizes analyzed

This ore breakage pattern can be justified by the presence of considerable silica content in the ore blend, mainly in the coarse fraction, characterizing a heterogeneous material. Such response may also be explained by the weak intergranular bonding among the individual grains that make up the ore (TAVARES, 2000), leading to a depletion of material in selected size ranges and accumulation in others. The result is that the breakage distribution functions may be normalized with respect to the feed-size material. As such, an estimation scheme based on interpolation between the two breakage distribution functions was proposed, given the difficulty of performing experiments with each feed size. Figure 4.8 compares the measured results to the interpolated results, which accounted for this non-normalizable character of the ore.

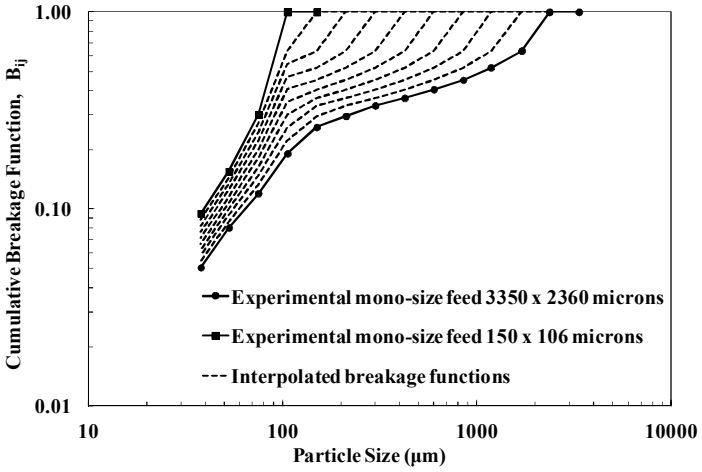

Figure 4.8: Experimental and interpolated breakage functions for wet grinding in the 25.4 cm diameter mill

Once the breakage functions were estimated, the individual breakage distribution functions values (b_{i1}) were estimated using Equation 2.45. Fortunately, results from previous studies (KIM, 1974, SIDDIQUE, 1977, HERBST *et al.,* 1985) suggest that the breakage functions for a given material is fairly insensitive to mill variables, so that they may be considered approximately independent of mill speed, ball load and particle load. Therefore, the b_{ij} values were considered as constants in the predictive simulations where the PBM approach was used. Detailed values of B_{ij} are shown in Appendix III.

4.2 Batch Grinding: Natural Feed Size

In this section, data obtained in the 25.4 cm diameter mill were used to demonstrate the application of the population balance model approach to optimizing ball milling in iron ore grinding as well as to test the predictive capability of this model.

As presented in detail in the methodology chapter, the variables investigated using this methodology were solids concentration, top ball size and slurry filling. Table 4.2 summarizes the conditions used in the batch wet grinding experiments.

Table 4.2: Batch wet experimental conditions

Batch Experiment Designation	*Tests Conditions*		
	Percent Solids (%)	*Slurry Filling (%)*	*Top Ball Size (mm)*
B3	72	100	30
B4	76		
B5	80		
B6	72	260	30
B7	76		
B8	80		
B9	72	100	25

Since the breakage functions are assumed to be independent of the environment, the selection function, described by Equation 2.47, was the function fitted for each experimental condition listed in Table 4.2. Firstly, the estimation of the selection function parameters (S_1 and ζ_1) was made using the non-linear regression program Estimill, from the initial estimation of $S_1 = 0.6512$ min^{-1} (Table 4.1) and $\zeta_1 = 0.5$ (as recommended by the EstiMill_User Manual). Secondly, these initial estimates needed to be improved, also using the Estimill software, considering the specific energy input. The resulting values of S_1^E and ζ_1^E that were estimated corresponded to the least squares best fit of the batch wet grinding model. Simulations considering the 3-parameters breakage rate function (S_1, ζ_1, ζ_2 - Equation 2.35) were also carried out, but the RMS (root mean of squares of residuals) was actually higher when comparing to the value obtained with simulations considering 2-parameters breakage rate function (S_1, ζ_1).

Since the specific selection function (S_i^E) is considered to be strongly dependent on the size consist in the mill in wet grinding, this function was estimated over a narrow range of specific energies corresponding to those that approximately matched the specific energy input to Vale's industrial grinding mill. In this case, the S_i^E was estimated on the basis of the batch grinding experiments that used the natural feed (minus 2360 μm), which correspond to the similar fineness of industrial mill feed and based on the specific energy range described in the Table 4.3. These values were chosen according to the actual specific energy range of the industrial mill, considering the mill net power.

Table 4.3: Specific energy ranges selected to estimate S_i^E

Specific Energy of Batch Experiments			
B3 (kWh/ton)	**B4 (kWh/ton)**	**B5 (kWh/ton)**	**B9 (kWh/ton)**
4.40	3.84	4.59	4.39
5.87	5.12	5.73	5.85

Figures 4.9 to 4.12 show the comparison of experimental product size distribution and "similar fineness of grind" prediction for wet grinding in 25.4 cm mill for each batch test condition. The agreement between experimental and predicted product size distributions confirms the validity of the method based on the so-called "similar fineness of grind procedure".

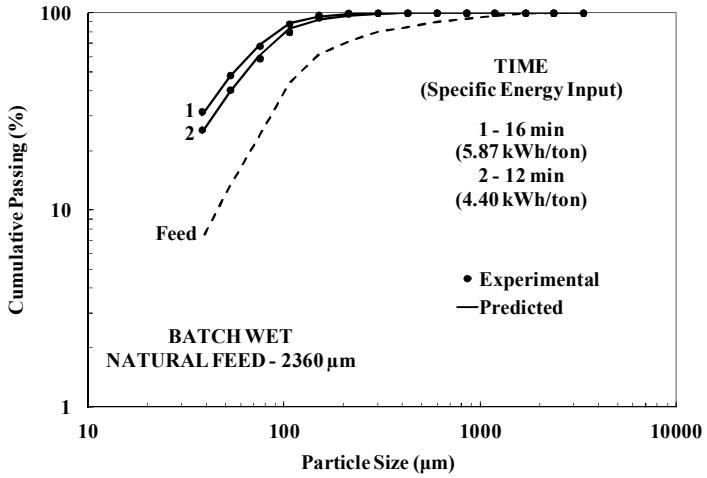

Figure 4.9: Comparison of experimental product size distribution and "similar fineness of grind" prediction for B3 test condition

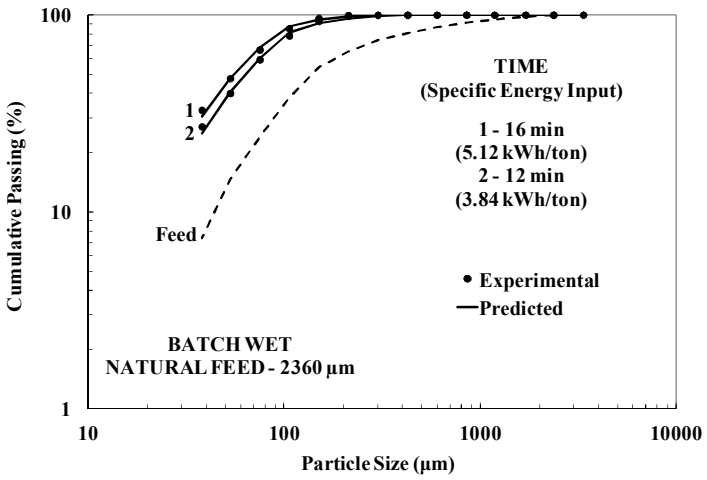

Figure 4.10: Comparison of experimental product size distribution and "similar fineness of grind" prediction for B4 test condition

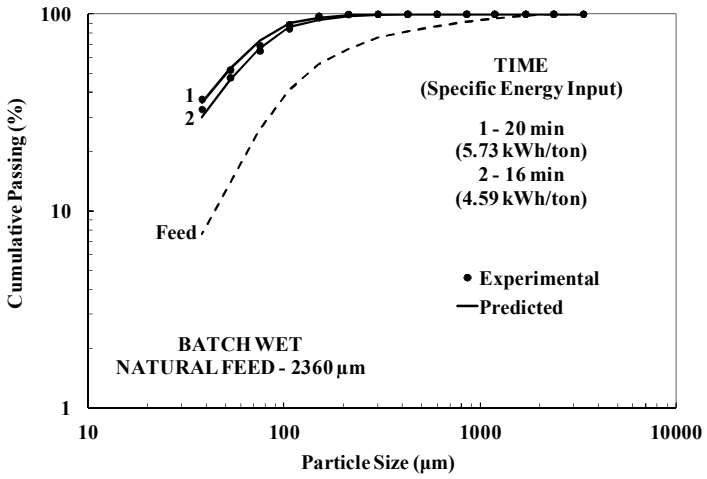

Figure 4.11: Comparison of experimental product size distribution and "similar fineness of grind" prediction for B5 test condition

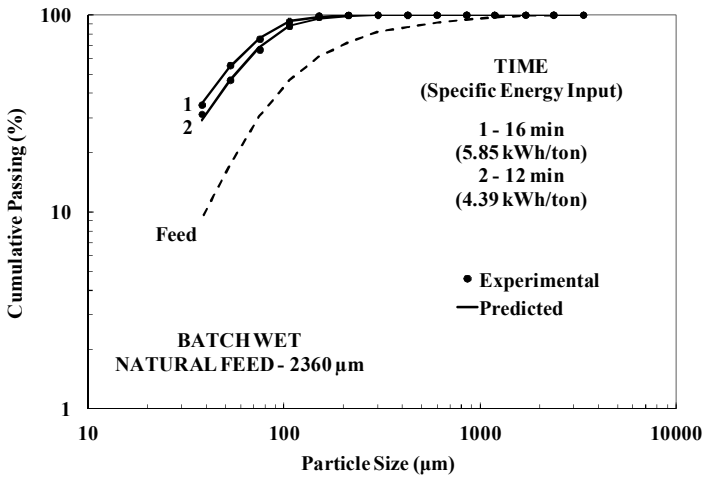

Figure 4.12: Comparison of experimental product size distribution and "similar fineness of grind" prediction for B9 test condition

The specific selection functions estimated for each experimental condition are plotted in Figures 4.13 and 4.14. They illustrate the dependence of specific selection functions on solids concentration and top ball size. Apparently the effect of change in top ball size was more significant than the variation in solids concentration, within the range of conditions tested. However, comparing to the experiments carried out at 72 and 76% solids, the batch experiment conducted at 80% solids presented a different behavior on its specific selection function. It shows a pivoting point at about 150 microns, indicating that particles finer than this size have higher breakage rates than particles of the same size but at different solids concentrations. This behavior could favor a greater fines generation when particles become finer than 150 microns, considering in this case a slurry filling of 100%. Details of S_i^E are shown in Appendix III.

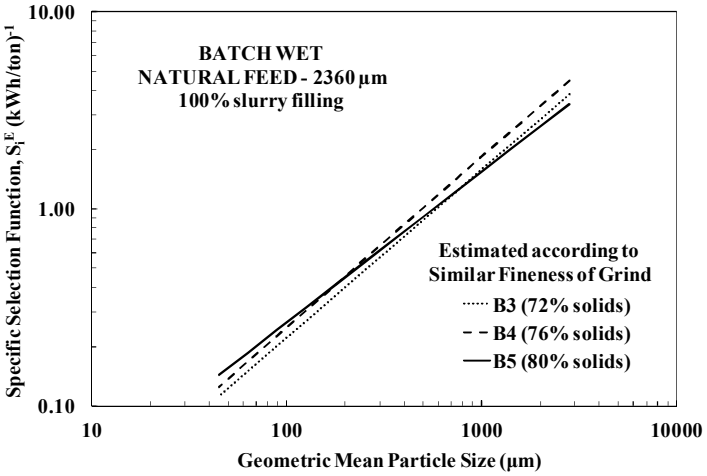

Figure 4.13: Specific selection functions estimated according to similar fineness of grind considering the influence of percent solids

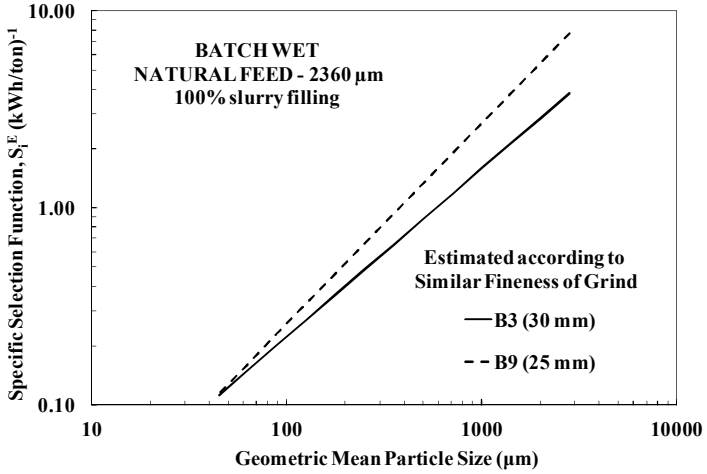

Figure 4.14: Specific selection functions estimated according to similar fineness of grind considering the influence of top ball size

The change in the specific selection function when the top ball size was reduced from 30 mm to 25 mm (Figure 4.14) shows that the specific breakage rates are higher when the top ball size is smaller. In other words, for this specific iron ore the top ball size of 25 mm could generate more fines during grinding probably due to the increased frequency of impacts that result from the larger number of smaller balls in the mill. MARTINOVIC *et al.* (1990) in their work with iron ore from Carol Pellet Plant found that the overall grinding efficiency could be improved by appropriately decreasing the

ball sizes. Indeed, the behavior found in their work (Figure 2.28) for the specific selection functions was very similar to the one shown in Figure 4.14.

Despite the fact that in some studies the breakage functions can be influenced by process variables (mainly the top ball size), in this estimate, the breakage function was considered to be the same as that determined with 30 mm of top ball size, which means that the influence of top ball size in this function was not considered. This consideration was made because several studies (MARTINOVIC *et al.* (1990), SAMSKOG *et al.* (1990), AUSTIN *et al.* (2007), etc), as mentioned previously, reported that the breakage functions (b_{ij}) have been found to be to a good approximation invariant with respect to design and operating variables over a wide range of conditions.

The selection function parameters estimated from each batch grinding condition and the mill power are shown in Table 4.4. The mill power was calculated according to Equation 2.11 (KING, 2001) considering the mill rotational speed and the average torque recorded during each experiment. The average torque was subtracted by the no-load torque previously measured. The specific energy input to batch wet experiments are presented in the Appendix II.

Table 4.4: Selection function parameters and the mill net power for tests conducted at 100% and 260% of slurry filling

Batch experiments	S_1 $(min)^{-1}$	S_1^E $(kWh/ton)^{-1}$	ζ_1^E	***Net Power (W)***
B3	1.398	3.816	0.853	81.3
B4	1.438	4.494	0.866	83.2
B5	0.976	3.410	0.766	84.7
B6	1.022	11.351	1.071	51.8
B7	1.499	20.273	1.329	51.3
B8	1.263	18.663	1.341	51.8
B9	2.805	7.666	1.016	83.9

Besides the evaluation of the influence of solids concentration and top ball size in the specific selection function, the influence of slurry filling on this function was also investigated. In this case it was identified that a higher value of slurry or interstitial filling (volumetric slurry hold-up divided by the volume of the ball charge voidage at rest) should be used in order to mimic conditions expected in overflow ball mills.

According to findings by SONGFACK (1996), for the interstitial filling of 100%, the slurry only partially fills the ball charge voidage, and its level is well below the bottom of the overflow opening, so there is not enough slurry to allow for pool formation, resulting in a configuration that is not likely to occur in practical applications involving overflow ball mills. The same behavior was found for a value of the interstitial filling equal to 200%. The dynamic profile showed a small pool formation with not enough slurry to allow for the mill discharge by overflow, because the slurry level is under the lip of the overflow opening. This also does not correspond to a normal mill operation.

As such, the value found by SONGFACK (1996) to be representative of conditions that exist inside a ball mill corresponds to 260% of slurry filling. In this condition, the slurry tends to completely fill the voidage of both the cascading and cataracting portions of the ball charge. A pool of slurry is formed in the bottom of the mill, left of the ball charge and after a few rotations of the mill, the free slurry surface just intersects the overflow opening, allowing the discharge by overflow. The predictions made by the author through simulations were in good agreement with experimental measurements. Despite the fact that this value of slurry filling could vary with the diameter of the discharge trunnion, the value of 260% was used in the present study, owing to similarities between Vale's industrial mill and the industrial mill studied by Songfack.

The product size distribution for each batch grinding condition is shown in Figure 4.15. It is evident that the resulting products of the tests at higher percent slurry filling (260%) were coarser than the products generated from tests conducted with 100% of slurry filling, when comparing the same grind time (12 min) and solids concentration (72%). This difference may be attributed to the combined effect of larger volume of slurry and the reduction of mill power with increased slurry filling. This reduction in mill power at higher slurry filling is due to the shift in the center of gravity of the charge towards the axis of the mill, resulting in a reduction in torque. Indeed, this is evident from Equation 2.10 and the studies of MORRELL (2014), described in Section 2.2.1.

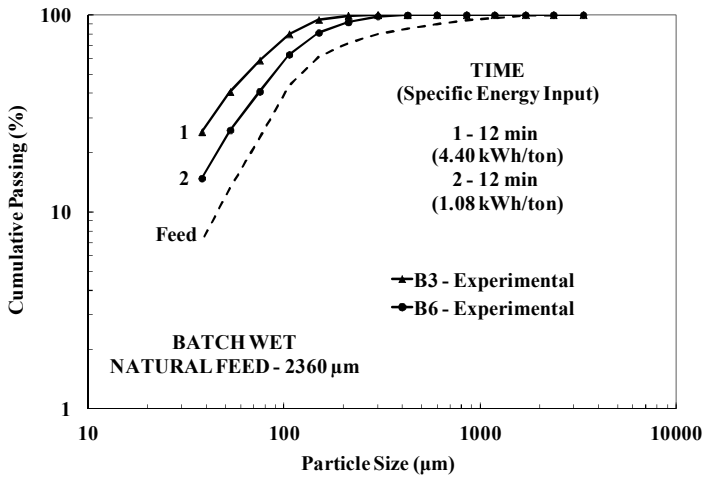

Figure 4.15: Comparison between the product fineness generated in a batch test with 100% of slurry filling (B3) and in a batch test with 260% of slurry filling (B6)

In order to achieve the same product fineness of the industrial mill and consequently a similar specific energy input, the batch experiments conducted with 260% of slurry filling should have been carried out up to, at least, 48 min of grind time. Unfortunately, these experiments were carried out only up to 16 min. As such, in the absence of experimental data with appropriately longer grind times, it was not possible to evaluate this experimental condition into industrial mill environment. Nevertheless, the predictive capability of the PBM was also proven with these batch test results, given the satisfactory agreement between experimental and predicted results shown in Figures 4.16 and 4.17, on the basis of the specific selection function estimated considering grinding data from 12 and 16 minutes.

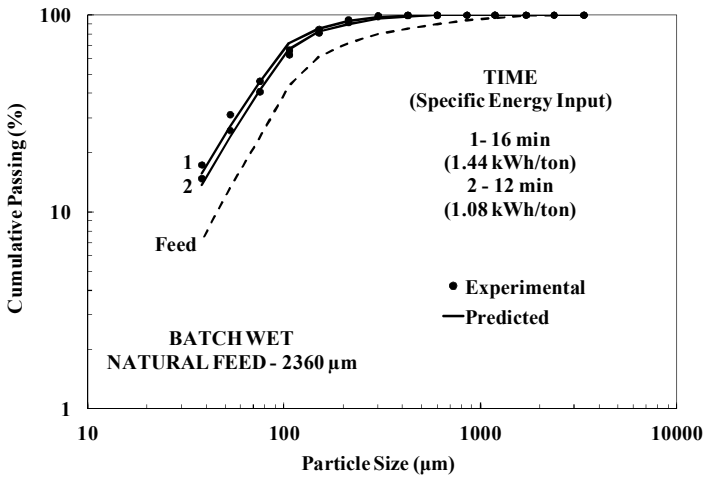

Figure 4.16: Comparison of experimental product size distribution and predicted results for B6 test condition

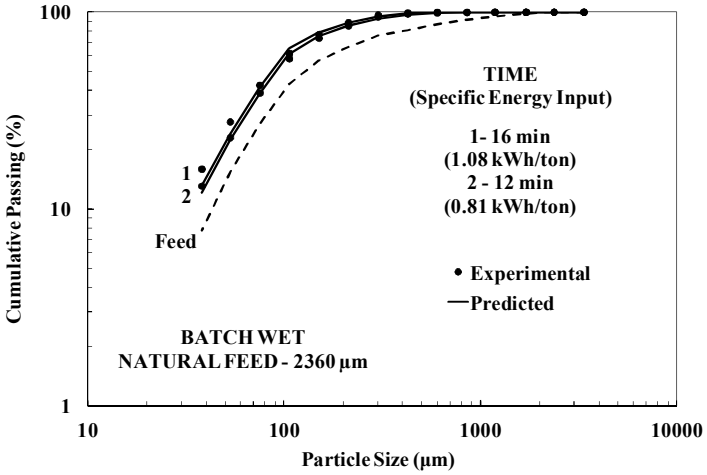

Figure 4.17: Comparison of experimental product size distribution and predicted results for B8 test condition

Figure 4.18 demonstrates the agreement between experimental and predicted results for B7 test condition, with 76% solids and 260% slurry filling. In this case the specific selection function was estimated considering grinding data from 4 and 12 minutes.

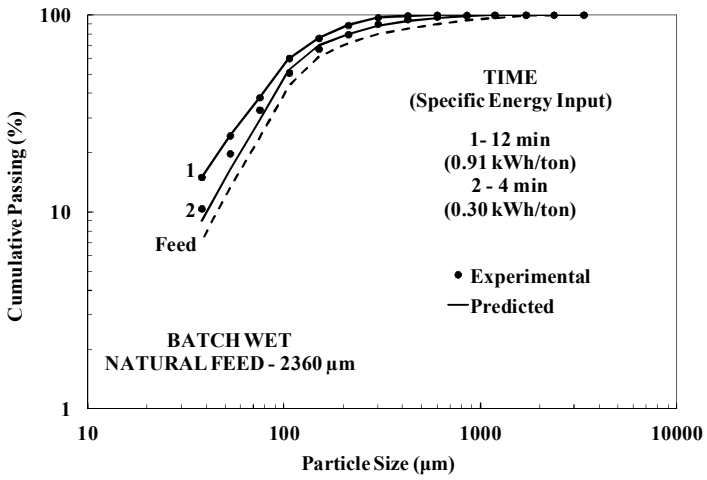

Figure 4.18: Comparison of experimental product size distribution and predicted results for B7 test condition

Figures 4.19 and 4.20 compare the breakage rate functions (S_i) determined at 100% and 260% of slurry filling for tests conducted at 72 and 80% solids, respectively. Parameters of both functions were estimated on the basis of grinding data from 12 and 16 minutes. As shown, batch experiments carried out at 260% of slurry filling presented lower breakage rates than those performed at 100% of slurry filling, regardless of the solids concentration. As previously mentioned, this behavior may be related to the higher volume of slurry, which directly impacts the selection function. As a result, higher breakage rates observed in the batch tests with 100% of slurry filling explain the product size distribution illustrated in Figure 4.15, where for the same time of grinding, the product generated from these experiments was finer than the one obtained with 260% of slurry filling.

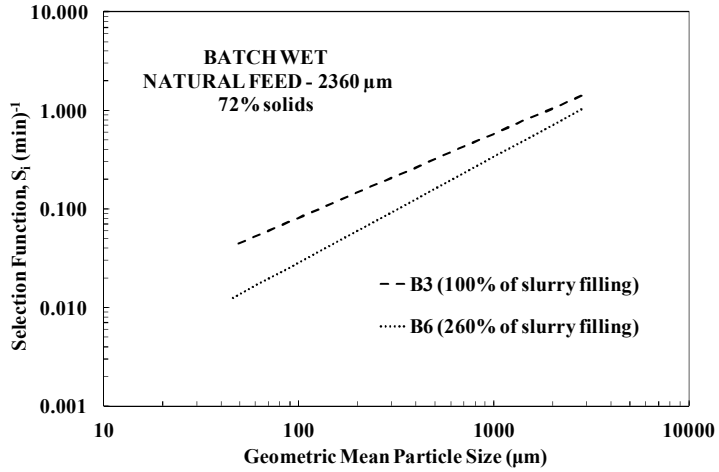

Figure 4.19: Breakage rate functions estimated on the basis of data from the feed, 12 and 16 minutes considering the influence of slurry filling in batch tests carried out with 72% of solids

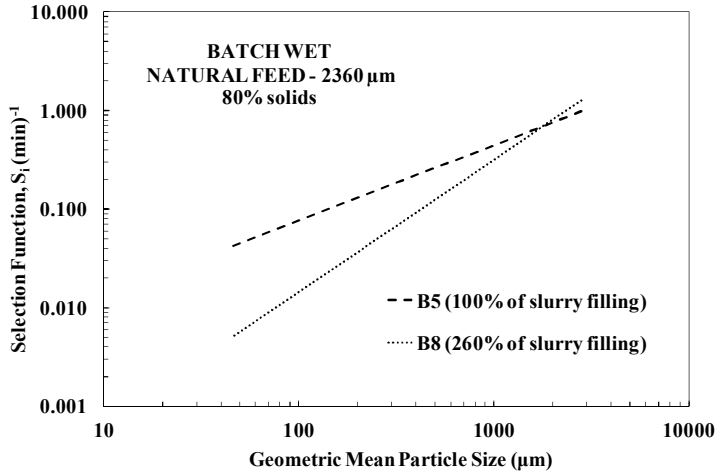

Figure 4.20: Estimated breakage rate functions considering the influence of slurry filling in batch tests carried out with 80% of solids

However, a different behavior of the specific selection functions determined with 260% of slurry filling can be observed in Figures 4.21 and 4.22. The specific breakage rates for this condition are significantly higher for coarse particles, while for particles finer than 150 µm breakage rates decrease and become similar to those corresponding to 100% of slurry filling. In these comparisons, the grinding time was the same but the product fineness was not, because during the batch experiments carried out with higher slurry filling, the net power input to the system was lower. Then, it is not possible to

confirm this same behavior if the experiments had been conducted until reaching the same product fineness. On the other hand, these results are coherent with the low power input and the potentially higher efficiency due to the higher filling of the ball charge voidage.

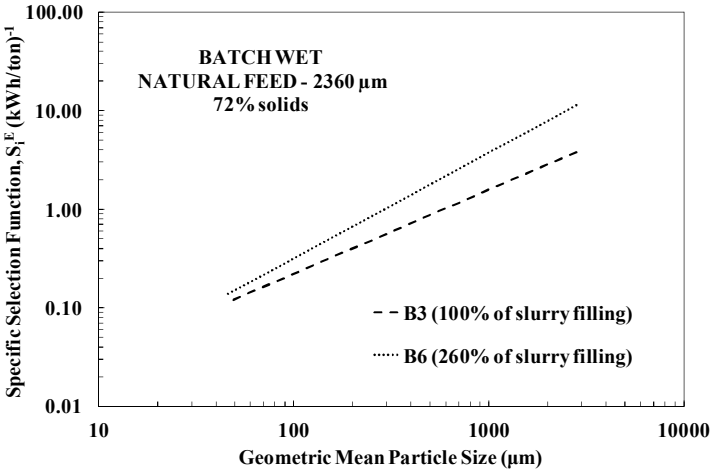

Figure 4.21: Specific selection functions estimated between feed, 12 and 16 minutes considering the influence of slurry filling in batch tests carried out with 72% of solids

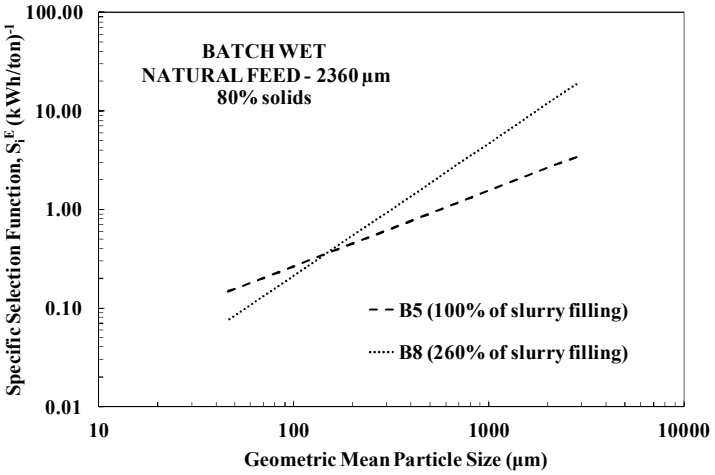

Figure 4.22: Specific selection functions estimated between feed, 16 and 20 minutes for batch test B5 and between feed, 12 and 16 minutes for batch test B8 considering the influence of slurry filling in batch tests carried out with 80% of solids

An additional analysis of the effect of percent solids is possible by comparison of the specific breakage rates at 260% of slurry filling (Figure 4.23) to those estimated from tests at 100% slurry filling (Figure 4.13). In this case, the batch experiment carried out with 72% of solids presented a different behavior on its specific selection function, indicating a pivoting point at about 425 µm, where particles finer than this size have higher breakage rates than particles generated in grinding tests at different solids concentrations. This behavior could favor a greater fines generation when particles become finer than 425 microns.

Analyzing these results it is possible to infer that at higher slurry filling, the lower percentage of solids will favor higher breakage rates for the finer particles. On the other hand, at lower slurry filling, the higher solids concentration will result in higher breakage rates of the finer particles. This behavior indicated that the combination of these two variables has great impact on the specific selection function. The optimal combination could contribute to better grinding process performance. This becomes more evident by analyzing the effect of these two variables on the breakage rate function parameters presented in Table 4.4 (Figures 4.24 and 4.25).

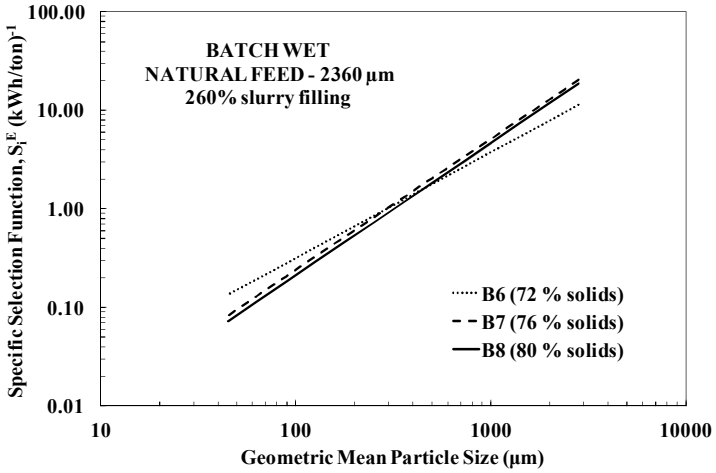

Figure 4.23: Specific selection functions estimated from the batch experiments carried out with 260% of slurry filling and considering the influence of percent solids

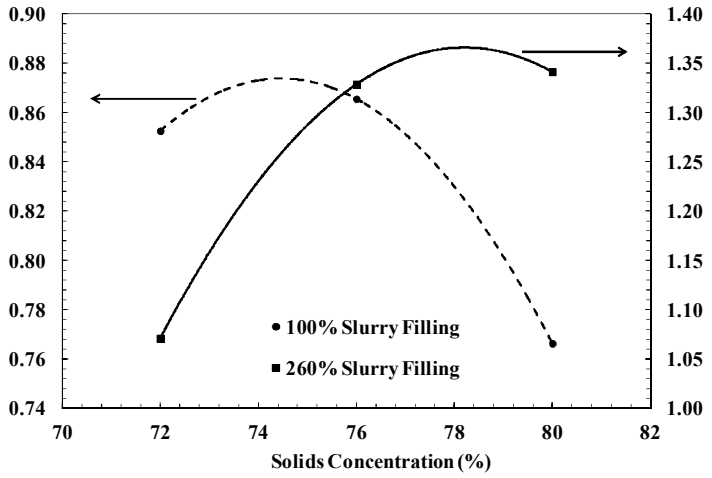

Figure 4.24: Relationship between solids concentration and ζ_1^E from batch tests carried out with 100% and 260% of slurry filling

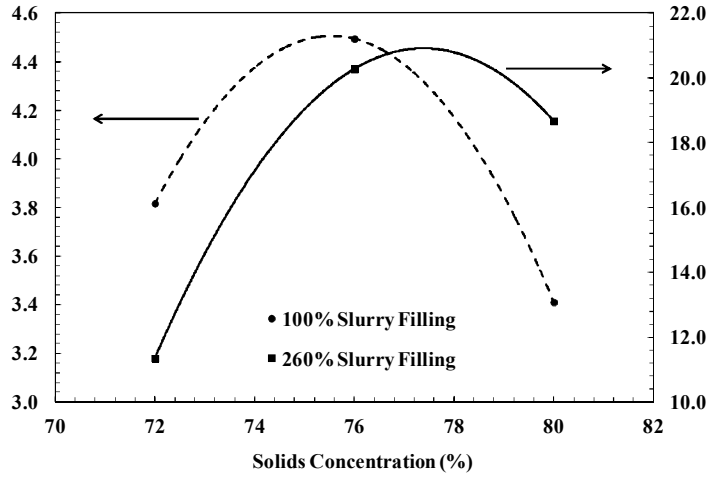

Figure 4.25: Relationship between solids concentration and feed size specific selection function parameter S_1^E (t/kWh) from batch tests carried out with 100% and 260% of slurry filling

4.3 Pilot-scale Mill Simulations

Validation of a model is critical to know if the simulation is an accurate representation of the real system considered. The validation is carried out by comparing the simulation results to what is generally accepted in the real system. As such, in order to validate the use of the population balance model as a predictive model capable of optimizing an industrial mill, the breakage function and selection function parameters fitted to data

from the batch mill were used to predict the performance of the pilot-scale mill for different percent solids, top ball size and slurry filling.

The pilot mill operating conditions are summarized in Table 4.5. The slurry filling was calculated considering the slurry hold up measured through the load cells during the steady state condition.

Table 4.5: Pilot mill experimental conditions

Pilot Experiment Designation	*Tests Conditions*			
	Percent Solids (%)	*Slurry Filling (%)*	*Top Ball Size (mm)*	*Ball Load (%)*
P1	74	167		
P2	76	139		
P3	79	245	30	35
P4	85	204		
P5 (grate discharge)	77	89		

Figure 4.26 summarizes the methodology used for simulation. The residence time distribution, the mill power and the feed size distribution were required, in addition to the selection and breakage functions fitted to batch data, to predict the size distribution of the mill discharge.

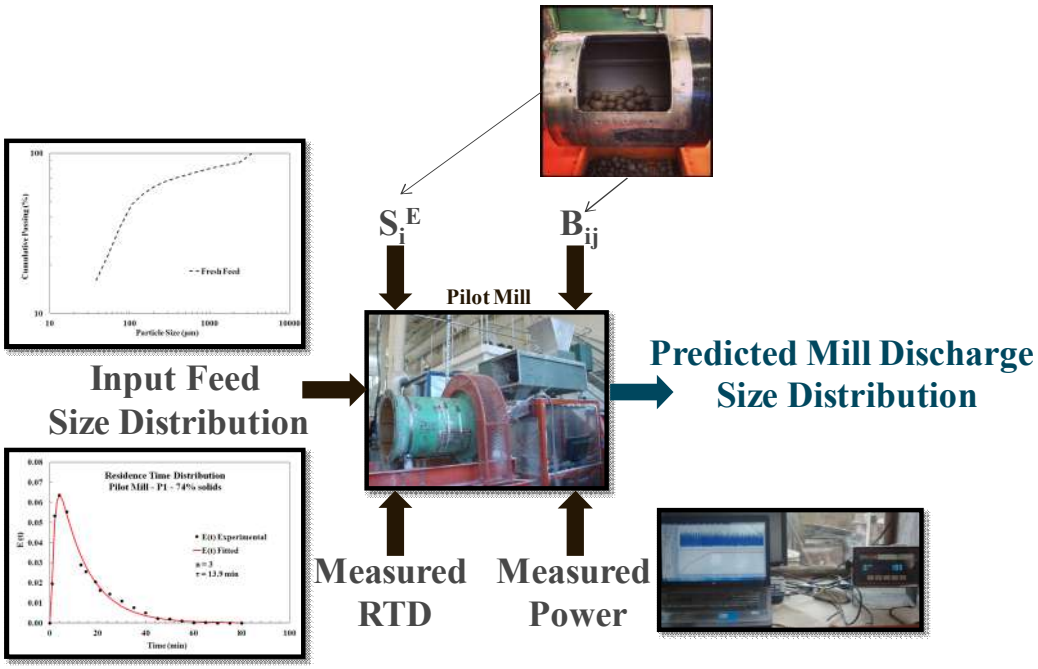

Figure 4.26: Prediction methodology scheme for the pilot scale mill

From the RTD measured using lithium chloride as tracer and the mixers-in-series models described by Equations 2.38 to 2.42, the number of mixers-in-series was estimated. The least squares best fit parameters were estimated using Matlab software. The comparison between experimental data and fitted RTD models for pilot tests P1 and P2 is presented in Figures 4.27 and 4.28, respectively, while results from P3, P4 and P5 are shown in Appendix IV.

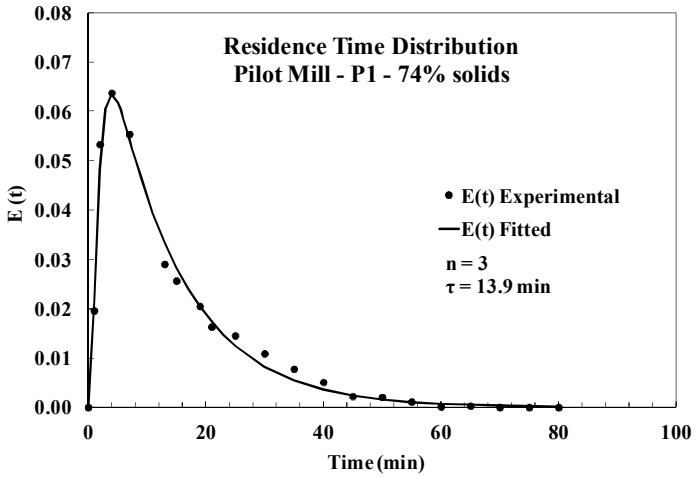

Figure 4.27: Comparison between experimental data and fitted RTD models for pilot test P1

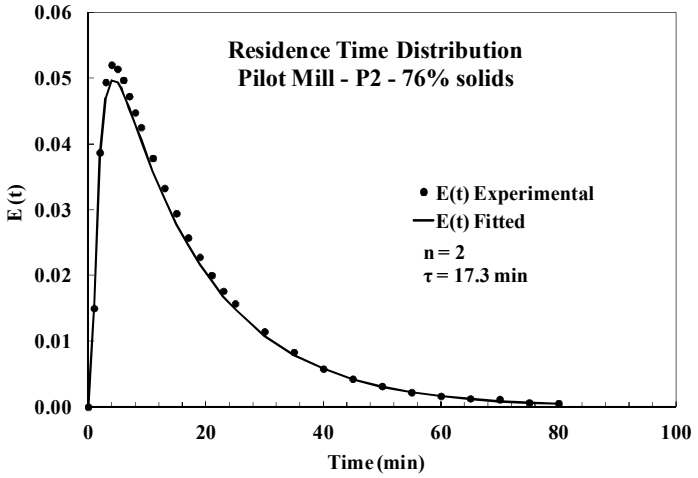

Figure 4.28: Comparison between experimental data and fitted RTD models for pilot test P2

The residence time distribution of each pilot test was modeled optimally with three mixers-in-series. Exception was pilot test P2, in which two mixers-in-series provided the best fit. The RTD model parameters and the pilot mill power and slurry hold-up recorded during the steady-state conditions are summarized in Table 4.6.

Table 4.6: RTD model parameters and the pilot mill power and slurry hold-up recorded during the steady state conditions

Pilot Experiment Designation	*RTD model parameters*					*Pilot mill measurements*	
	n	τ	τ_1	τ_2	τ_3	*Power (kW)*	*Hold-up (kg)*
P1	3.0	13.9	12.1	0.9	0.9	0.67	47
P2	2.0	17.3	15.9	1.4	-	0.68	41
P3	3.0	20.3	19.6	0.6	0.03	0.59	77
P4	2.5	39.6	-	-	-	0.61	91
P5 (grate discharge)	3.0	7.4	6.0	0.7	0.7	0.60	27

Figure 4.29 shows the experimental product size distributions for pilot tests conditions P3, P4 and P5. The mill discharge with higher percent of solids presented a coarser product size distribution and comparing the product obtained with grate discharge with that obtained with overflow discharge for similar solids concentration, the condition with grate discharge provided a slightly finer product.

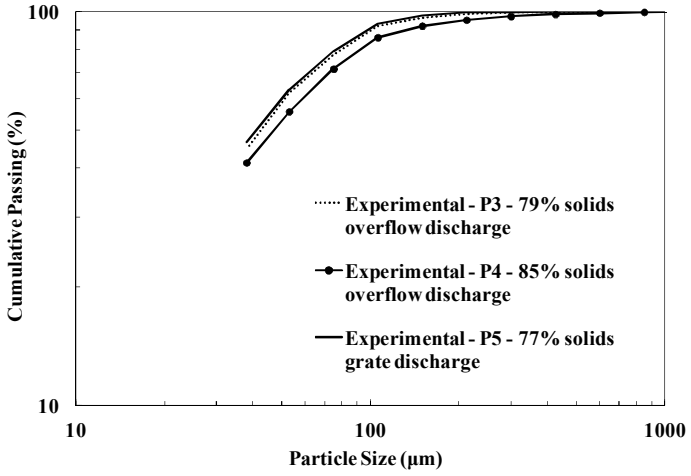

Figure 4.29: Experimental product size distributions for pilot tests conditions P3, P4 and P5

However, the agreement between experimental and predicted product size distributions was not satisfactory for the majority of tested conditions. The model predictions resulted in product size distributions finer than those obtained in the pilot mill experimental tests. This difference could be, perhaps, attributed to liner design that influences the motion of the media and which could have caused a vertical shift in the selection function for any given percent solids. Another assumption is that this difference could be also attributed to the mismatch between the slurry filling levels used in the batch experiments and the actual values found in the pilot mill, which were in the range of 139 to 245% (Table 4.5).

The validity of the second one can be confirmed from the good agreement between experimental and predicted results shown in Figure 4.30. In this test condition, the pilot mill was configured with grate discharge instead of overflow discharge. With this configuration, the slurry filling was approximately 89% under steady-state conditions. As such, the pilot mill discharge size distribution was predicted on the basis of the specific selection function estimated considering grinding data from test B4 due to the similarities with respect to solids concentration and slurry filling. In this case, the S_i^E was estimated on the basis of data from the feed, 16 and 20 min of grind in order to follow the similar fineness methodology, using the specific selection function parameters $\zeta_1^E = 0.85$ and $S_1^E = 4.079$ (kWh/ton)$^{-1}$.

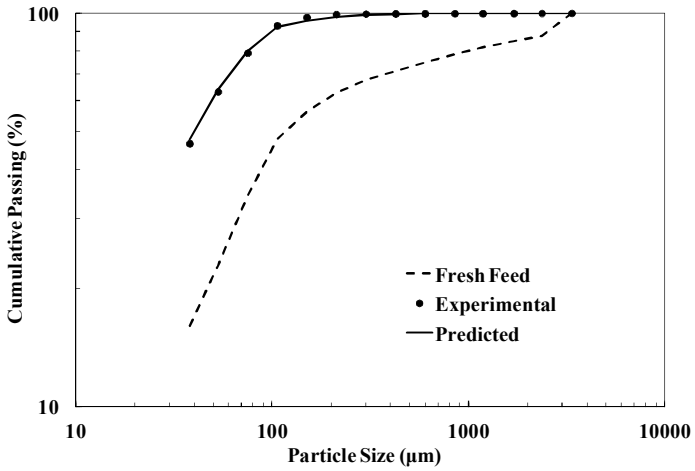

Figure 4.30: Comparison between the experimental and predicted size distribution for P5 test condition considering the breakage parameters fitted from the batch test B4

Now analyzing pilot plant data gathered from tests at higher slurry fillings (P3 pilot test at 79% solids and 245% of slurry filling), discharge size distributions were predicted using the specific breakage parameters estimated from B8 batch test condition (80% solids and 260% of slurry filling). The agreement between the experimental and predicted results is demonstrated in Figure 4.31, showing once again that the slurry filling influenced grinding kinetics, besides material transport through the mill.

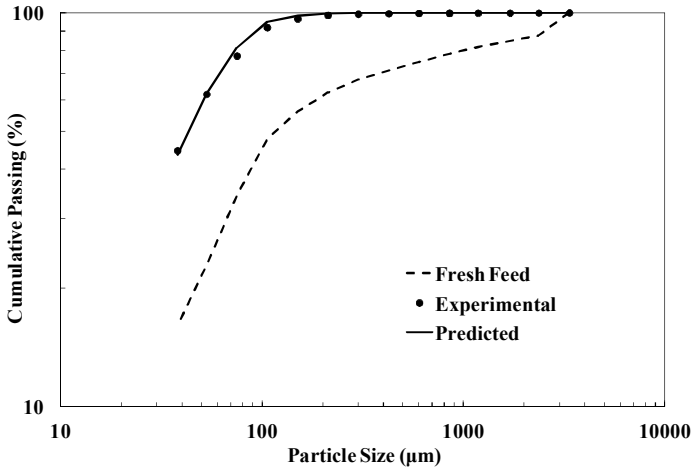

Figure 4.31: Comparison between the experimental and predicted size distribution for P3 test condition considering the breakage parameters fitted from the batch test B8

Since experimental conditions tested in the batch mill were somewhat different from those tested in the pilot mill, besides the conditions found in the industrial mill, the specific selection functions estimated on the basis of batch experiments needed to be adjusted. As such, it has been assumed that the industrial mill operates with similar slurry fillings to the pilot mill.

The adjustment procedure was based on the relationship between solids concentration and ζ_1^E from batch tests carried out with 100% of slurry filling (Figure 4.24). According to the fitted polynomial function, the ζ_1^{E*} was estimated considering the solids concentration of the pilot tests experiments (74, 76, 79 and 85%). Figure 4.32 shows the relationship between ζ_1^{E*} and the pilot mill solids concentration.

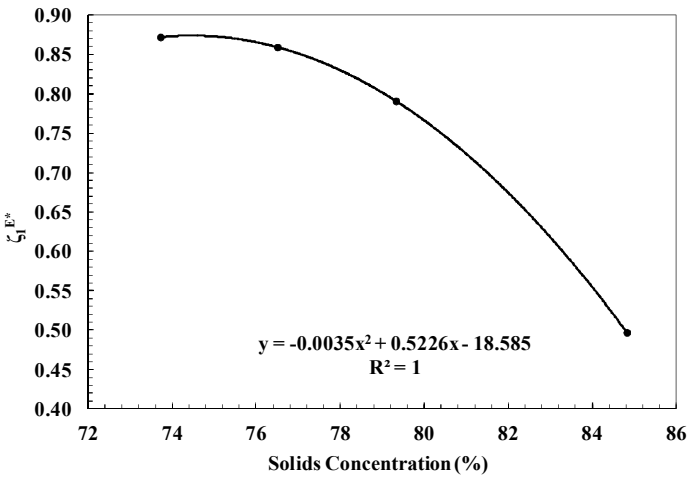

Figure 4.32: Relationship between ζ_1^{E*} and the solids concentration in the pilot mill tests for top ball size of 30 mm and 68.3% of critical speed

The "new" specific selection functions (S_1^{E*}) were estimated considering the value of ζ_1^{E*} and the lowest RMS (root mean squares of residuals). Figure 4.33 demonstrates that there is a shift between S_1^E from the batch tests and S_1^{E*} from the pilot tests. This shift corresponds to a multiplier of about 0.9, which should be applied to the S_1^E from batch data to predict the continuous mill operation. The differences in slurry filling and liners design could be related to the appearance of this factor.

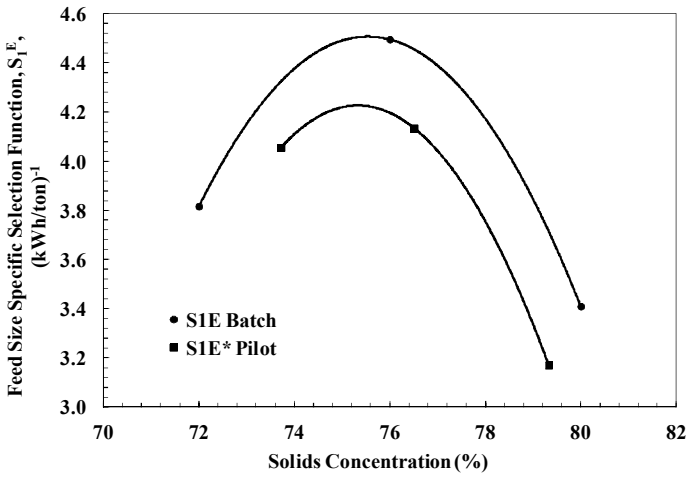

Figure 4.33: Relationship between solids concentration and feed size specific selection functions, S_1^E

The specific selection functions (S_1^{E*}) estimated for 74, 76, 79 and 85% solids of slurry in the pilot mill are demonstrated in Figure 4.34.

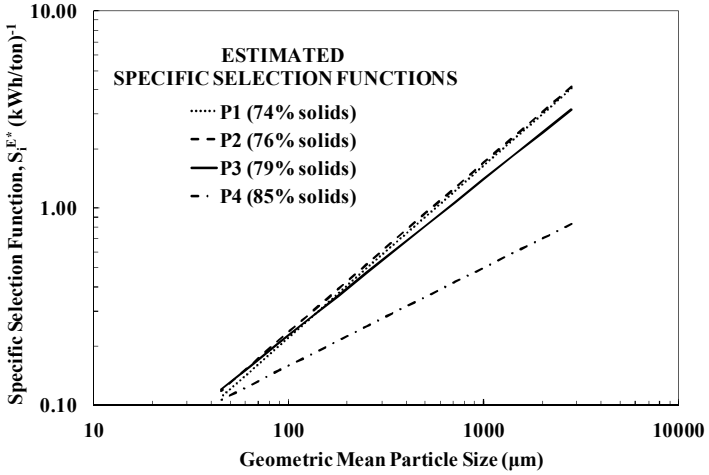

Figure 4.34: Specific selection functions (S_1^{E*}) estimated for slurry with 74, 76, 79 and 85% solids in the pilot mill

In order to evaluate the top ball size reduction from 30 to 25 mm and also to assess the influence of discharge type in mill performance, the same fitting factor of 0.9 was applied in the feed size specific selection function previously determined from the batch test B9 (Table 4.4) and from the batch test B4 where S_1^E was estimated on the basis of data from the feed, 16 and 20 min of grind in order to simulate the P5 pilot test condition (Figure 4.30). The parameter ζ_1^{E*} was calculated according to the polynomial equation described in Figure 4.32, considering the solids concentration of the pilot mill experiments.

The specific selection function parameters used to predict the pilot mill operation are shown in Table 4.7, whereas the specific selection functions (S_i^{E*}) estimated for different top ball size and mill discharge are demonstrated in Figures 4.35 and 4.36, respectively.

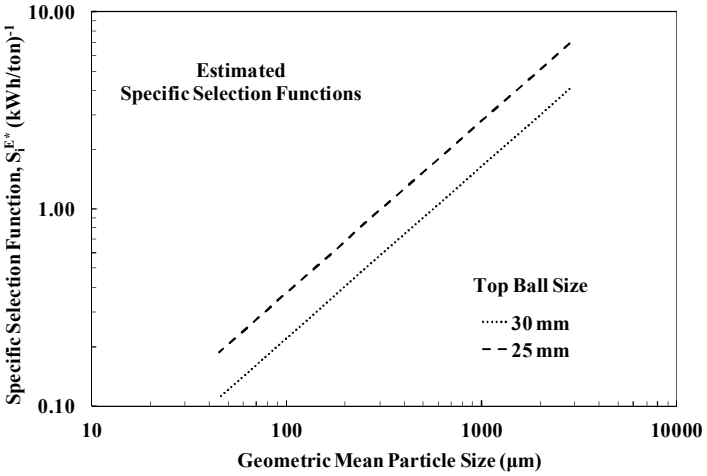

Figure 4.35: Specific selection functions estimated for different top ball size considering 74% solids

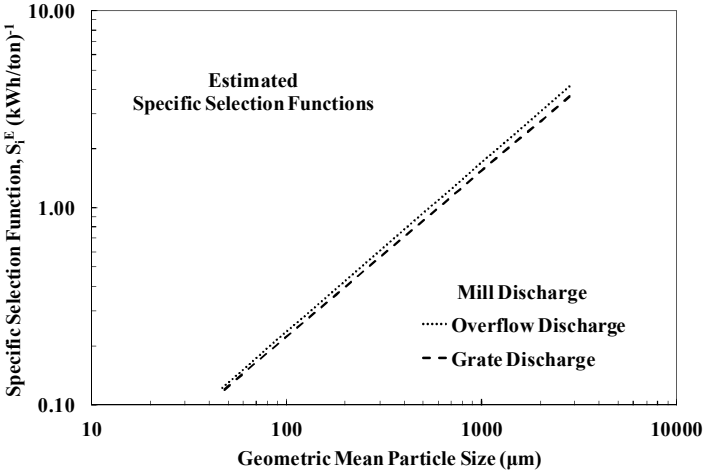

Figure 4.36: Specific selection functions estimated for different mill discharge

Table 4.7: Specific selection function parameters used to predict the pilot mill operation

Simulated conditions	S_I^{E*} $(kWh/ton)^{-1}$	ζ_I^{E*}
1. 74% solids; top ball size of 30 mm; overflow discharge	4.055	0.872
2. 74% solids; top ball size of 25 mm; overflow discharge	6.899	0.872
3. 76% solids; top ball size of 30 mm; overflow discharge	4.134	0.859
4. 79% solids; top ball size of 30 mm; overflow discharge	3.172	0.791
5. 85% solids; top ball size of 30 mm; overflow discharge	0.834	0.497
6. 77% solids; top ball size of 30 mm; grate discharge	3.671	0.840

The reasonable agreement between experimental and predicted product size distributions demonstrated in Figures 4.37 to 4.40 confirms the validity of this fitting factor and also the use of PBM as a predictive model.

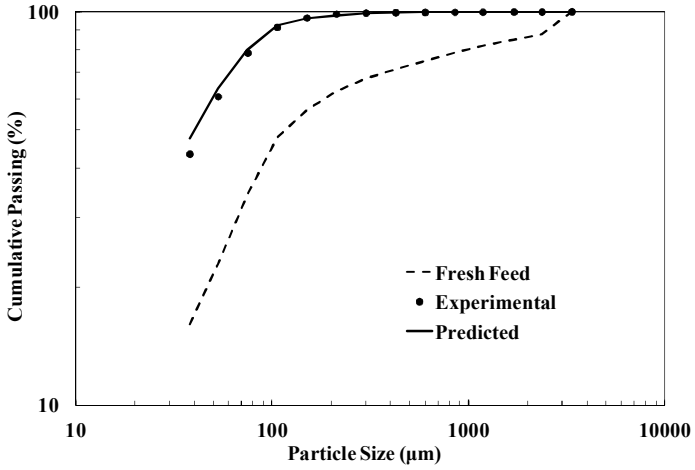

Figure 4.37: Comparison between the experimental and predicted product size distribution for P1 test condition (simulated condition #1 from Table 4.7)

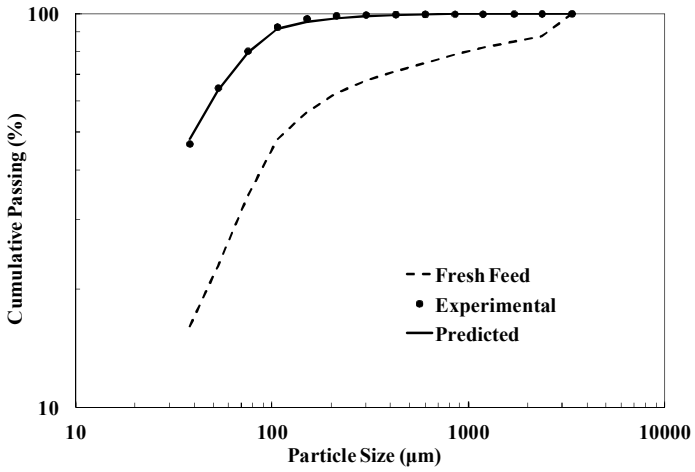

Figure 4.38: Comparison between the experimental and predicted product size distribution for P2 test condition (simulated condition #3 from Table 4.7)

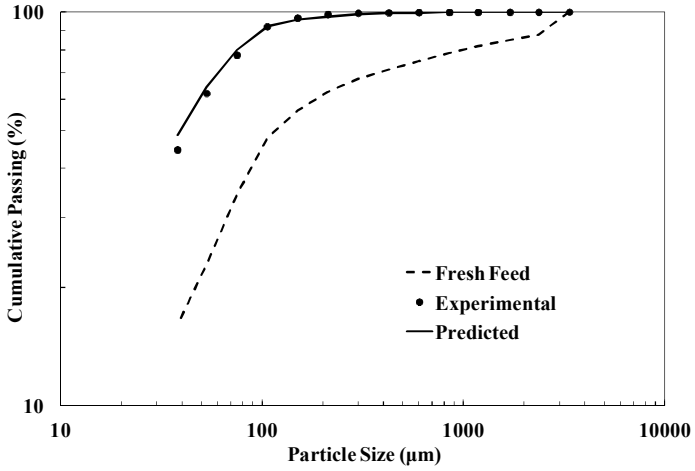

Figure 4.39: Comparison between the experimental and predicted product size distribution for P3 test condition (simulated condition #4 from Table 4.7)

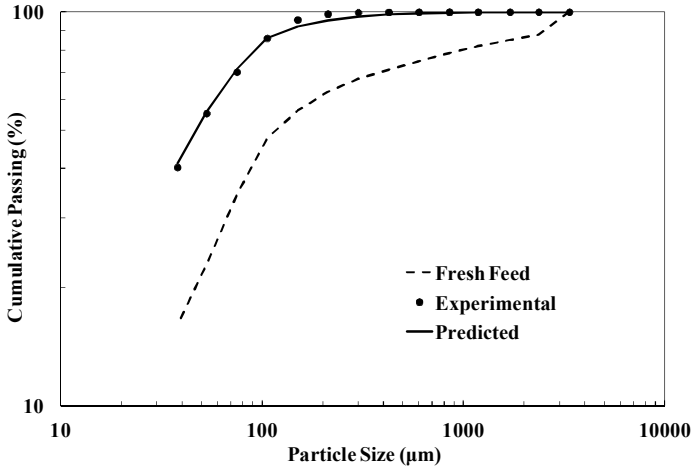

Figure 4.40: Comparison between the experimental and predicted product size distribution for P4 test condition (simulated condition #5 from Table 4.7)

4.4 Simulations of Vale's Industrial Mill Using the PBM Approach

The specific selection function parameters used to predict the pilot mill operation were also used to predict the discharge size distribution of the industrial mill (Table 4.7). The residence time distribution, the mill power (shown in Table 3.6) and the feed size distribution were then required in this simulation. The RTD and the number of mixers-in-series were determined following the same procedure used in the pilot mill

experiments, as described previously. In this case, the industrial mill was best modeled with one mixer and the data related with the closed circuit (points after 35 min shown in Figure 4.41) were disregarded in this modeling.

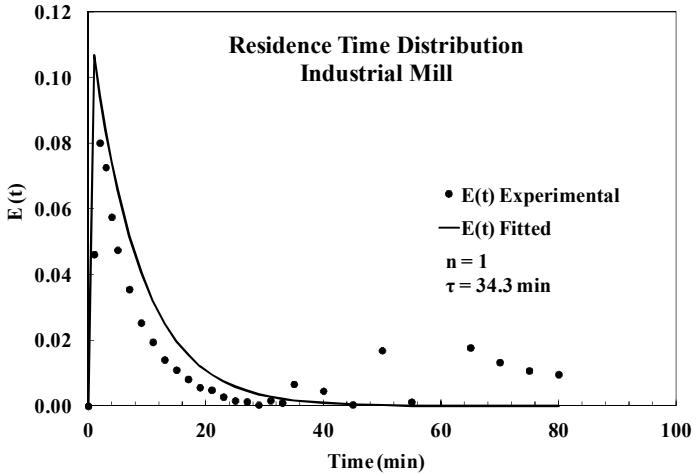

Figure 4.41: Comparison between experimental data and fitted RTD model for industrial mill

Since the performance of the hydrocyclones can be analyzed independently of mill performance, the hydrocyclone performance was not evaluated in the industrial mill simulations. The closed circuit was simulated using the Estimill program considering the partition curve estimated on the basis of data from the sampling campaigns (Appendix I).

As mentioned in Chapter 1 the quality of the iron ore pellet in the pelletizing process is directly related to the amount of fines contained in the mill product (mainly the cumulative passing 45 microns). Under this circumstance the predictive capability of the PBM approach was evaluated through the comparison between the predicted amount of -38 microns and -45 microns produced in the mill as a function of solids concentration with the experimental results obtained through the three sampling campaigns that were carried out in the industrial mill (as described in section 3.4.3.1). The predicted and the experimental results from the sampling campaigns are shown in Figures 4.42 to 4.44.

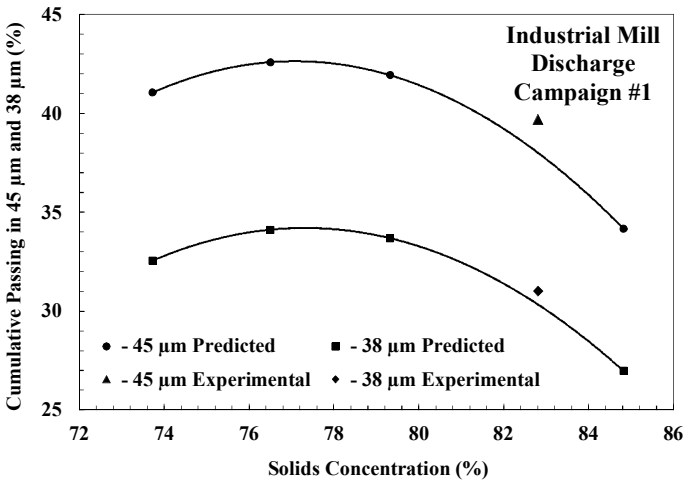

Figure 4.42: Fineness of industrial mill discharge as a function of solids concentration – predicted and experimental results from campaign #1

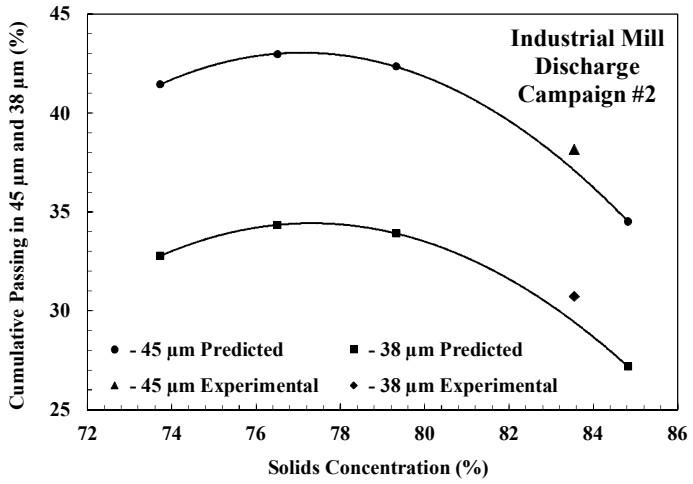

Figure 4.43: Fineness of industrial mill discharge as a function of solids concentration – predicted and experimental results from campaign #2

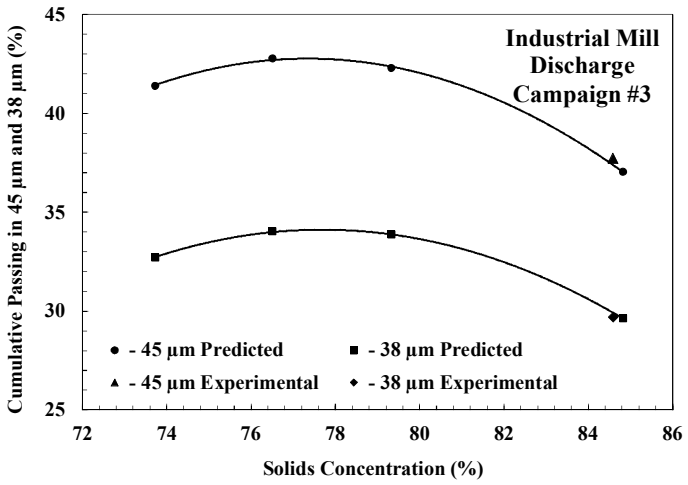

Figure 4.44: Fineness of industrial mill discharge as a function of solids concentration – predicted and experimental results from campaign #3

Considering the iron ore type used in all experiments, Figures 4.42 to 4.44 can be used to identify the optimal operating condition for Vale's industrial mill, which should be in the range from 76 to 80 percent solids. This operational condition would be optimal for the pelletizing process because both the amount of -38 microns and -45 microns, which are used in the plant to characterize process performance, were the highest.

For a given product size (40% passing 45 microns), simulation results indicated that lowering percent solids in the mill from 83 (current condition of industrial mill) to 76 or 80 increased mill capacity by about 10% (Figure 4.45). An opposite behavior is shown in the energy requirement (Figure 4.46), since decreasing percent solids in the mill would reduces the specific energy consumption. Similar results were found by MARTINOVIC *et al* (1990) at Carol Pellet Plant of the Iron Ore Company of Canada.

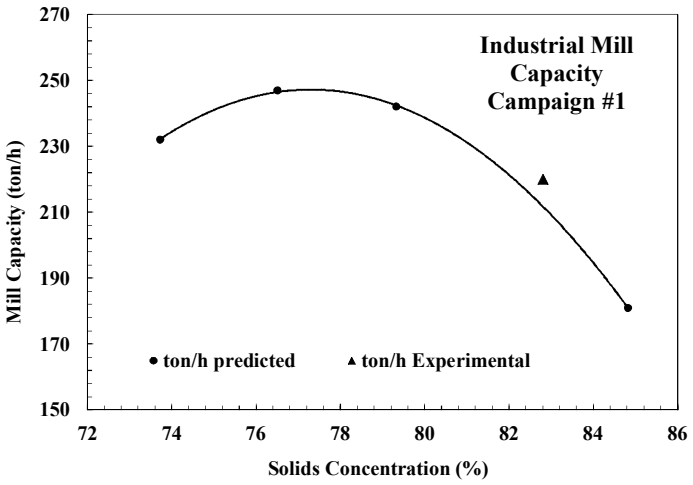

Figure 4.45: Predictions of industrial mill capacity as a function of percent solids for a product size of 40% passing 45 microns

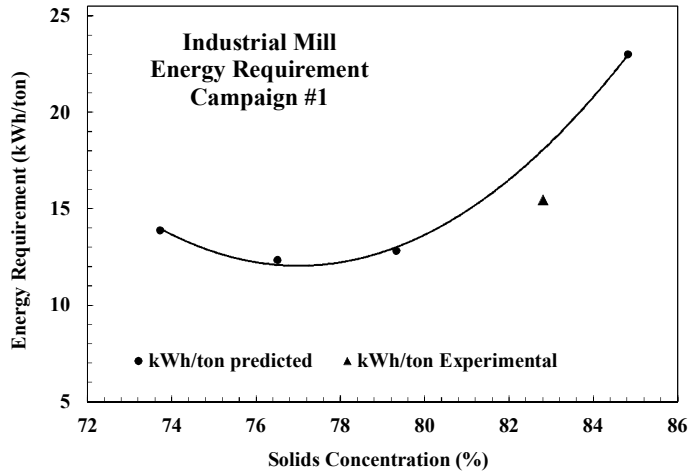

Figure 4.46: Predictions of energy requirements for the industrial mill with percent solids for a product size of 40% passing 45 microns

The good agreement between experimental and predicted results, shown in previous graphs, demonstrates the validity of the PBM approach as a predictive method and also as a good optimization methodology for the industrial mill. The simulated results indicated that the mill operation between 76 and 80% solids (or 42 and 48% in volume) would lead to higher grinding efficiency, considering the iron ore density around 4.34 g/cm^3.

The predicted industrial mill performance with 30 mm and 25 mm of top ball size was compared and it was found that the overall grinding efficiency could be improved by appropriately reducing the ball size. This is evident from the specific selection functions presented in Figure 4.35. Figures 4.47 to 4.49 show that the product mill discharge in each industrial mill campaign was finer when the top ball size was reduced to 25 mm.

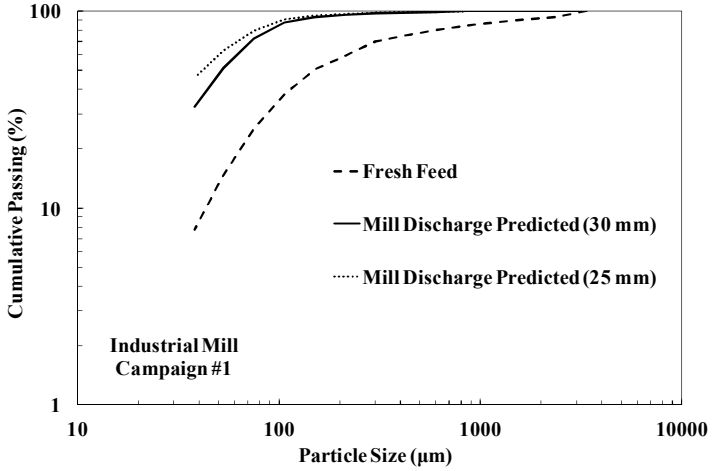

Figure 4.47: Predicted product size distribution of industrial mill discharge as a function of top ball size – predicted results considering mill feed from campaign #1

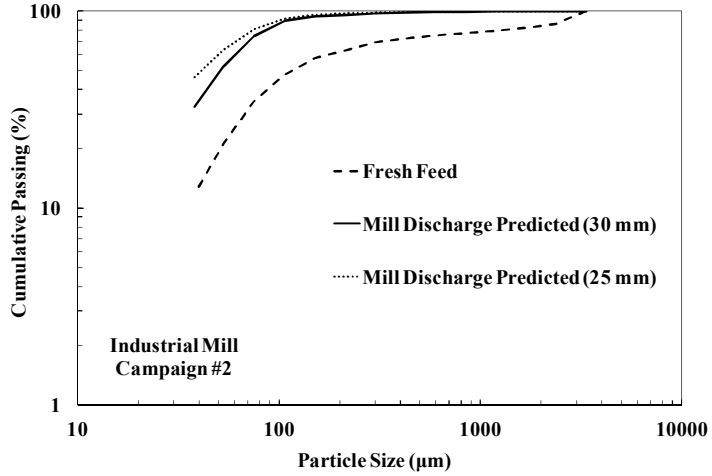

Figure 4.48: Predicted product size distribution of industrial mill discharge as a function of top ball size – predicted results considering mill feed from campaign #2

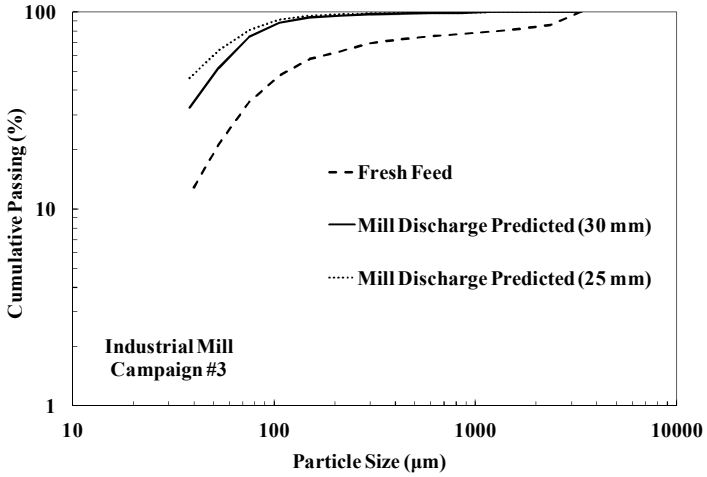

Figure 4.49: Predicted product size distribution of industrial mill discharge as a function of top ball size – predicted results considering mill feed from campaign #3

The type of discharge on the industrial mill performance was also simulated on the basis of specific selection functions estimated for the pilot mill tests with similar solids concentration while operating with overflow and grate discharge. Table 4.7 and Figure 4.36 present the specific selection function parameters used to predict the industrial mill discharge.

The difference between product size distribution of the industrial mill considering overflow discharge and grate discharge was not significant. In this simulated condition (percent of solids around 76) the industrial mill performance was nearly identical for these two types of discharge.

4.5 DEM Simulations

At first, simulations using the Discrete Element Method were carried out for the entire industrial mill and a typical result is presented in Figure 4.50. However, in order to optimize the time required for the simulations, it was considered a slice measuring 0.1 m of the mil, resulting in a total of 61.878 particles. The energies dissipated in each of the collisions during 5 seconds of analyzes were registered and post-processed using the software LTM Analyst (CARVALHO, 2013) to generate the collision energy spectra. As an illustration, a typical result is presented in Figure 4.51 for the simulation considering a slice.

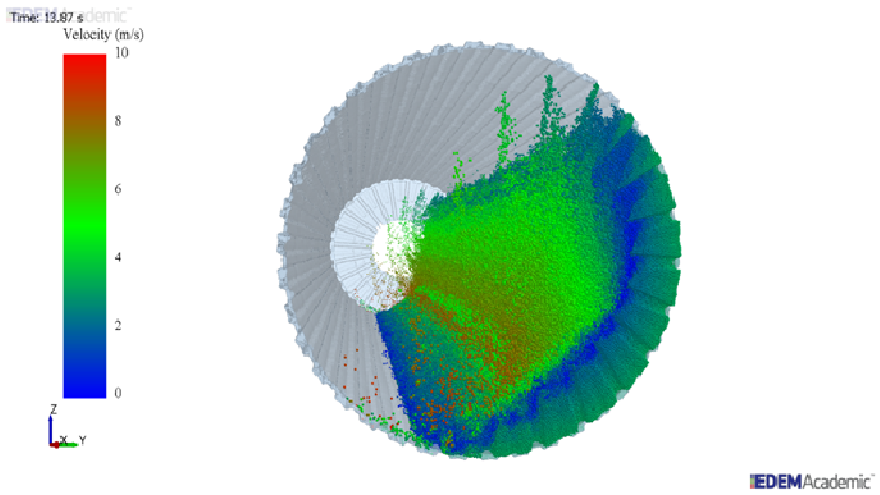

Figure 4.50: DEM simulations of the entire industrial mill

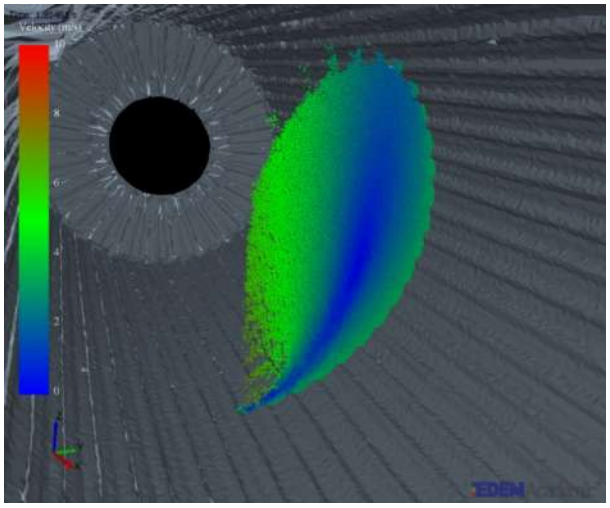

Figure 4.51: DEM simulations of a 0.1 m slice of the mill

Further, simulations of the batch mill were carried out in order to generate data for back-calculating the fracture energy distribution parameters. Typical simulation results are shown in Figure 4.52.

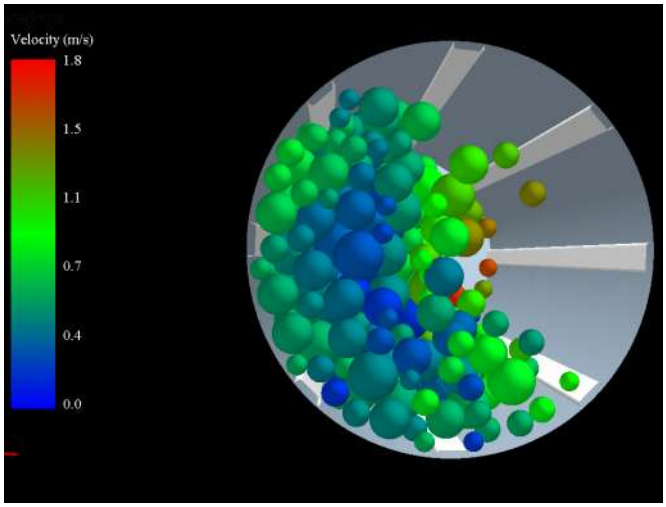

Figure 4.52: Simulations of the batch ball mill, with a top ball size of 30 mm (ball filling of 40% and 68.3% of critical speed)

4.6 UFRJ Mechanistic Model Parameter Estimation and Simulation framework

The approach that was adopted for application of the UFRJ mechanistic mill model in the industrial mill simulations is illustrated in Figure 4.53. The gray background represents the area of application of the model to grinding, which is fed by parameters from sub models describing the different breakage mechanisms, estimated on the basis of Drop Weight Tests (DWT), repeated impact tests, abrasion breakage tests and also batch grinding tests.

In the present work it was assumed that data from an earlier study (CARVALHO and TAVARES, 2013) on breakage of coarser particles could be used to describe data on finer size from the present work, and these are listed in Table 3.10. As such, parameters that describe the ore fragmentation pattern, the amenability to breakage by repeated impacts and response to abrasion breakage were assumed to be the same as those from the previous study. On the other hand, it is considered that the variation of particle fracture energies with size is a characteristic that varies significantly for different ores and materials (TAVARES and KING, 1998). As such, a back-calculation procedure on the basis of batch grinding tests was proposed for parameters describing this relationship.

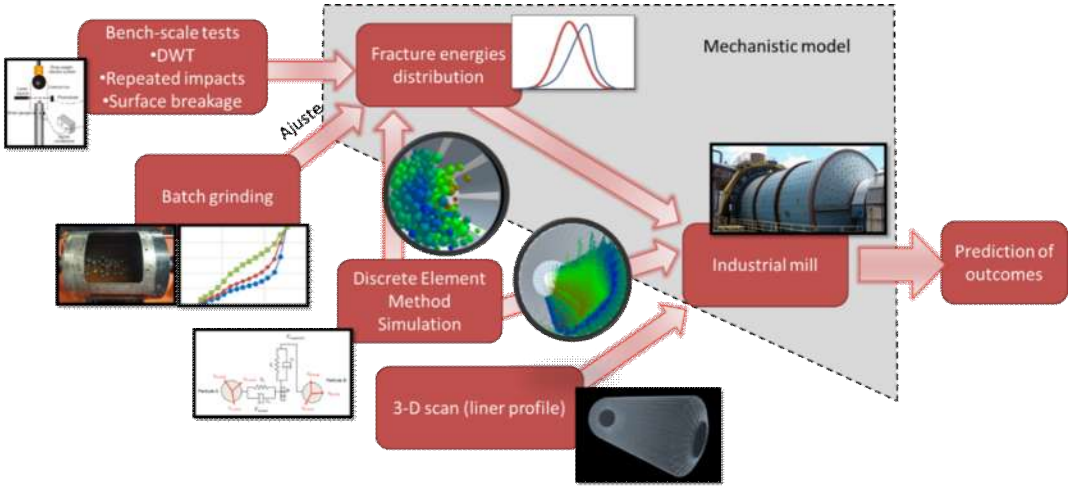

Figure 4.53: General scheme of the application of the mechanistic mill model to simulate the industrial mill.

As such, assuming that the mechanistic ball mill model provides a realistic description of batch grinding, results from selected batch grinding tests (Table 4.8) have been used as a basis for back-calculating the fracture energy model parameters (Equation 2.59). A comparison between experiments and simulations using the best fit parameters is shown in Figures from 4.54 to 4.58, which demonstrates the reasonable agreement between both.

Table 4.8: Tests used to fit the fracture energy distribution parameters

Batch Experiments Designation	***Percent Solids (%)***	***Slurry Filling (%)***	***TopBall Size (mm)***	***Grind Times (min)***
B1	72	100	30	1/2/4
B2	72	100	30	1/2/4
B3	72	100	30	4/8/12/16/20
B4	76	100	30	8/12/16/20
B6	72	260	30	4/8/12/16
B9	72	100	25	8/12/16/20

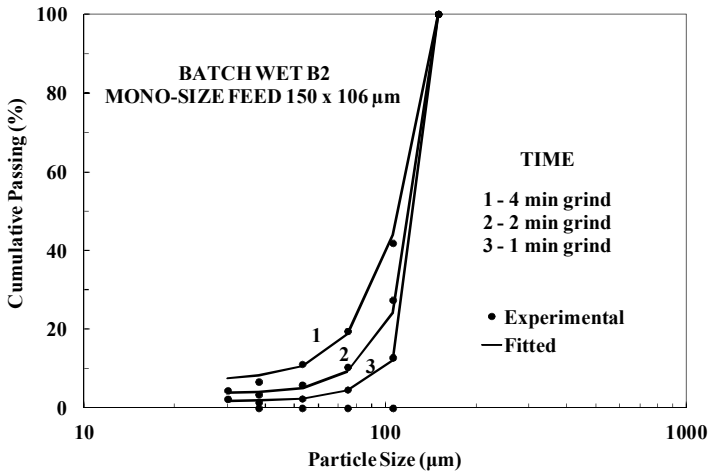

Figure 4.54: Comparison between experimental and fitted results using the best fit parameters in UFRJ mechanistic ball mill model for batch test B2

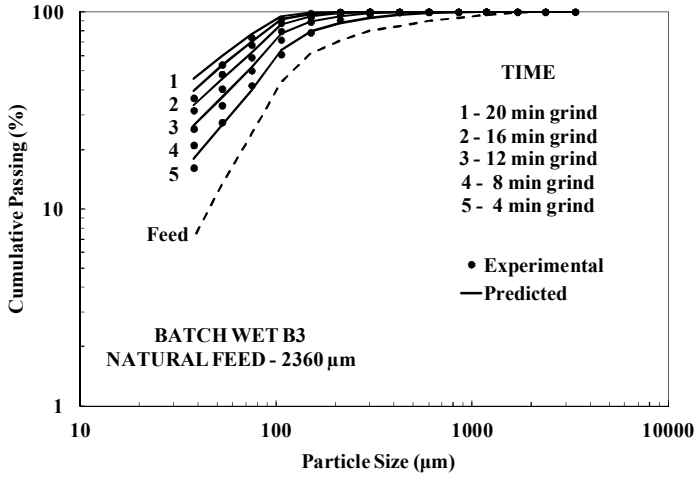

Figure 4.55: Comparison between experimental and fitted results using the best fit parameters in UFRJ mechanistic ball mill model for batch test B3

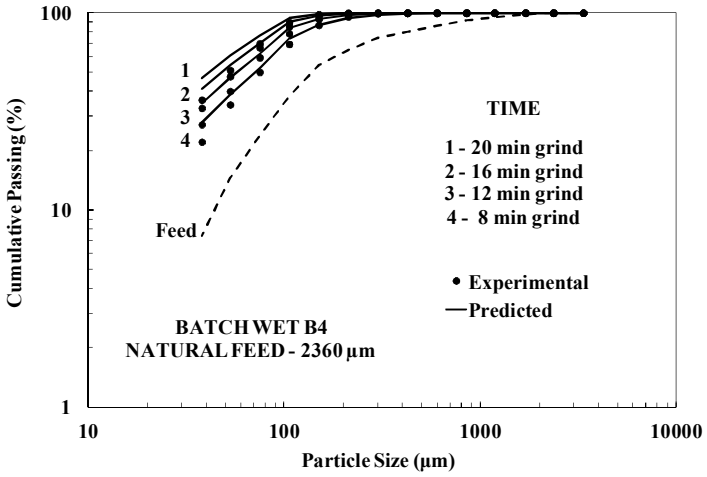

Figure 4.56: Comparison between experimental and fitted results using the best fit parameters in UFRJ mechanistic ball mill model for batch test B4

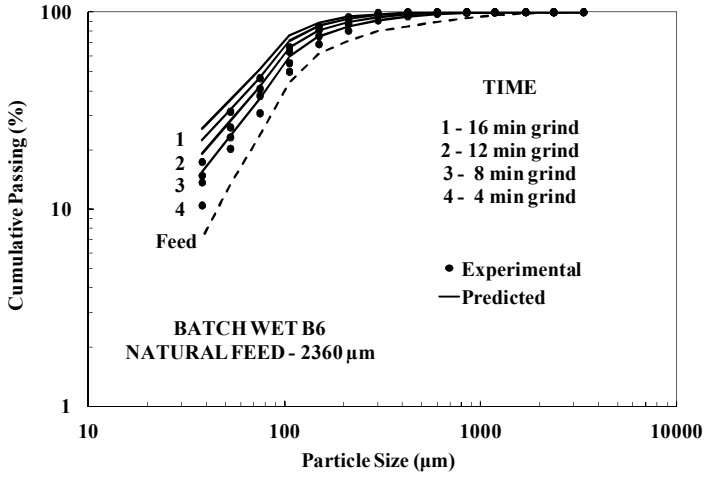

Figure 4.57: Comparison between experimental and fitted results using the best fit parameters in UFRJ mechanistic ball mill model for batch test B6

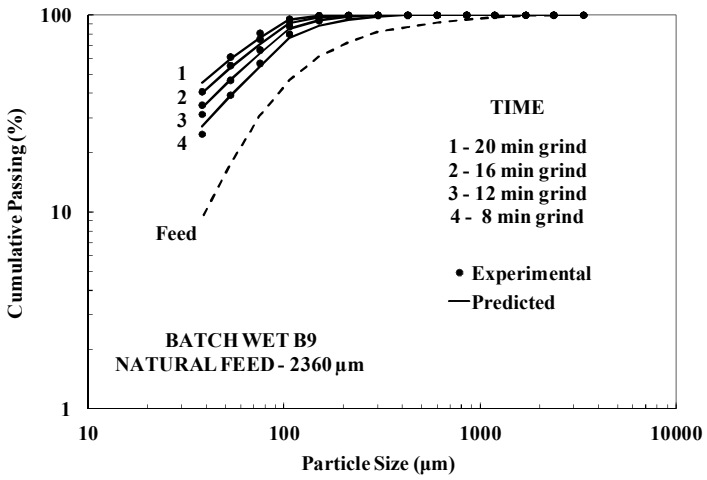

Figure 4.58: Comparison between experimental and fitted results using the best fit parameters in UFRJ mechanistic ball mill model for batch test B9

Figure 4.59 compares the fracture energy distributions of the base ore (TAVARES and CARVALHO, 2013) to the results from back-calculation. They demonstrate that the ore in the present study would present higher fracture energies for particles coarser than about 3 mm, but lower for finer particles, being more amenable to breakage.

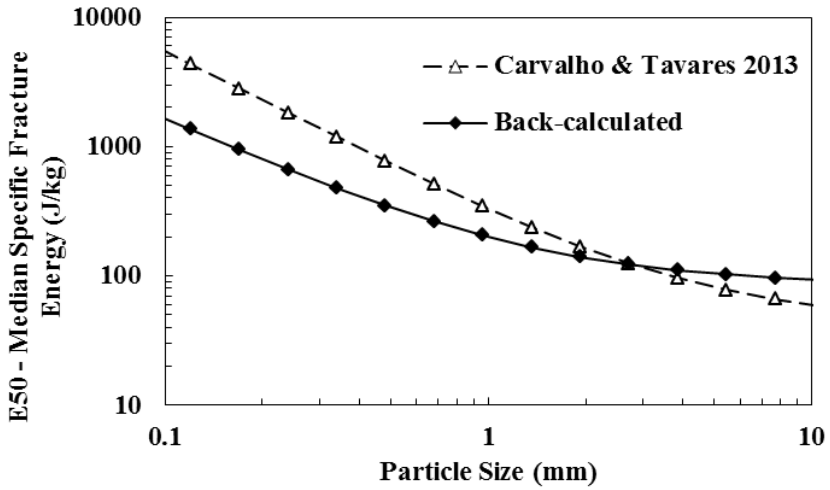

Figure 4.59: Comparison of back-calculated median fracture energies (present work) and data from measurements for another iron ore (CARVALHO and TAVARES, 2013)

DEM simulations of Vale's industrial mill for the 0.1 m slice are presented in Figure 4.60, which demonstrates that the effect of liner wear caused no visually noticeable difference in the charge motion.

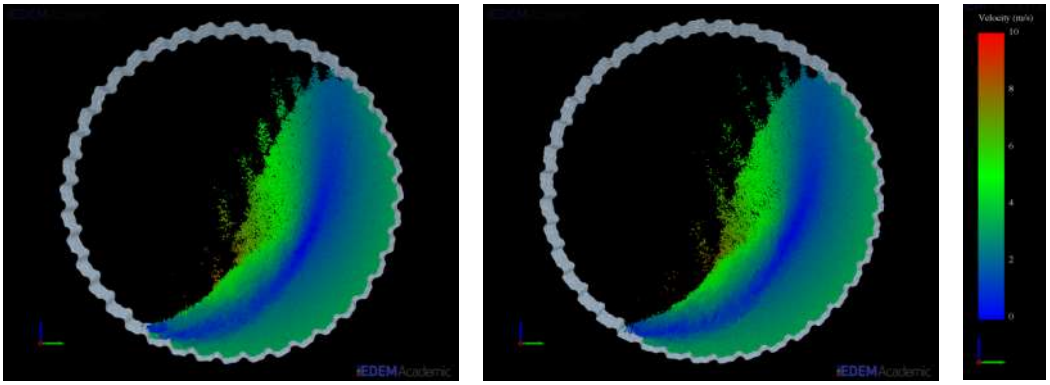

(a) (b)

Figure 4.60: Simulations of the charge motion for the mill with new mill liners (a) and after 12,000 hours of operation (b)

The collision energy spectra calculated from DEM simulations of the industrial mill is shown in Figure 4.61. In this graph, the collision frequencies were calculated per 10 centimeters of mill length, which is the mill slice (0.1 meter) considered in the DEM simulations. Taking the initial life of the liner as listed in Table 3.9, which is the laser scanning data from survey #2, which had 31.7% of ball filling and comparing with both the mid-life (survey #3) and end-life (survey #1) simulations under the same mill filling conditions i.e. (same ball charge). The results showed that these three collision energy distribution almost overlap at low energy collisions such as those bellow 2 J. However, in Figure 4.62 which shows the same data displayed in Figure 4.61, but with rearranged scales, a slight difference appears at higher collision energies.

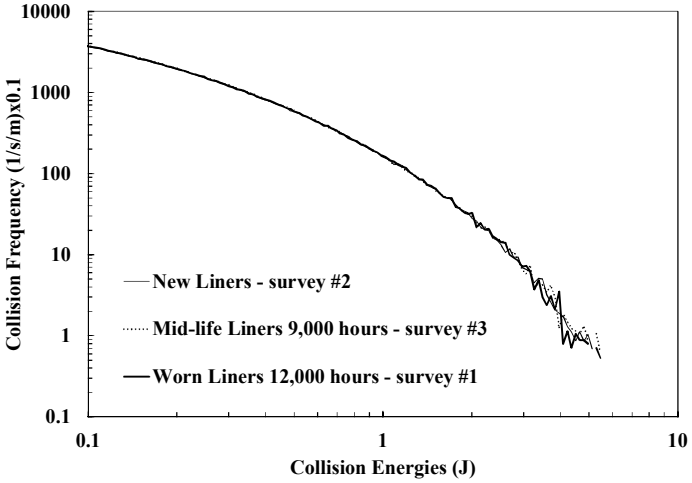

Figure 4.61: Collision energy spectra calculated from DEM simulations of the industrial mill

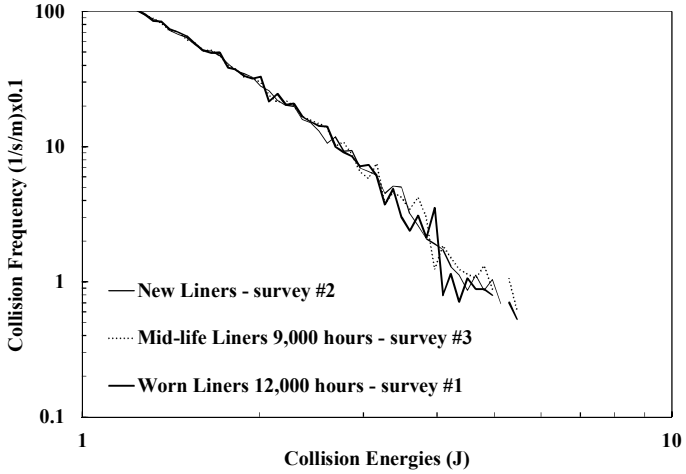

Figure 4.62: Collision energy spectra calculated from DEM simulations of the industrial mill with rearranged scales

As a first attempt to test the model to the regrind stage of the comminution, the industrial mill was considered as a batch reactor. To compare the measured discharge product size distribution of the industrial mill to those obtained from the batch model of the simulations, the average residence time measured was considered. So the grinding time of the batch simulation that produced a comparable product to the continuous operation was around 16 minutes. In addition, the initial particle size distribution of the batch simulations was equivalent to the mill feed, which is the fresh feed plus the recycle stream. Even with this simplistic approach, the order of the magnitude of the

error, when compared the measured discharge was of 1-5% when considered the cumulative passing distribution (Figure 4.63).

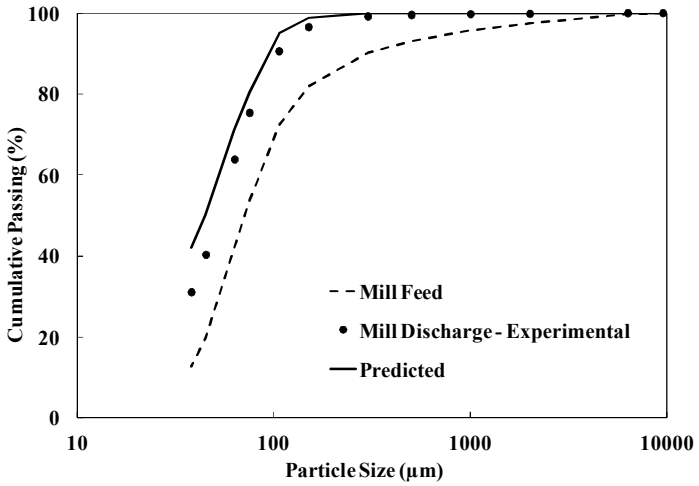

Figure 4.63: Comparison between experimental and predicted result obtained from the batch model of the simulations

In order to compare what would be the model predictions as function of the different liner profiles surveyed in this work, the simulations performed by setting the ball filling of 31.7% that generated the collision spectra shown in Figure 4.61 resulted in almost no difference among the three simulations in terms of the product size distribution. This confirms, as warned by CARVALHO and TAVARES (2013), that the mechanistic approach is indeed sensitive to the quality of the DEM simulations, in other words, the collision energy spectrum, thus will not result in significant differences in the particle size distribution of the product.

One of the advantages of having such tool to predict the outcomes of the grinding is the capability to extrapolate the limits of operation. A set of three new simulations using the mechanistic approach were performed to check if there would be any difference in the product size distribution if the mill was subjected to a coarse feed in respect to the three liner profiles (new, mid-life and end-life). The results are shown in Figure 4.64. The product size distributions almost overlap each other, being almost difficult to see any differences. For the same grinding time, the mill was able to produce 100% passing minus 500 micrometers.

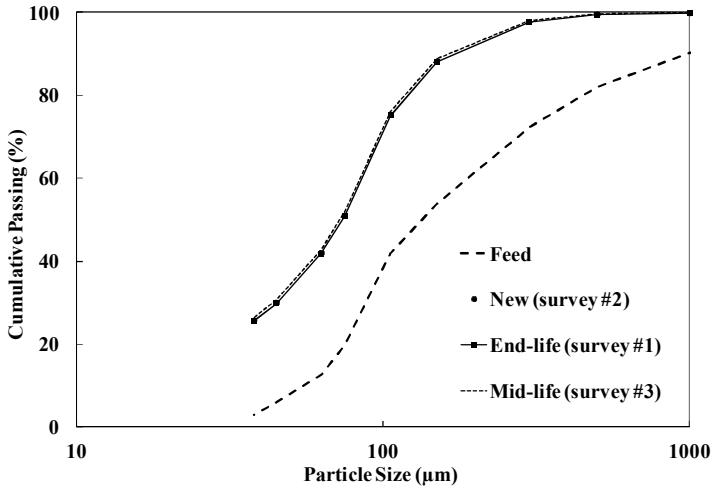

Figure 4.64: Predicted product size distribution when the mill was simulated with coarse feed in respect to the three liner profiles (new, mid-life and end-life)

5. CONCLUSIONS

Fitting the population balance model of batch grinding to data from a 25.4 cm mill in size reduction of an iron ore from Brazil resulted in non-normalizable breakage functions and breakage rate distributions that varied with percent solids, top ball size and slurry filling. From these, as well as the residence time distribution, it was possible to predict the product size distributions from a pilot scale mill operating in open circuit. This, however, required the introduction of a fitting factor to the specific selection function which was explained on the basis of differences in liner design and slurry filling content within the mill, that could not be properly matched in the laboratory mill.

Using the same correction value of the factor for the specific breakage function, the full scale mill performance was predicted as well using the population balance model. It allowed concluding that the range of solids concentration from 76 to 80% was optimal since the fines generation and the amount of -45 microns was the highest, which would favor the pelletizing process. It was also found that the overall grinding efficiency can be improved by reducing the top ball size from 30 to 25 mm. No measurable difference was observed in industrial mill performance in the operational conditions simulated for overflow discharge and grate discharge.

For a given product size (40% passing 45 microns), simulation results also indicated that reducing the percent solids in the industrial mill from the currently used 83% to a value between 76% and 80% would result in an increase in mill capacity of about 10% and consequently decrease the specific energy consumption (kWh/ton) for the ore in question. Thus, the industrial mill performance could be optimized in terms of energy consumption.

The good agreement between experimental and predicted results, shown in this study, demonstrates the applicability of the PBM approach as a predictive method and also for grinding process optimization of a selected closed-circuit ball mill producing fines for pelletizing process.

The predictions related with process optimization have been implemented in Vale's industrial mill. Given the success achieved in demonstrated benefits quantitatively for this plant scale mill, it is expected that the application of this approach will result in significantly improved mill product quality.

An approach was proposed to predict the performance of the industrial mill using UFRJ mechanistic mill model. It was based on fitting the fracture energy distribution parameters, the most critical part of the model, to data from the batch grinding tests previously conducted to model using the traditional PBM. Results showed that the model, after fitting only three parameters, could describe the batch grinding results with good confidence, providing data that could be used as the basis of full-scale mill simulations.

Scannings of the mill internals when they were new and nearly fully worn followed by DEM simulations of the mill operating under the same mill filling resulted in nearly identical collision energy spectra. Indeed, simulations using the mechanistic ball mill model of the industrial mill showed nearly no effect of liner wear on mill performance.

6. SUGGESTIONS FOR FUTURE WORK

In this investigation, it has been found that the influence of slurry filling in the specific selection function is very significant and affected the predictive capability of the PBM approach. Thus, in order to investigated the appearance of the fitting factor of 0.9, it is suggested to study in greater detail the effect of this variable on the specific selection function to improve the predictive capability of PBM approach when this methodology is applied in an industrial mill scale-up grinding iron ore for pellet production. In this case, the batch experiments should be planned considering the slurry filling within the range of values that correspond to normal mill operation (the diameter of the discharge trunnion also should be considered in the determination of the slurry filling ranges).

Taking into consideration the grinding of a heterogeneous mixture of iron ore, as used in this study, other required study is the top ball size effect. As such it is recommended to study the effect of ball size on the breakage function, demonstrating or not the validity of the assumption considered in several studies that this function is invariant with respect to operating variables, such as top ball size, over a wide range of conditions.

Investigate comminution of iron ore considering its multicomponent nature, taking into account the different breakage response of silica and the iron-rich minerals, which likely differ.

Investigate further the applicability of the mechanistic ball mill model, analyzing the effect of several other variables, including mill filling and ball size, on the mill performance.

7. REFERENCES

AGRAWALA, S., RAJAMANI, R.K., SONGFACK, P. *et al.*, "Mechanics of Media Motion in Tumbling Mills with 3D Discrete Element Method", **International Journal of Mineral Processing**, v.10, pp. 215-227, 1997.

ALVES, V.K., **Otimização de Carga Moedora Utilizando Ferramentas de Modelamento Matemático e Simulação de Moagem**, M.Sc., Universidade Federal de Minas Gerais, 2006.

AMELUNXEN, P.A., MEADOWS, D., "Not Another HPGR Trade-off Study!", **Minerals and Metallurgical Processing**, v.28, pp. 1-7, 2011.

AUSTIN, L.G., "Understanding Ball Mill Sizing", **Industrial & Engineering Chemistry Research - Process Design and Development**, v.12, pp.121, 1973.

AUSTIN, L.G., "A Mill Power Equation for SAG Mills", **Minerals and Metallurgical Processing**, pp. 57-62, 1990.

AUSTIN, L.G., CONCHA, F.A., "Diseño y Simulación de Circuitos de Molienda y Clasificación", **In: CYTED: Programa Iberoamericano de Ciencia y Tecnologia para el Desarrollo**, Chapter 7: Distribución de Tiempos de Residencia, pp. 155-174 1994.

AUSTIN, L.G., GARDNER, R.P., "Prediction of Size-Weight Distribution from Selection and Breakage Data", **Proceedings: 1st European Symposium Zerkleinern, H. Rumpf and D. Behrens Data**, eds., pp. 232-248, Verlag Chemie, Weinheim, 1962.

AUSTIN, L.G., JULIANELLI, K., SOUZA, A.S. *et al.*, "Simulation of Wet Ball Milling of Iron Ore at Carajas, Brazil", **International Journal of Mineral Processing**, v.84, pp. 157-171, 2007.

AUSTIN, L.G., KLIMPEL, R.R., BEATTIE, A.N., "Solutions of Grinding", **Zerkleinern, 2nd European Symposium on Comminution**, Dechema-Monographien, v. 57, pp. 281-312, Amsterdam, 1967.

AUSTIN, L.G., KLIMPEL, R.R., LUCKIE, P.T., **Process Engineering of Size Reduction: Ball Milling**, New York, SME, AIME, 1984.

AUSTIN, L.G., LUCKIE, P.T., "Methods for Determination of Breakage Distribution Parameter Scale", **Powder Technology**, v.5, pp. 251, 1971-72.

AUSTIN, L.G., TANGSATHITKULCHAI, C., "Comparison of Methods for Sizing Ball Mills Using Open-Circuit Wet Grinding of Phosphate Ore as a Test Sample ", **Industrial & Engineering Chemistry Research**, v.26, pp. 997-1003, 1987.

BARRIOS, G.K.P., CARVALHO, R.M., TAVARES, L.M., "Modeling Breakage of Monodispersed Particles in Unconfined Beds", **Minerals Engineering**, v.24, pp. 308-318, 2011.

BOND, F.C., "The Third Theory of Comminution - Discussion", **Mining Engineering, Trans. AIME**, pp. 1071-1074, 1952a.

BOND, F.C., "The Third Theory of Comminution", **Mining Engineering, Trans. AIME**, pp. 484-494, 1952b.

BOND, F.C., "Crushing and Grinding Calculations", **British Chemical Engineering**, v.6, pp. 378-391, 543-548, 1960.

BOND, F.C., "Crushing and Grinding Calculations", **Allis-Chalmers Publications**, Milwaukee, Wisconsin, 16 pp, 1962.

BOND, F.C., **Crushing and Grinding Calculations**. In: Selection Circuits to Prepare Beneficiation Feeds, Allis Chalmers Bulletin, 1983.

CARVALHO, R.M., **Desenvolvimento de Modelo Matemático Generalizado da Cominuição**, M.Sc., Universidade Federal do Rio de Janeiro, 2009.

CARVALHO, R.M., **Mechanistic Modelling of Semi-Autogenous Grinding**, D.Sc., Universidade Federal do Rio de Janeiro, 2013.

CARVALHO, R.M., TAVARES, L.M., "Simulação Dinâmica da Moagem a Seco em Moinho de Bolas", **In: Anais do IX Encontro de Modelagem Computacional**, Belo Horizonte, Brazil, 2006.

CARVALHO, R.M., TAVARES, L.M., "Dynamic Modeling of Comminution Using a General Microscale Breakage Model", **Computer Aided Chemical Engineering**, v.27, pp. 519-524, 2009.

CARVALHO, R.M., TAVARES, L.M., "Predicting the Effect of Operating and Design Variables on Breakage Rates Using the Mechanistic Ball Mill Model", **Minerals Engineering**, v.43-44, pp. 91-101, 2013.

CHO, K., **Breakage Mechanisms in Size Reduction**, Ph.D., University of Utah, 1987.

CLEARY, P.W., "Predicting Charge Motion, Power Draw, Segregation and Wear in Ball Mill Using Discrete Element Methods", **Minerals Engineering**, v.11, pp. 1061-1080, 1998.

CLEARY, P.W., "Charge Behavior and Power Consumption in Ball Mills: Sensitivity to Mill Operating Conditions, Liner Geometry and Charge Composition", **International Journal of Mineral Processing**, pp. 63, 2001.

CLEARY, P.W., "Ball Motion, Axial Segregation and Power Consumption in a Full Scale Two Chamber Cement Mill", **Minerals Engineering**, v.22, pp.809-820, 2009.

CLEARY, P., HOYER, D., "Centrifugal Mill Charge Motion and Power Draw: Comparison of DEM Predictions with Experiment", **International Journal of Mineral Processing**, v.59, pp. 131-148, 2000.

CLEARY, P.W., SINNOTT, M.D., MORRISON, R.D.,"DEM Prediction of Particle Flows in Grinding Processes", **International Journal for Numerical Methods in Fluids**, pp. 58, 2008.

COLLINAO, E., DAVILA, P., IRARRAZABAL, R., *et al.*, "Continuous Improvement in SAG Mill Liner Design Using New Technologies", **International Mineral Processing Congress**, paper 636, Santiago, Chile, October, 2014.

CUNDALL, P., STRACK, O., "A Discrete Numerical Model for Granular Assemblies", **Geotechnique**, v.29, pp. 517, 1979.

DAVIS, E.W., "Pulp Densities within Operating Ball Mills", **Trans. SME, AIME**, v.163, pp. 155, 1946.

DONDA, J.D., **Um Método para Prever o Consumo Especifico de Energia na (Re)moagem de Concentrados de Minério de Ferro em Moinho de Bolas**, D.Sc., Universidade Federal de Minas Gerais, 2003.

DONDA, J.D., ROSA, A.C., **A Lei de Moagem – Comprovação para Minério de Ferro**, 1st edition, Ouro Preto-MG, Livraria & Editora Graphar, 2014.

FARIA, P.M.C., TAVARES, L.M., RAJAMANI, R.K. *et al.*, "Scale-up and Optimization of Ball Mills in Iron Ore Grinding", **COREM: 3rd Symposium on Iron Ore Pelletizing**, paper 039, Quebec, Canada, September, 2013.

FARIA, P.M.C., TAVARES, L.M., RAJAMANI, R.K., "Population Balance Model Approach to Ball Mill Optimization in Iron Ore Grinding", **15º Brazilian Symposium on Iron Ore**, paper 25363, Belo Horizonte, Brazil, September, 2014a.

FARIA, P.M.C., TAVARES, L.M., RAJAMANI, R.K., "Population Balance Model Approach to Ball Mill Optimization in Iron Ore Grinding", **XXVI IMPC 2014**, paper 684, Santiago, Chile, October, 2014b.

HERBST, J.A., **Batch Ball Mill Simulation: An Approach for Wet Systems**, D.Sc., University of California, 1971.

HERBST, J.A., FUERSTENAU, D.W., "The Zero Order Production of Fine Sizes in Comminution and Its Implications in Simulation", **Trans. SME, AIME**, v.241, pp. 538-548, 1968.

HERBST, J.A., FUERSTENAU, D.W., "Influence of Mill Speed and Ball Loading on the Parameters of the Batch Grinding Equation", **Trans. SME, AIME**, v.252, pp. 169-176, 1972.

HERBST, J.A., FUERSTENAU, D.W., "Mathematical Simulation of Dry Ball Milling Using Specific Power Information", **Trans. SME, AIME**, v.254, pp. 343-348, 1973.

HERBST, J.A., FUERSTENAU, D.W., "Scale-Up Procedure for Continuous Grinding Mill Design Using Population Balance Models", **International Journal of Mineral Processing**, v.7, pp. 1-31, 1980.

HERBST, J.A., GRANDY, G.A., FUERSTENAU, D.W., "Population Balance Models for the Design of Continuous Grinding Mills", **X International Mineral Processing Congress**, paper 19, London, 1973.

HERBST, J.A., LO, Y.C., "Grinding Efficiency with Balls or Cones as Media", **International Journal of Mineral Processing**, pp. 141, 1989.

HERBST, J.A., LO, Y.C., RAJAMANI, K., "Population Balance Model Predictions of the Performance of Large-Diameter Mills", **Minerals and Metallurgical Processing**, pp. 114-120, 1985.

HERBST, J.A., MIKA, T.S., "Linearization of Tumbling Mill Models Involving Nonlinear Breakage Phenomena", **Eleventh International Symposium on Computer Applications in Mineral Industries**, Tucson, Arizona, 1973.

HERBST, J.A., RAJAMANI, K., KINNEBERG, D.J., **Estimill - A Program for Grinding Simulation and Parameter Estimation with Linear Models**, Program Description and User Manual, Utah Comminution Center, University of Utah, Salt Lake City, Utah, 1977.

HERBST, J.A., RAJAMANI, K., LO, Y.C., "Ball Mill Scale-up Testing at Carol Lake Pellet Plant", **University of Utah Grinding Project**, pp. 1-61, 1982.

HERBST, J.A., SIDDIQUE, K., RAJAMANI, K. *et al.*, "Population Balance Approach to Ball Mill Scale-Up: Bench and Pilot Scale Investigations", **Trans. SME, AIME**, v. 272, pp. 1945-1953, 1983.

HÖFLER, A., **Fundamental Breakage Studies of Mineral Particles with an Ultrafast Load Cell Device**, Ph.D., University of Utah, 1990.

HOGG, R., FUERSTENAU, D.W., "Power Relationships for Tumbling Mills", **Trans. SME, AIME**, v.252, pp. 418-423, 1972.

HUKKI, R.T., "Proposal for a Solomonic Settlement between The Theories of Von Rittinger, Kick and Bond", **Trans. SME, AIME**, v.223, pp. 403-408, 1962.

HUKKI, R.T., "The Principles of Comminution: An Analytical Summary", **Engineering & Mining Journal**, v.176, pp. 106, 1975.

KATZER, M., KLIMPEL, R., SEWELL, J., "Example of the Laboratory Characterization of Grinding Aids in the Wet Grinding of Ores", **Mining Engineering**, v.30, n. 10, pp.1471-1476, 1981.

KELSALL, D.F., REID, K.J., RESTARICK, C.J., "Continuous Grinding in a Small Wet Ball Mill. Part III. A Study of Distribution of Residence Time", **Powder Technology**, v.3, pp.170, 1970.

KIM, J.H., **A Normalized Model for Wet Batch Ball Milling**, Ph.D., University of Utah, 1974.

KING, R.P., "Comminution Operations", **Modeling and Simulation of Mineral Processing Systems,** 1st edition, Chapter 5, Great Britain, Butterworth-Heinemann, 2001.

KING, R.P., BOURGEOIS, F., "Measurement of Fracture Energy During Single Particle Fracture", **Minerals Engineering**, v.6, pp. 353-367, 1993.

LISBOA, V., SUAREZ, D., DEHART, I., "Applications of Vertimill in Grinding Circuits", **In: 15º Brazilian Symposium on Iron Ore**, paper 25378, Belo Horizonte, Brazil, September, 2014.

LO, Y.C., HERBST, J.A., "Considerations of Ball Size Effect in Population Balance Approach to Mill Scale-Up", **Advances in Mineral Processing**, pp. 33, 1986.

LO, Y.C., HERBST, J.A., "Analysis of the Performance of Large-Diameter Ball Mills at Bougainville Using the Population Balance Approach", **Minerals and Metallurgical Processing**, pp. 221-226, 1988.

LO, Y.C., OBLAD, A.E., HERBST, J.A., "Cost Reduction in Grinding Plants Through Process Optimization and Control", **Trans. SME, Minerals and Metallurgical Processing** , pp. 19-21, 1996.

MARTINOVIC, T.I., HERBST, J.A., LO, Y.C., "Optimization of Regrinding Ball Mills at Carol Pellet Plant of the Iron Ore Company of Canada", **Trans. SME, Minerals and Metallurgical Processing** , v.7, pp. 223-231, 1990.

MAZZINGHY, D.B., SCHNEIDER, C.L., "Applying the Austin Model for Vertical Mill Simulation", **15º Brazilian Symposium on Iron Ore**, paper 25396, Belo Horizonte, Brazil, September, 2014.

MEYER, K., **Pelletizing of Iron Ores.** 1st edition, New York, Spring-Verlag, 1980.

MIKA, T.S., BERLIOZ, L.M., FUERSTENAU, D.W., "An Approach to Kinetics of Dry Batch Ball Milling", **Zerkleinern, 2nd European Symposium on Comminution**, Dechema-Monographien, v.57, pp. 205-240, Amsterdam, 1967.

MISHRA, B.K, RAJAMANI, R.K., "The Discrete Element Method for the Simulation of Ball Mills", **Applied Mathematical Modeling**, v.16, pp. 598-604, 1992.

MORRELL, S., **Simulation of Bauxite Grinding in a Semi-Autogenous Mill and DSM Screen Circuit**, M.Sc., University of Queensland, 1989.

MORRELL, S., **The Prediction of Power Draw in Wet Tumbling Mills**, Ph.D., University of Queensland, 1993.

MORRELL, S., "Power Draw of Wet Tumbling Mills and Its Relationship to Charge Dynamics, Part 1: A Continuum Approach to Mathematical Modelling of Mill Power

Draw", **Transactions of the Institute of Mining and Metallurgy**, v.105, Section C, pp. C43–53, 1996a.

MORRELL, S., "Power Draw of Wet Tumbling Mills and Its Relationship to Charge Dynamics, Part 2: An Empirical Approach to Modeling of Mill Power Draw", **Transactions of the Institute of Mining and Metallurgy**, v.105, Section C, pp. C54–62, 1996b.

MORRELL, S., "Modelling the Influence on Power Draw of the Slurry Phase in Autogenous (AG), Semi-autogenous (SAG) and Ball Mills", **Comminution'14**, Cape Town, South Africa, April, 2014.

MORRELL, S., KOJOVIC, T., "The Influence of Slurry Transport on the Power Draw of Autogenous and Semi-autogenous Mills", **Proc. of 2nd Int. Conf. on Autogenous and Semi-autogenous Grinding Technology**, Vancouver, Canada, pp.378-389, 1996.

NAPIER-MUNN, T.J., MORREL, S., MORRISON, R.D., *et al.*, "Mineral Comminution Circuits: Their Operation and Optimization", **In: JKMRC Monograph Series in Mining and Mineral Processing**, p 2, 1996.

NARAYANAN, S.S., WHITEN, W.J., "Determination of Comminution Characteristics from Single-Particle Breakage Tests and Its Application to Ball–Mill Scale-up", **Trans. Instn. Min. Metal**, C 97, C115-124, 1988.

POWELL, M.S., WEERASEKARA, N.S., "Building the Unified Communition Model", **XXV International Mineral Processing Congress**, Brisbane, Australia, pp. 1133-1142, 2010.

POWELL, M.S., WEERASEKARA, N.S., COLE, S. *et al.*, "DEM Modeling of Liner Evolution and Its Influence on Grinding Rate in Ball Mills", **Minerals Engineering**, v.24, pp.341-351, 2011.

PRATHY, S.K, **Grinding Mill Shell Liner Wear and Its Influence on the Breakage Field**, M.Sc., University of Utah, 2005.

RAJAMANI, R., MISHRA, B., VENUGOPAL, R. *et al* "Discrete Element Analysis of Tumbling Mills", **Power Technology**, 109, pp. 105, 2000.

RAMOS, E.S., CARVALHO, R.M., TAVARES, L.M., "Simulação do Movimento da Carga em Moinhos de Bolas Utilizando o Método dos Elementos Discretos", **In: XXIV**

Brazilian Meeting of Mineral Processing and Extractive Metallurgy, v.1, pp. 440-447, Salvador, Brazil, 2011.

REID, K.J., "A Solution to the Batch Grinding Equation", **Chemical Engineering Science**, v.20, pp. 953-963, 1965.

ROSE, H.E., SULLIVAN, R.M.E., "A Treatise on the Internal Mechanics of Ball, Tube and Rod Mills", **Chemical Publishing Company**, New York, 258 pp, 1958a.

ROSE, H.E., SULLIVAN, R.M., "Ball, Tube and Rod Mills", **Chemical Publishing Co**, New York, pp. 140-177, 1958b.

ROWLAND, C.A, "The Tools of Power: The Bond Work Index, A Tool to Measure Grinding Efficiency", **SME, AIME**, pp. 1-22, 1976.

ROWLAND, C.A., MULAR, A.L.; GERALD II, V.J., "Selection of Rod Mills, Ball Mills, Pebble Mills and Regrind Mills", In: Design and Installation of Comminution Circuits, **American Institute of Mining, Metallurgical and Petroleum Engineers**, pp. 393- 438, New York, 1982.

SAMSKOG, P.O, BJORKMAN, J., HERBST, J.A. *et al.*, "Optimization of the Grinding Circuit at Kiruna Plant of LKAB Using Modeling and Simulation Techniques", **Trans. SME, Minerals and Metallurgical Processing** , v.7, pp. 279-287, 1990.

SCHÖNERT, K., **Advances in the Physical Fundamentals of Comminution. In Advances in Mineral Processing**, Edited by P. Somasundaran. Littleton, Colo. SME, 1986.

SCHÖNERT, K., "A First Survey of Grinding with High-Compression Roller Mills", **International Journal of Mineral Processing**, v.22, pp. 401-412, 1988.

SEPÚLVEDA, J. E., "Criterios para la Selección, Aplicación y Evaluación de Medios de Molienda", **I Encuentro Internacional de Procesamiento de Minerales**, Antofagasta, Chile, Julio, 2006.

SIDDIQUE, M., **A Kinetic Approach to Ball Mill Scale-Up for Dry and Wet Systems**, M.Sc., University of Utah, 1977.

SONGFACK, P.K., **Mass Transport in Wet Overflow Ball Mills**, D.Sc., University of Utah, 1996.

TAVARES, L.M., "Breakage of Particles: Quase-static", **In: M. Ghadiri, M. Hounslow, Handbook of Powder Technology**, v.12, pp.3-68, 2007.

TAVARES, L.M., "Analysis of Particle Fracture by Repeated Loading as Damage Accumulation", **Powder Technology**, v.190, pp. 327-339, 2009.

TAVARES, L.M., CARVALHO, R.M., "Modeling Breakage Rates of Coarse Particles in Ball Mills", **Minerals Engineering**, v.22, pp. 650-659, 2009.

TAVARES, L.M., CARVALHO, R.M., "A Mechanistic Model of Batch Grinding in Ball Mills", **In: XXV International Mineral Processing Congress**, v.1, pp. 1287-1297, AUSIMM, Brisbane, 2010.

TAVARES, L.M., CARVALHO, R.M., ALVES, V.K. *et al.*, "On Design of Ball Mills for Grinding Itabirite Ores", **In: 6th International Congress on the Science and Technology of Ironmaking 2012, ICSTI 2012 - Including Proceedings from the 42nd Ironmaking and Raw Materials Seminar, and the 13th Brazilian Symposium on Iron Ore**, Rio de Janeiro, Brazil, 2012.

TAVARES, L.M., KING, R.P., "Single-Particle Fracture Under Impact Loading", **International Journal of Mineral Processing**, v.54, pp. 1-28, 1998.

TAVARES, L.M., KING, R.P., "Modeling Particle Breakage by Repeated Impacts Using Continuum Damage Mechanics", **Powder Technology**, v.123, n. 2-3, pp.138-146, 2002.

TAVARES, L.M., KING, R.P., "Modeling of the Load-Deformation Response from Impact-Breakage of Particles", **International Journal of Mineral Processing**, v.74, pp. 267–277, 2004.

TOOR, P., PERKINS, T., POWELL, M.S. *et al.*, "The Influence of Liner Wear on Milling Efficiency", **Metallurgical Plant Design and Operating Strategies (MetPlant 2011)**, Perth, WA, 2011.

WEERASEKARA, N.S., POWELL, M.S., "The New Energy Logging from the Discrete Element Method", **CSRP'08 2nd Annual Conference**, Brisbane, Australia, 2008.

WEERASEKARA, N.S., POWELL, M.S., CLEARY, P.W. *et al.*, "The Contribution of DEM to the Science of Comminution", **Powder Technology**, v.248, pp.3-24, 2013.

WILLS, B.A., NAPIER-MUNN, T. “Comminution”, In: Elsevier Science & Technology Books, **Mineral Processing Technology - An Introduction to the Practical Aspects of Ore Treatment and Mineral Recovery,** 7th edition, Chapter 5, Butterworth-Heinemann, 2006.

I. APPENDIX I: Experimental Particle Size Distributions for Iron Ore Grinding

Table I.1: Particle size distribution of Vale's samples

Size		*Cumulative Passing (%)*	
Mesh	**Micron**	**Vale's Analysis**	**MPL Analysis**
0.371"	**9475**	100.00	100.00
3	**6700**	99.54	99.53
4	**4738**	97.52	98.91
6	**3350**	95.21	97.04
8	**2360**	92.93	94.62
10	**1700**	90.50	92.46
14	**1180**	87.49	90.23
20	**850**	84.19	86.57
28	**600**	80.10	82.50
35	**425**	75.32	77.69
48	**300**	69.82	72.51
65	**212**	59.39	63.72
100	**150**	50.56	52.08
150	**106**	37.59	35.41
200	**75**	25.18	21.60
270	**53**	14.67	12.15
400	**38**	7.75	6.33

Table I.2: Particle size distribution of batch test B1

Batch Wet Test Conditions	
Mono-Size Feed: 3350 x 2360 µm	Bulk density (ρ_{bulk}) = 2.81 g/cm^3
Mill Size: 25.4 x 29.2 cm	Slurry density (ρ_s) = 2.24 g/cm^3
Average Net Torque = 12.4 Nm	Solids Concentration = 72%
Slurry Filling (U) = 1.0	Solids Hold-up = 3.8 kg
Ball filling (J_b) = 0.4	Critical Speed (φ_c) = 0.683
Ball Top Size = 30 mm	Mill Speed = 61.3 rpm

Cumulative Passing (%)					
Size		**Grind Time (min)**			
Mesh	**Micron**	**0.0**	**1.0**	**2.0**	**4.0**
6	**3350**	100.00	100.00	100.00	100.00
8	**2360**	0.00	61.56	79.95	89.81
10	**1700**	0.00	41.35	58.29	78.06
14	**1180**	0.00	33.99	47.86	70.57
20	**850**	0.00	29.40	41.24	65.01
28	**600**	0.00	26.34	36.58	60.16
35	**425**	0.00	23.81	32.61	55.12
48	**300**	0.00	21.81	29.68	50.63
65	**212**	0.00	19.28	26.25	44.56
100	**150**	0.00	16.94	22.93	38.90
150	**106**	0.00	12.45	16.87	29.31
200	**75**	0.00	7.82	11.73	20.82
270	**53**	0.00	5.23	8.09	14.33
400	**38**	0.00	3.29	5.303	9.53

Table I.3: Particle size distribution of batch test B2

Batch Wet Test Conditions	
Mono-Size Feed: 150 x 106 µm	Bulk density (ρ_{bulk}) = 2.81 g/cm^3
Mill Size: 25.4 x 29.2 cm	Slurry density (ρ_s) = 2.24 g/cm^3
Average Net Torque = 12.6 Nm	Solids Concentration = 72%
Slurry Filling (U) = 1.0	Solids Hold-up = 3.8 kg
Ball filling (J_b) = 0.4	Critical Speed (φ_c) = 0.683
Ball Top Size = 30 mm	Mill Speed = 61.3 rpm

Cumulative Passing (%)					
Size		**Grind Time (min)**			
Mesh	**Micron**	**0.0**	**1.0**	**2.0**	**4.0**
100	**150**	100.00	100.00	100.00	100.00
150	**106**	0.00	12.85	27.43	41.87
200	**75**	0.00	4.67	10.42	19.53
270	**53**	0.00	2.40	5.89	11.17
400	**38**	0.00	1.47	3.45	6.69

Table I.4: Particle size distribution of batch test B3

Bach Wet Test Conditions	
Natural Feed: -2360 µm	Bulk density (ρ_{bulk}) = 2.81 g/cm^3
Mill Size: 25.4 x 29.2 cm	Slurry density (ρ_s) = 2.24 g/cm^3
Average Net Torque = 12.7 Nm	Solids Concentration = 72%
Slurry Filling (U) = 1.0	Solids Hold-up = 3.8 kg
Ball filling (J_b) = 0.4	Critical Speed (φ_c) = 0.683
Ball Top Size = 30 mm	Mill Speed = 61.3 rpm

Cumulative Passing (%)

Size		**Grind Time (min)**					
Mesh	**Micron**	**Feed**	**4.0**	**8.0**	**12.0**	**16.0**	**20.0**
8	**2360**	100.00	100.00	100.00	100.00	100.00	100.00
10	**1700**	98.86	99.99	99.99	100.00	100.00	100.00
14	**1180**	96.58	99.89	99.98	99.99	100.00	100.00
20	**850**	93.46	99.80	99.98	99.99	100.00	100.00
28	**600**	89.62	99.66	99.97	99.98	100.00	100.00
35	**425**	84.91	99.27	99.93	99.98	99.97	100.00
48	**300**	80.05	97.90	99.75	99.91	99.89	99.95
65	**212**	71.61	90.89	97.38	99.19	99.72	99.85
100	**150**	61.46	78.52	89.07	94.51	97.35	98.58
150	**106**	43.83	60.84	72.04	79.86	87.91	91.78
200	**75**	23.72	42.32	50.30	58.73	67.91	73.97
270	**53**	13.28	27.49	33.50	40.67	48.22	53.85
400	**38**	7.08	16.16	21.06	25.51	31.61	36.49

Table I.5: Particle size distribution of batch test B4

Bach Wet Test Conditions	
Natural Feed: -2360 µm	Bulk density (ρ_{bulk}) = 2.81 g/cm^3
Mill Size: 25.4 x 29.2 cm	Slurry density (ρ_s) = 2.41 g/cm^3
Average Net Torque = 13.0 Nm	Solids Concentration = 76%
Slurry Filling (U) = 1.0	Solids Hold-up = 4.3 kg
Ball filling (J_b) = 0.4	Critical Speed (φ_c) = 0.683
Ball Top Size = 30 mm	Mill Speed = 61.3 rpm

Cumulative Passing (%)						
Size		**Grind Time (min)**				
Mesh	**Micron**	**Feed**	**8.0**	**12.0**	**16.0**	**20.0**
8	**2360**	100.00	100.00	100.00	100.00	100.00
10	**1700**	98.12	99.98	99.99	99.99	100.00
14	**1180**	94.86	99.96	99.99	99.99	100.00
20	**850**	91.23	99.95	99.99	99.99	99.99
28	**600**	86.45	99.93	99.99	99.98	99.99
35	**425**	80.52	99.85	99.97	99.97	99.99
48	**300**	74.79	99.45	99.92	99.95	99.98
65	**212**	65.04	95.80	98.79	99.51	99.84
100	**150**	54.08	86.60	92.94	96.39	98.31
150	**106**	37.88	69.42	78.54	85.27	89.37
200	**75**	23.90	50.06	59.38	66.59	69.77
270	**53**	14.54	34.22	40.04	47.63	51.19
400	**38**	7.37	22.15	27.11	32.90	36.20

Table I.6: Particle size distribution of batch test B5

Bach Wet Test Conditions	
Natural Feed: -2360 µm	Bulk density (ρ_{bulk}) = 2.81 g/cm^3
Mill Size: 25.4 x 29.2 cm	Slurry density (ρ_s) = 2.60 g/cm^3
Average Net Torque = 13.2 Nm	Solids Concentration = 80%
Slurry Filling (U) = 1.0	Solids Hold-up = 4.9 kg
Ball filling (J_b) = 0.4	Critical Speed (φ_c) = 0.683
Ball Top Size = 30 mm	Mill Speed = 61.3 rpm

Cumulative Passing (%)						
Size		**Grind Time (min)**				
Mesh	**Micron**	**Feed**	**8.0**	**12.0**	**16.0**	**20.0**
8	**2360**	100.00	100.00	100.00	100.00	100.00
10	**1700**	98.11	100.00	100.00	100.00	100.00
14	**1180**	95.01	99.99	100.00	100.00	100.00
20	**850**	91.17	99.98	100.00	100.00	100.00
28	**600**	86.69	99.96	99.99	99.99	99.99
35	**425**	81.15	99.88	99.98	99.97	99.99
48	**300**	75.77	99.37	99.90	99.95	99.99
65	**212**	66.11	95.39	98.50	99.46	99.81
100	**150**	55.40	86.57	92.04	95.81	97.86
150	**106**	41.14	71.26	77.34	84.31	88.53
200	**75**	25.89	51.32	59.08	65.11	69.30
270	**53**	13.80	34.54	42.69	47.56	52.09
400	**38**	7.65	21.67	27.53	32.85	36.97

Table I.7: Particle size distribution of batch test B6

Bach Wet Test Conditions	
Natural Feed: -2360 µm	Bulk density (ρ_{bulk}) = 2.81 g/cm^3
Mill Size: 25.4 x 29.2 cm	Slurry density (ρ_s) = 2.24 g/cm^3
Average Net Torque = 8.1 Nm	Solids Concentration = 72%
Slurry Filling (U) = 2.6	Solids Hold-up = 9.6 kg
Ball filling (J_b) = 0.4	Critical Speed (φ_c) = 0.683
Ball Top Size = 30 mm	Mill Speed = 61.3 rpm

Cumulative Passing (%)						
Size		**Grind Time (min)**				
Mesh	**Micron**	**Feed**	**4.0**	**8.0**	**12.0**	**16.0**
8	**2360**	100.00	100.00	100.00	100.00	100.00
10	**1700**	98.86	99.90	99.99	100.00	100.00
14	**1180**	96.58	99.63	99.94	99.99	99.99
20	**850**	93.46	99.17	99.87	99.97	99.99
28	**600**	89.62	98.16	99.65	99.93	99.98
35	**425**	84.91	95.36	98.75	99.67	99.89
48	**300**	80.05	90.64	96.05	98.45	99.35
65	**212**	71.61	80.45	87.15	91.81	94.60
100	**150**	61.46	68.73	75.52	81.17	84.69
150	**106**	43.83	49.92	55.17	62.90	66.46
200	**75**	23.72	30.72	37.66	40.84	46.22
270	**53**	13.28	20.28	23.20	26.00	31.26
400	**38**	7.08	10.44	13.68	14.81	17.37

Table I.8: Particle size distribution of batch test B7

Bach Wet Test Conditions	
Natural Feed: -2360 µm	Bulk density (ρ_{bulk}) = 2.81 g/cm^3
Mill Size: 25.4 x 29.2 cm	Slurry density (ρ_s) = 2.41 g/cm^3
Average Net Torque = 8.0 Nm	Solids Concentration = 76%
Slurry Filling (U) = 2.6	Solids Hold-up = 11.3 kg
Ball filling (J_b) = 0.4	Critical Speed (φ_c) = 0.683
Ball Top Size = 30 mm	Mill Speed = 61.3 rpm

Cumulative Passing (%)				
Size		**Grind Time (min)**		
Mesh	**Micron**	**Feed**	**4.0**	**12.0**
8	**2360**	100.00	100.00	100.00
10	**1700**	98.86	99.94	99.99
14	**1180**	96.58	99.60	99.96
20	**850**	93.46	99.05	99.91
28	**600**	89.62	97.84	99.81
35	**425**	84.91	94.89	99.27
48	**300**	80.05	89.98	97.12
65	**212**	71.61	79.58	88.60
100	**150**	61.46	67.20	76.27
150	**106**	43.83	50.90	60.23
200	**75**	23.72	32.95	38.11
270	**53**	13.28	19.79	24.39
400	**38**	7.08	10.39	15.03

Table I.9: Particle size distribution of batch test B8

Bach Wet Test Conditions	
Natural Feed: -2360 µm	Bulk density (ρ_{bulk}) = 2.81 g/cm^3
Mill Size: 25.4 x 29.2 cm	Slurry density (ρ_s) = 2.60 g/cm^3
Average Net Torque = 8.1 Nm	Solids Concentration = 80%
Slurry Filling (U) = 2.6	Solids Hold-up = 12.8 kg
Ball filling (J_b) = 0.4	Critical Speed (φ_c) = 0.683
Ball Top Size = 30 mm	Mill Speed = 61.3 rpm

Cumulative Passing (%)						
Size		**Grind Time (min)**				
Mesh	**Micron**	**Feed**	**4.0**	**8.0**	**12.0**	**16.0**
8	**2360**	100.00	100.00	100.00	100.00	100.00
10	**1700**	98.12	99.71	99.84	99.93	99.99
14	**1180**	94.87	99.09	99.54	99.81	99.94
20	**850**	91.00	98.02	99.16	99.66	99.87
28	**600**	86.39	95.92	98.26	99.32	99.71
35	**425**	80.82	91.65	95.64	97.98	99.02
48	**300**	75.81	86.05	90.81	94.32	96.70
65	**212**	66.64	75.63	80.88	85.09	88.39
100	**150**	56.47	64.65	69.65	73.70	77.06
150	**106**	42.95	48.14	53.93	58.19	61.75
200	**75**	26.96	30.09	34.63	38.91	42.56
270	**53**	15.23	17.78	20.94	23.08	27.71
400	**38**	7.75	10.04	11.89	13.10	15.98

Table I.10: Particle size distribution of batch test B9

Bach Wet Test Conditions	
Natural Feed: -2360 µm	Bulk density (ρ_{bulk}) = 2.81 g/cm^3
Mill Size: 25.4 x 29.2 cm	Slurry density (ρ_s) = 2.24 g/cm^3
Average Net Torque = 13.1 Nm	Solids Concentration = 72%
Slurry Filling (U) = 1.0	Solids Hold-up = 3.8 kg
Ball filling (J_b) = 0.4	Critical Speed (φ_c) = 0.683
Ball Top Size = 25 mm	Mill Speed = 61.3 rpm

Cumulative Passing (%)						
Size		**Grind Time (min)**				
Mesh	**Micron**	**Feed**	**8.0**	**12.0**	**16.0**	**20.0**
8	**2360**	100.00	100.00	100.00	100.00	100.00
10	**1700**	98.96	99.98	100.00	100.00	100.00
14	**1180**	96.97	99.97	100.00	100.00	100.00
20	**850**	94.37	99.96	99.99	100.00	100.00
28	**600**	91.02	99.95	99.98	100.00	99.99
35	**425**	86.65	99.91	99.97	99.97	99.98
48	**300**	81.76	99.82	99.93	99.96	99.95
65	**212**	72.65	98.90	99.69	99.87	99.88
100	**150**	61.14	93.67	97.59	99.01	99.44
150	**106**	46.50	80.03	87.84	92.86	95.45
200	**75**	30.79	56.97	66.62	75.54	81.06
270	**53**	17.35	39.27	46.70	55.49	61.36
400	**38**	9.25	24.88	31.37	34.96	40.85

Table I.11: Particle size distribution of pilot test P1

Pilot Wet Test Conditions	
Fresh Feed: -3350 µm	Bulk density (ρ_{bulk}) = 2.81 g/cm^3
Mill Size: 41.6 x 64.1 cm	Slurry density (ρ_s) = 2.31 g/cm^3
Average Net Torque = 5.8 Nm	Solids Concentration = 73.7%
Slurry Filling (U) = 1.67	Fresh Feed Rate = 1.2 kg/min
Ball filling (J_b) = 0.35	Critical Speed (φ_c) = 0.683
Ball Top Size = 30 mm	Mill Speed = 46.5 rpm

Cumulative Passing (%)			
Size		**Grind Time (min)**	
Mesh	**Micron**	**Feed**	**Mill Discharge**
6	**3350**	100.00	100.00
8	**2360**	87.46	99.85
10	**1700**	84.88	99.83
14	**1180**	81.80	99.76
20	**850**	78.53	99.71
28	**600**	75.04	99.63
35	**425**	71.26	99.50
48	**300**	67.76	99.26
65	**212**	62.80	98.61
100	**150**	56.09	96.44
150	**106**	47.88	91.33
200	**75**	34.38	78.62
270	**53**	22.85	60.89
400	**38**	16.06	43.53

Table I.12: Particle size distribution of pilot test P2

Pilot Wet Test Conditions	
Fresh Feed: -3350 µm	Bulk density (ρ_{bulk}) = 2.81 g/cm^3
Mill Size: 41.6 x 64.1 cm	Slurry density (ρ_s) = 2.43 g/cm^3
Average Net Torque = 5.9 Nm	Solids Concentration = 76.5%
Slurry Filling (U) = 1.39	Fresh Feed Rate = 1.1 kg/min
Ball filling (J_b) = 0.35	Critical Speed (φ_c) = 0.683
Ball Top Size = 30 mm	Mill Speed = 46.5 rpm

Cumulative Passing (%)			
Size		**Grind Time (min)**	
Mesh	**Micron**	**Feed**	**Mill Discharge**
6	**3350**	100.00	100.00
8	**2360**	87.46	99.93
10	**1700**	84.88	99.86
14	**1180**	81.80	99.79
20	**850**	78.53	99.74
28	**600**	75.04	99.68
35	**425**	71.26	99.55
48	**300**	67.76	99.37
65	**212**	62.80	98.80
100	**150**	56.09	97.09
150	**106**	47.88	92.51
200	**75**	34.38	80.38
270	**53**	22.85	64.79
400	**38**	16.06	46.74

Table I.13: Particle size distribution of pilot test P3

Pilot Wet Test Conditions	
Fresh Feed: -3350 µm	Bulk density (ρ_{bulk}) = 2.81 g/cm^3
Mill Size: 41.6 x 64.1 cm	Slurry density (ρ_s) = 2.57 g/cm^3
Average Net Torque = 5.2 Nm	Solids Concentration = 79.3%
Slurry Filling (U) = 2.45	Fresh Feed Rate = 1.1 kg/min
Ball filling (J_b) = 0.35	Critical Speed (φ_c) = 0.683
Ball Top Size = 30 mm	Mill Speed = 46.5 rpm

Cumulative Passing (%)			
Size		**Grind Time (min)**	
Mesh	**Micron**	**Feed**	**Mill Discharge**
6	**3350**	100.00	100.00
8	**2360**	87.46	99.92
10	**1700**	84.88	99.89
14	**1180**	81.80	99.85
20	**850**	78.53	99.81
28	**600**	75.04	99.73
35	**425**	71.26	99.56
48	**300**	67.76	99.32
65	**212**	62.80	98.65
100	**150**	56.09	96.57
150	**106**	47.88	91.81
200	**75**	34.38	77.74
270	**53**	22.85	62.16
400	**38**	16.06	44.71

Table I.14: Particle size distribution of pilot test P4

Pilot Wet Test Conditions	
Fresh Feed: -3350 µm	Bulk density (ρ_{bulk}) = 2.81 g/cm^3
Mill Size: 41.6 x 64.1 cm	Slurry density (ρ_s) = 2.88 g/cm^3
Average Net Torque = 5.4 Nm	Solids Concentration = 84.8%
Slurry Filling (U) = 2.04	Fresh Feed Rate = 0.7 kg/min
Ball filling (J_b) = 0.35	Critical Speed (φ_c) = 0.683
Ball Top Size = 30 mm	Mill Speed = 46.5 rpm

Cumulative Passing (%)			
Size		**Grind Time (min)**	
Mesh	**Micron**	**Feed**	**Mill Discharge**
6	**3350**	100.00	100.00
8	**2360**	87.46	100.00
10	**1700**	84.88	100.00
14	**1180**	81.80	100.00
20	**850**	78.53	99.99
28	**600**	75.04	99.96
35	**425**	71.26	99.90
48	**300**	67.76	99.73
65	**212**	62.80	98.87
100	**150**	56.09	95.54
150	**106**	47.88	85.80
200	**75**	34.38	70.41
270	**53**	22.85	55.28
400	**38**	16.06	40.36

Table I.15: Particle size distribution of pilot test P5

Pilot Wet Test Conditions	
Fresh Feed: -3350 µm	Bulk density (ρ_{bulk}) = 2.81 g/cm^3
Mill Size: 41.6 x 64.1 cm	Slurry density (ρ_s) = 2.48 g/cm^3
Average Net Torque = 5.3 Nm	Solids Concentration = 77.5%
Slurry Filling (U) = 0.89	Fresh Feed Rate = 1.2 kg/min
Ball filling (J_b) = 0.35	Critical Speed (φ_c) = 0.683
Ball Top Size = 30 mm	Mill Speed = 46.5 rpm

Cumulative Passing (%)			
Size		**Grind Time (min)**	
Mesh	**Micron**	**Feed**	**Mill Discharge**
6	**3350**	100.00	100.00
8	**2360**	87.46	100.00
10	**1700**	84.88	100.00
14	**1180**	81.80	100.00
20	**850**	78.53	99.99
28	**600**	75.04	99.96
35	**425**	71.26	99.90
48	**300**	67.76	99.73
65	**212**	62.80	98.87
100	**150**	56.09	95.54
150	**106**	47.88	85.80
200	**75**	34.38	70.41
270	**53**	22.85	55.28
400	**38**	16.06	40.36

Table I.16: Particle size distribution of Vale's industrial mill – Campaign #1

Industrial Mill Sampling Campaign	
Fresh Feed: -3350 µm	Ore density (ρ_{ore}) = 5.13 g/cm^3
Mill Size: 5.2 x 10.6 m	Circulating Load (CL) = 2.37
Mill Power = 3405 kW	Specific Energy = 15.47 kW/ton
Feed Rate = 220 t/h (dry basis)	Specific Energy (with CL) = 4.59 kW/ton
Ball filling (J_b) = 0.31	Critical Speed (φ_c) = 0.683
Ball Top Size = 30 mm	Mill Speed = 12.7 rpm

Cumulative Passing (%)						
Size		**Grind Time (min)**				
Mesh	**Micron**	**Fresh Feed**	**Mill Discharge**	**Cyclone Overflow**	**Cyclone Underflow**	**Partition Curve**
6	**3350**	100.00	100.00	100.00	100.00	100.00
8	**2360**	92.92	99.85	99.99	99.79	100.00
10	**1700**	90.50	99.81	99.99	99.74	100.00
14	**1180**	87.49	99.78	99.98	99.70	100.00
20	**850**	84.19	99.72	99.98	99.60	100.00
28	**600**	80.10	99.60	99.97	99.45	100.00
35	**425**	75.32	99.43	99.96	99.20	100.00
48	**300**	69.82	99.18	99.94	98.86	100.00
65	**212**	59.39	97.86	99.85	97.01	100.00
100	**150**	50.55	96.56	99.76	95.21	100.00
150	**106**	37.59	90.59	99.35	86.90	99.99
200	**75**	25.17	75.35	97.92	65.84	97.09
270	**53**	14.67	50.40	87.04	34.17	68.49
400	**38**	7.74	31.01	69.55	14.77	37.28

Table I.17: Particle size distribution of Vale's industrial mill – Campaign #2

Industrial Mill Sampling Campaign	
Fresh Feed: -3350 µm	Ore density (ρ_{ore}) = 4.95 g/cm^3
Mill Size: 5.2 x 10.6 m	Circulating Load (CL) = 2.57
Mill Power = 3378 kW	Specific Energy = 14.29 kW/ton
Feed Rate = 237 t/h (dry basis)	Specific Energy (with CL) = 4.00 kW/ton
Ball filling (J_b) = 0.31	Critical Speed (φ_c) = 0.683
Ball Top Size = 30 mm	Mill Speed = 12.7 rpm

Cumulative Passing (%)						
Size		**Grind Time (min)**				
Mesh	**Micron**	**Fresh Feed**	**Mill Discharge**	**Cyclone Overflow**	**Cyclone Underflow**	**Partition Curve**
6	**3350**	100.00	100.00	100.00	100.00	100.00
8	**2360**	85.63	99.72	99.97	99.62	100.00
10	**1700**	82.22	99.63	99.95	99.51	100.00
14	**1180**	79.59	99.55	99.94	99.39	100.00
20	**850**	77.31	99.38	99.92	99.17	100.00
28	**600**	74.98	99.10	99.89	98.80	100.00
35	**425**	72.28	98.82	99.85	98.41	100.00
48	**300**	69.17	98.51	99.82	98.00	100.00
65	**212**	63.12	97.01	99.63	95.99	100.00
100	**150**	57.62	95.54	99.45	94.02	100.00
150	**106**	47.26	89.30	98.69	85.65	99.97
200	**75**	34.65	73.52	96.73	64.49	95.87
270	**53**	21.19	47.09	85.49	31.32	68.04
400	**38**	11.78	30.72	69.73	15.55	40.83

Table I.18: Particle size distribution of Vale's industrial mill – Campaign #3

Industrial Mill Sampling Campaign	
Fresh Feed: -3350 µm	Ore density (ρ_{ore}) = 4.72 g/cm^3
Mill Size: 5.2 x 10.6 m	Circulating Load (CL) = 2.67
Mill Power = 3463 kW	Specific Energy = 14.65 kW/ton
Feed Rate = 236 t/h (dry basis)	Specific Energy (with CL) = 3.99 kW/ton
Ball filling (J_b) = 0.31	Critical Speed (φ_c) = 0.683
Ball Top Size = 30 mm	Mill Speed = 12.7 rpm

Cumulative Passing (%)						
Size		**Grind Time (min)**				
Mesh	**Micron**	**Fresh Feed**	**Mill Discharge**	**Cyclone Overflow**	**Cyclone Underflow**	**Partition Curve**
6	**3350**	100.00	100.00	100.00	100.00	100.00
8	**2360**	85.63	99.72	99.97	99.62	100.00
10	**1700**	82.22	99.70	99.97	99.60	100.00
14	**1180**	79.59	99.77	99.98	99.69	100.00
20	**850**	77.31	99.68	99.99	99.56	100.00
28	**600**	74.98	99.42	99.97	99.21	100.00
35	**425**	72.28	99.12	99.96	98.80	100.00
48	**300**	69.17	98.77	99.95	98.33	100.00
65	**212**	63.12	97.19	99.88	96.19	100.00
100	**150**	57.62	95.65	99.81	94.10	100.00
150	**106**	47.26	89.26	99.49	85.44	99.97
200	**75**	34.65	72.98	97.43	63.83	93.77
270	**53**	21.19	47.56	85.81	32.45	58.17
400	**38**	11.78	29.69	70.74	14.34	29.78

II. APPENDIX II: The Specific Energy Input to the Mill

Table II.1: Specific energy input to batch wet experiments

Test	P/H (kW/ton)	kWh/ton for each grind times (in minutes)						
		1.0	2.0	4.0	8.0	12.0	16.0	20.0
B1	21.5	0.36	0.72	1.43	-	-	-	-
B2	21.9	0.36	0.73	1.46	-	-	-	-
B3	22.0	-	-	1.47	2.93	4.40	5.87	7.33
B4	19.2	-	-	-	2.56	3.84	5.12	6.40
B5	17.2	-	-	-	2.29	3.44	4.59	5.73
B6	5.4	-	-	0.36	0.72	1.08	1.44	-
B7	4.6	-	-	0.30	-	0.91	-	-
B8	4.0	-	-	0.27	0.54	0.81	1.08	-
B9	22.0	-	-	-	2.93	4.39	5.85	7.32

III. APPENDIX III: Estimated Feed Size Breakage Functions and Specific Selection Functions

Table III.1: Estimated feed size breakage functions

Size		B1: Mono-size 3350 x 2360 µm	B2: Mono-size 150 x 106 µm
Mesh	**Micron**	B_{ij}	B_{ij}
6	**3350**	1.0000	
8	**2360**	1.0000	
10	**1700**	0.6350	
14	**1180**	0.5220	
20	**850**	0.4515	
28	**600**	0.4044	
35	**425**	0.3657	
48	**300**	0.3349	
65	**212**	0.2961	
100	**150**	0.2601	1.0000
150	**106**	0.1911	1.0000
200	**75**	0.1200	0.3023
270	**53**	0.0803	0.1554
400	**38**	0.0505	0.0949

Table III.2: Estimated specific selection functions (S_i^E) based on batch experiments with 100% of slurry filling

Size		Specific Selection Function (kWh/ton)$^{-1}$			
Mesh	**Micron**	**Test B3 Feed, 12.0, 16.0 min grinds**	**Test B4 Feed, 12.0, 16.0 min grinds**	**Test B5 Feed, 16.0, 20.0 min grinds**	**Test B9 Feed, 12.0, 16.0 min grinds**
6	**3350**	3.8163	4.4937	3.4102	7.6655
8	**2360**	2.8581	3.3506	2.6298	5.4314
10	**1700**	2.1269	2.4823	2.0165	3.8196
14	**1180**	1.5829	1.8390	1.5462	2.6861
20	**850**	1.1864	1.3723	1.1933	1.9052
28	**600**	0.8829	1.0167	0.9150	1.3398
35	**425**	0.6571	0.7532	0.7016	0.9422
48	**300**	0.4885	0.5575	0.5375	0.6618
65	**212**	0.3635	0.4130	0.4121	0.4654
100	**150**	0.2705	0.3060	0.3160	0.3273
150	**106**	0.2013	0.2267	0.2423	0.2302
200	**75**	0.1498	0.1679	0.1858	0.1619
270	**53**	0.1121	0.1251	0.1432	0.1146
400	**38**	0.0000	0.0000	0.0000	0.0000

Table III.3: Estimated specific selection functions (S_i^E) based on batch experiments with 260% of slurry filling

Size		Specific Selection Function (kWh/ton)$^{-1}$		
Mesh	**Micron**	**Test B6 Feed, 12.0, 16.0 min grinds**	**Test B7 Feed, 4.0, 12.0 min grinds**	**Test B8 Feed, 16.0, 20.0 min grinds**
6	**3350**	11.3511	20.2730	18.6629
8	**2360**	7.8945	12.9187	11.8419
10	**1700**	5.4472	8.1516	7.4396
14	**1180**	3.7585	5.1436	4.6739
20	**850**	2.6168	3.2820	2.9697
28	**600**	1.8055	2.0710	1.8657
35	**425**	1.2458	1.3068	1.1721
48	**300**	0.8585	0.8233	0.7352
65	**212**	0.5924	0.5195	0.4619
100	**150**	0.4087	0.3278	0.2902
150	**106**	0.2820	0.2068	0.1823
200	**75**	0.1946	0.1305	0.1145
270	**53**	0.1352	0.0831	0.0726
400	**38**	0.0000	0.0000	0.0000

Table III.4: Estimated specific selection functions (S_i^{E*}) used to predict the pilot and industrial mill operation

Size		Specific Selection Function $(kWh/ton)^{-1}$		
Mesh	**Micron**	**Simulated condition: 74% solids; top ball size 30 mm; overflow discharge**	**Simulated condition: 74% solids; top ball size 25 mm; overflow discharge**	**Simulated condition: 76% solids; top ball size 30 mm; overflow discharge**
6	**3350**	4.0548	6.8990	4.1342
8	**2360**	3.0170	5.1331	3.0893
10	**1700**	2.2303	3.7947	2.2939
14	**1180**	1.6488	2.8053	1.7032
20	**850**	1.2278	2.0891	1.2739
28	**600**	0.9077	1.5443	0.9459
35	**425**	0.6710	1.1417	0.7023
48	**300**	0.4955	0.8431	0.5210
65	**212**	0.3663	0.6233	0.3868
100	**150**	0.2708	0.4608	0.2872
150	**106**	0.2002	0.3406	0.2133
200	**75**	0.1480	0.2518	0.1584
270	**53**	0.1100	0.1872	0.1183
400	**38**	0.0000	0.0000	0.0000

Table III.5: Estimated specific selection functions (S_i^{E*}) used to predict the pilot and industrial mill operation

Size		Specific Selection Function $(kWh/ton)^{-1}$		
Mesh	**Micron**	**Simulated condition: 79% solids; top ball size 30 mm; overflow discharge**	**Simulated condition: 85% solids; top ball size 30 mm; overflow discharge**	**Simulated condition: 77% solids; top ball size 30 mm; grate discharge**
6	**3350**	3.1715	0.8340	3.6705
8	**2360**	2.4256	0.7046	2.7605
10	**1700**	1.8442	0.5931	2.0633
14	**1180**	1.4022	0.4993	1.5422
20	**850**	1.0733	0.4220	1.1608
28	**600**	0.8160	0.3553	0.8676
35	**425**	0.6205	0.2990	0.6485
48	**300**	0.4713	0.2516	0.4842
65	**212**	0.3584	0.2118	0.3619
100	**150**	0.2725	0.1783	0.2705
150	**106**	0.2072	0.1501	0.2022
200	**75**	0.1575	0.1263	0.1511
270	**53**	0.1204	0.1067	0.1136
400	**38**	0.0000	0.0000	0.0000

IV. APPENDIX IV: Conductivity Calibration Curve and Residence Time Distribution

In order to obtain the concentration of lithium chloride in the samples collected at mill discharge during RTD experiments, the conductivity curve (LiCl concentration x conductivity – Figure IV.1) was determined in Mineral Processing Laboratory at University of Utah through standard solutions of LiCl. The conductivity of these solutions was measured by a conductivimeter.

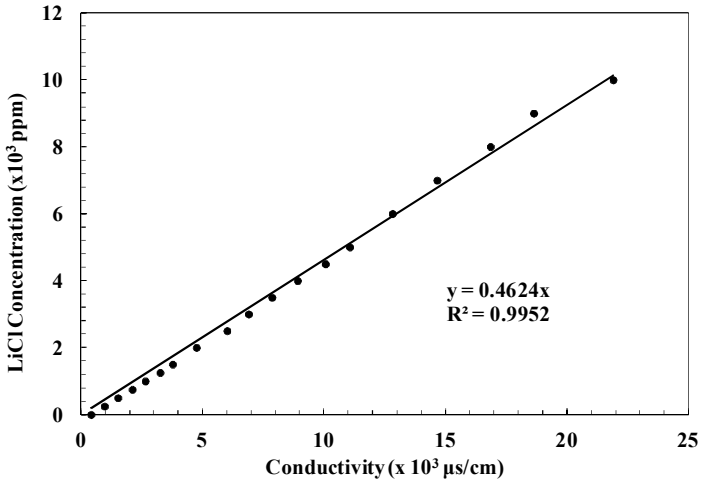

Figure IV.1: Conductivity calibration curve

The comparison between experimental data and fitted RTD models for pilot tests P3, P4 and P5 are presented in Figures from IV.2 to IV.4.

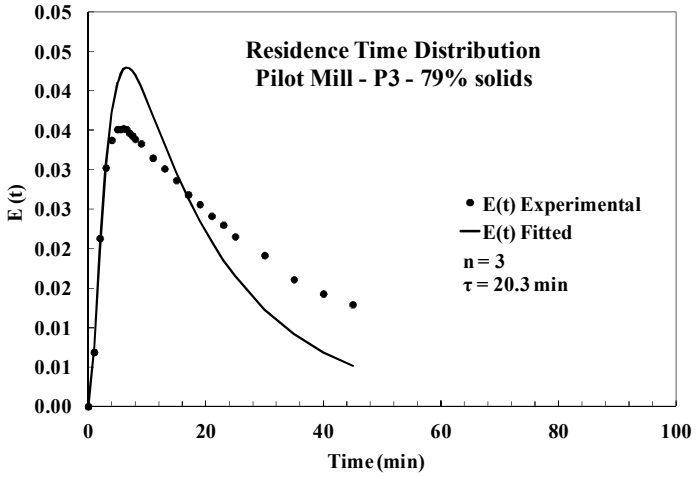

Figure IV.2: Comparison between experimental data and fitted RTD models for pilot test P3

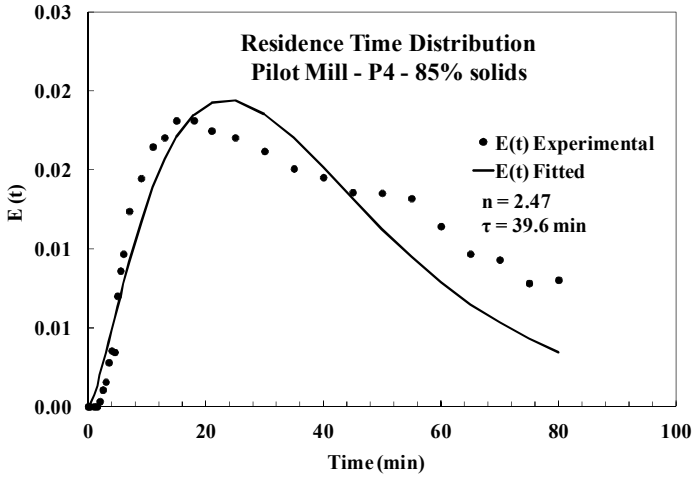

Figure IV.3: Comparison between experimental data and fitted RTD models for pilot test P4

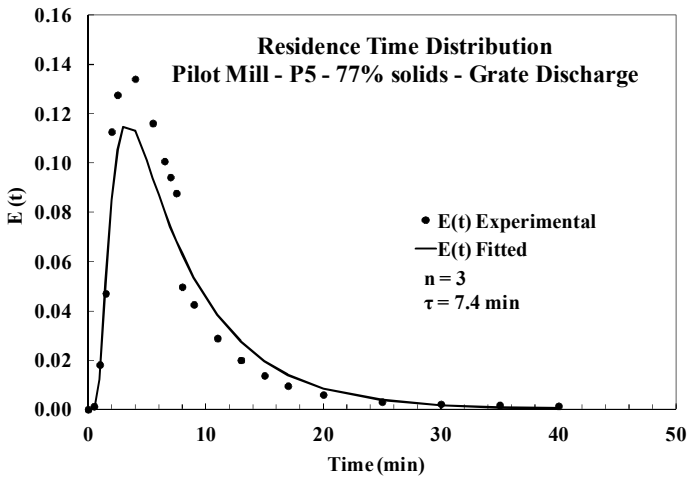

Figure IV.4: Comparison between experimental data and fitted RTD models for pilot test P5

V. APPENDIX V: List of Publications

FARIA, P.M.C., TAVARES, L.M., RAJAMANI, R.K. *et al.*, "Scale-up and Optimization of Ball Mills in Iron Ore Grinding", **COREM: 3rd Symposium on Iron Ore Pelletizing**, paper 039, Quebec, Canada, September, 2013.

FARIA, P.M.C., TAVARES, L.M., RAJAMANI, R.K., "Population Balance Model Approach to Ball Mill Optimization in Iron Ore Grinding", **15º Brazilian Symposium on Iron Ore**, paper 25363, Belo Horizonte, Brazil, September, 2014a.

FARIA, P.M.C., TAVARES, L.M., RAJAMANI, R.K., "Population Balance Model Approach to Ball Mill Optimization in Iron Ore Grinding", **XXVI IMPC 2014**, paper 684, Santiago, Chile, October, 2014b.